Volume 7 March 1961 No. 3

Canadian Aeronautical Journal

CONTENTS

Published by the
CANADIAN AERONAUTICAL INSTITUTE
Commonwealth Building, 77 Metcalfe Street
OTTAWA

Certainly new aviation projects take many forms, but manned, unmanned, research or commercial, they all depend on efficient hydraulics.

The drawing board stage, or before, is the time to consult Dowty Equipment of Canada Ltd. . . a self contained organization dedicated to the highest standard of quality.

EXPERIENCE • SPECIALIZATION • SERVICE

DOWTY *first in hydraulics in Canada*

DOWTY EQUIPMENT OF CANADA LIMITED, AJAX, ONTARIO

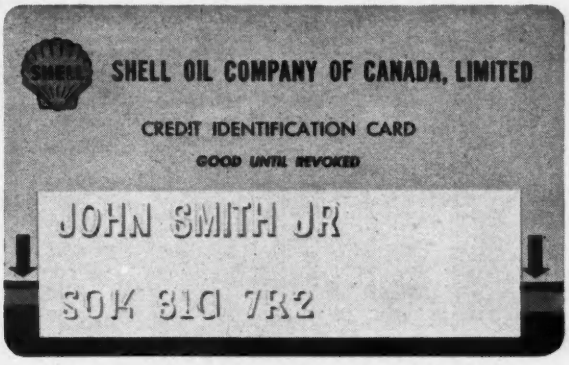

BULLETIN:

Mail coupon for Shell credit card —honoured by an ever-expanding network of airports throughout Canada and the U.S.

Shell is North America's largest supplier of commercial jet fuel and aviation gasoline. Send for your Shell credit card—and charge famous Shell products at any of hundreds of airports across the continent.

You can be sure that Shell quality will never vary no matter where you buy Shell products.

SHELL has pioneered many of the most important advances in aviation and aerospace fuels and lubricants. 100-octane gasoline is one example. Another is the new ashless dispersant oils now widely used by piston engine operators. Yet another example: the rocket fuel used to put U.S. satellites in orbit.

The same kind of research that produced these products has gone into all Shell fuels and lubricants in use today. Here is a brief rundown of these outstanding aviation products:

Shell aviation fuels. Shell gasolines are available in grades 80/87, 100/130, and 115/145. Also available: Aeroshell* turbine fuels 650 and JP-4.

Aeroshell Oils. Aeroshell Oil W is Shell's unique non-ash, dispersant oil with multi-viscosity characteristics. Use grade 80 for small engines, grade 100 for large engines.

Shell also makes outstanding straight mineral oils in grades 65, 80, 100, and 120.

Aeroshell Fluids. Shell offers you nine Aeroshell lubricating fluids—everything from squirt-can oil to a low-volatility instrument oil that is effective to −65 degrees F.

Aeroshell Greases. The nine Aeroshell greases include a high temperature grease, a graphite grease, a grease with an extreme pressure additive, and a special grease for helicopters.

Aeroshell Compounds. These include two anti-corrosion compounds, a de-icer, an anti-frost compound, and an anti-seize compound containing graphite.

You can charge these and many other Shell aviation products with a Shell credit card.

You can also charge a number of services, according to the conditions specified on Shell's credit card. These services include minor emergency repairs; transient hangar and tie-down fees; landing fees; and tires, batteries and accessories.

Mail coupon today for Shell credit card

Shell Oil Company of Canada, Limited
Aviation Division
505 University Avenue
Toronto, Ontario

Gentlemen: I would like to have a Shell credit card.

NAME_____

ADDRESS_____

CITY_____ ZONE_____ PROVINCE_____

EMPLOYER_____ YEARS EMPLOYED_____

EMPLOYER'S ADDRESS_____

YOUR OCCUPATION_____

BANK_____ BRANCH_____

T-AV-261

*T.M. Reg'd.

PT6

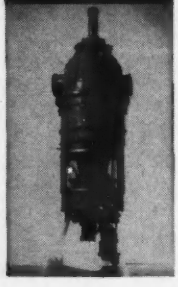

turboprop

Versatile New Engine
by CANADIAN PRATT & WHITNEY

Canada's first turboprop is a radical departure in engine design. The PT6 is an axial-centrifugal flow, moderate pressure ratio turbine engine with a free turbine drive for either turboprop or turboshaft installations. This 500 h.p. power plant is ideally suited for single or multi-engine fixed wing aircraft, helicopters or high speed marine installations. From a functional point of view, it weighs just 250 pounds, yet combines rugged service and dependable performance with the practical economies of low fuel consumption and ease of maintenance.

Canadian Pratt & Whitney Aircraft

COMPANY, LIMITED Longueuil, Montreal, P.Q.

A subsidiary of United Aircraft Corporation, East Hartford, Conn.

PRATT & WHITNEY ENGINES • SIKORSKI HELICOPTERS • HAMILTON STANDARD PRODUCTS • NORDEN ELECTRONICS

CANADIAN AERONAUTICAL INSTITUTE

CANADIAN AERONAUTICAL JOURNAL

Subscription—$4.00 a year Single copies—50 cents each
Copies prior to 1959—$1.00 each
Bound Volumes—Orders for binding readers' own copies will be accepted in January and February, 1962, at $5.00 a volume.
Published monthly, except July and August

All communications should be addressed to The Secretary, Canadian Aeronautical Institute, 77 Metcalfe St, Ottawa 4, Ontario, Canada

Authorized as second class mail, Post Office Department, Ottawa

Printed by The Runge Press Ltd., Ottawa, Ontario, Canada

AIRBORNE FROM OTTAWA

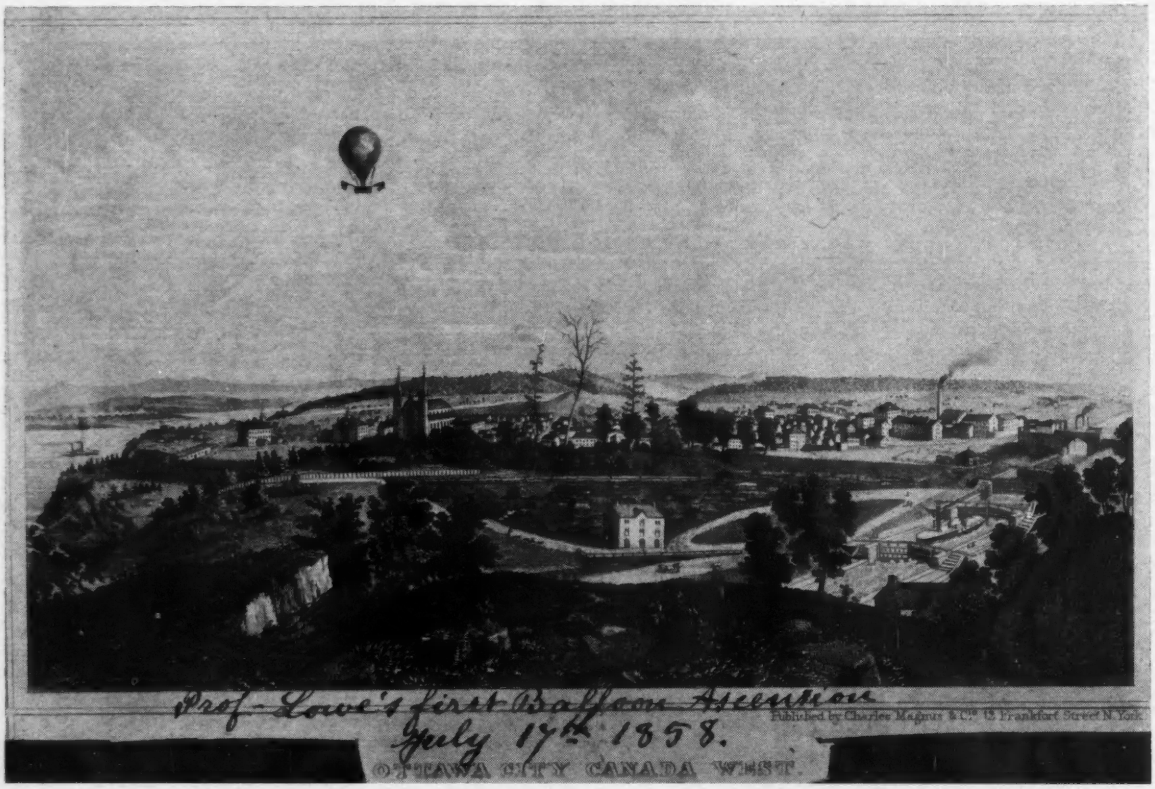

Professor T. S. Lowe's first balloon ascent over Ottawa on the 17th July, 1858. This ascent is believed to have been the first man-carrying flight in Canada.

EDITORIAL

ACHIEVEMENTS IN COOPERATIVE RESEARCH AND DEVELOPMENTS IN NATO

I AM particularly pleased to have been asked to contribute to your Journal in a guest editorial capacity. The reason for this is not only that I have another opportunity to develop a topic that I have been advocating for many years but because, judging from the response Canada has made through her participation in cooperative international endeavour, I have readers who are already largely convinced. I have been the Chairman of the Advisory Group for Aeronautical Research and Development and, after some ten years of experience in seeing put into practice, in a significant way, those terms and expressions everyone recognizes as being desirable aims, I am more than ever convinced that international cooperative activity at the most creative level is correct in principle and, much more significant, possible in practice. Ten years ago we were told that the nations would not be able to cooperate effectively, because reasons of national security, national proprietary interests, national pride, creative individuality etc would prevent any real achievement. In spite of these counsels we persisted in the formation of our Advisory Group, with its permanent secretariat in Paris and its voluntarily subscribed panels. From the beginning, at which time we had 3 panels drawing together some 80 talented NATO nationals in the study of three broad scientific disciplines, we have built up, by 1961, 7 panels involving over 250 of among the foremost scientists of the NATO nations. The thought and effort of these people is put voluntarily at the disposal of NATO in meetings normally held twice a year; the work of each panel is monitored by an executive officer, who is a member of the permanent secretariat located in Paris. Dr. John J. Green, with his early enthusiastic support of AGARD, was a great help in this development. In 1955 we were able to hold the Fifth General Assembly in Ottawa, and were fully supported by your Government. Examples of achievements to which Canada, as one of the NATO nations, can point with pride are various and occur at all scientific levels and in every scientific discipline:

- Work on the NATO Light Strike Fighter
- The Training Center for Experimental Aerodynamics, Brussels
- Design criteria for aircraft undercarriages; roughness of NATO runways
- Missile Range in Greece
- A large number of publications which provide a review of certain research endeavours and often give member countries access to information otherwise only available through costly and time consuming research programs. Examples:
  - Flight Test Manual
  - Manual on Aeroelasticity
  - Materials Handbook
  - Multi-Lingual Dictionary
- Symposia on Operational Research
- Work in the area of documentation. That the acceleration of scientific activity has resulted in an overwhelming increase in the quantity of technical literature is apparent to everyone — what is not exactly clear is the response that should be made to the problem, in the international sense.

The list of accomplishments is long — and gratifying. It is gratifying to me personally but this is of small importance. It is more important that it be a source of gratification to the nations, such as yours, which made it possible. Make no mistake, the achievements did not come about through some form of international prestidigitation: no magic formulae have produced these results. In each case dedicated men of many nations have given of their time and effort to find a solution to a scientific situation, exactly as has always been done in national practice; having found a possible approach, they have applied the normal development routines to achieve the progress we now see. The only magical element that can be found is that, in many cases, the result has the status of an agreement among nations, or a course of action which is acceptable to these nations. When one realizes that it took years to agree on a standard atmosphere in the West, one begins to appreciate the significance of what has been accomplished.

To the individuals who have worked on your behalf within our framework we all owe many thanks – not simply because they have displayed a great deal of energy within our organization but because they have helped to show the way. In most panels, there are Canadians directly involved. I cannot name all of the excellent participants from Canada. I shall name only a few. Dr. MacPhail of the National Research Council, who is Chairman of the Fluid Dynamics Panel; Mr. Wood of the National Aeronautical Establishment, Chairman of our Flight Mechanics Panel. To Mr. F. R. Thurston of the National Aeronautical Establishment, we all owe much for the application of his considerable energy and talent to the Structures and Materials Panel, for five years as a member and then as Chairman. The same panel also has an excellent executive officer from Canada, Mr. Gerald H. Cooper. The work of these men indicates that in Canada, as in the other nations which are contained in our structure, significant progress in cooperation on an international scale is inevitable, providing that (a) there exists a strong structure of organization within which their combined talents can find application, and (b) the value of their work within this structure is so fully appreciated nationally that they are supported in their participation.

In closing, I should like to sound a note of cautious optimism. In my almost sixty years of intimate involvement in science, I have never lost sight of the possibility for good of international actions – we are further toward this goal now than I would have thought possible even fifteen years ago. But we have a tremendous distance yet to go. All that can be said is that a start has been made; a possibility has been demonstrated; a series of tests, statistically not sufficient, has confirmed an hypothesis. The future is up to the workers of the nations, which, like yours, show a will.

Dr. Theodore von Kármán,
Chairman, Advisory Group for Aeronautical Research and Development, NATO

AIRBORNE FROM OTTAWA

We are indebted to Mr. K. M. Molson, Curator of the National Aviation Museum, for our frontispiece this month.

The complete story of this balloon ascent has not yet been assembled but it seems that Professor T. S. Lowe was an American, invited to Ottawa to take part in the celebrations marking the laying of the first trans-Atlantic cable. (A balloon ascent was justifiably regarded as a telling feature of any celebrations in those days, whether it was appropriate or not.) Though his balloon had been built in the States, apparently Professor Lowe had not made an ascent before coming to Ottawa, so that the flight in Ottawa on the 17th July, 1858, was his first. It is reported that he made other ascents in the area that summer.

It is believed to have been the first man-carrying flight in Canada.

Later Professor Lowe became possibly the foremost US balloonist and was placed in charge of the balloon unit of the Union forces in the American Civil War.

Those who know Ottawa can get their bearings from the Rideau Canal Locks. The picture was apparently "taken" from the site of the present Parliament Buildings, looking east. Though appearances may be misleading – and probably are in this case – Professor Lowe seems to have taken off, appropriately enough, from the neighbourhood of Rockcliffe.

Prof. Lowe's first balloon ascent over Ottawa on the 17th July, 1858.

MAN-POWERED FLIGHT IN 1935-37 AND TODAY†

by Helmut Haessler

Two of the greatest pioneering achievements in the realm of man-powered flight were the Haessler-Villinger and Bossi-Bonomi aircraft of the mid-30s. In the December 1960 issue of the Journal we published a paper by Mr. Bossi reporting on his work and we have now received this paper from Mr. Haessler giving details of his aircraft and some stimulating observations about future possibilities. – Sec.

SUMMARY

This paper reviews the flights of the Haessler-Villinger man-powered aircraft in the years 1935-37 and gives the specification of this aircraft. It considers the influence of weight and span on performance, and wing weights are calculated for a range of spans, areas and loads, on the basis of the weight of the Haessler-Villinger aircraft. It concludes with a proposal for a man-powered aircraft capable of restricted flights of 1 hour, with and without ground effect, by a trained racing cyclist, or unrestricted flights with glide ratio improved to 1:100, by an average amateur.

INTRODUCTION

When the early aeronautical pioneers tried to fly, they thought the use of man-power would be the quickest and easiest way to do it. For centuries they were unable to succeed by this means and the first actual flights were made with gliders, without any power at all. When power was used, they found that much more was needed than a human being could develop. Aircraft powerplants, which in the early days developed about 10 hp, now have more than a thousand times this power output, making it possible to fly beyond the limits of the atmosphere into outer space.

It seems that with the beginning of the space age, which coincides with the completion of the conquest of the air, interest in man-powered flight is becoming livelier than ever. There can be no practical reason for this, unless man considers the conquest of the air to be incomplete until he can fly with his own muscles. It is not surprising that this could not be done at the beginning of the development of aircraft, since a horizontal flight with that wee bit of man-power demands extraordinary refinements in the airplane shape and structure.

I have been asked to report on the development and flying of the Haessler-Villinger man-powered aircraft 26 years ago and I would like to add some thoughts about the present situation.

†Received on the 17th January, 1961.

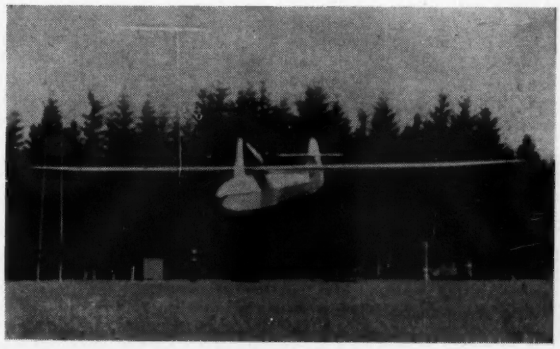

Figure 1

FIRST HORIZONTAL MAN-POWERED FLIGHTS

First flight

On the 29th August, 1935, at the airport of Frankfurt/M in Germany, the Haessler-Villinger man-powered aircraft was carried out of the hangar to the airfield to attempt its first man-powered flight; some previous test flights had been made without power on the airport at Dessau. The airplane looked like an ordinary sailplane of 45 ft span, except for the propeller mounted on a pylon over the fuselage (Figures 1 and 2). The technical specification is given in Table 1.

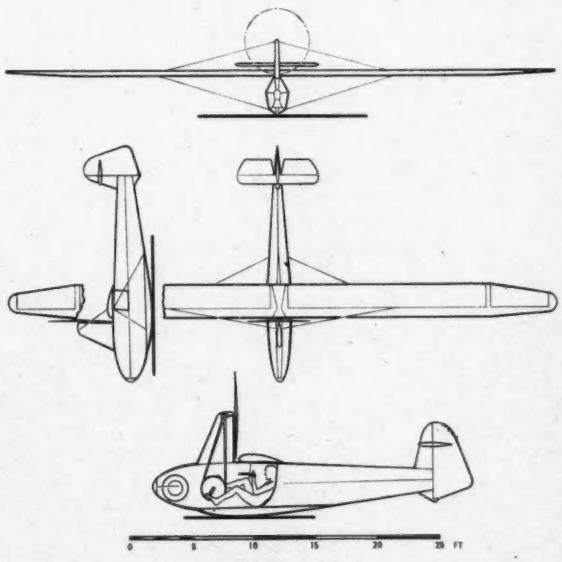

Figure 2
Man-powered aircraft — Haessler-Villinger

TABLE 1

SPECIFICATION OF THE HAESSLER-VILLINGER AIRCRAFT

Wing area	9.65 sq m	104 sq ft
Span	13.5 m	44.3 ft
Wing loading	11.5 kg/sq m	2.29 lb/sq ft
Aspect ratio	18.8	18.8
Wing section	Gottingen 535	
Rib distance	20 cm	7.9 in
Chord	76 cm	30.0 in
Sinking speed	0.52 m/sec	20.5 in/sec or 102.5 ft/min
Fuselage cross-section	0.33 sq m	3.56 sq ft
Prop dia.	1.5 m	4.9 ft
Prop rpm	600 rpm	600 rpm
Prop eff.	0.82	0.82
Glide ratio	1:24	1:24
Empty weight	34 kg	75 lb
Energy acc.	10 kg	22 lb
Pilot	65 kg	143 lb

A prize had been instituted by the Polytechnische Gesellschaft of Frankfurt for the first flight by man-power. There were regulations covering the distance to be flown and the storage of the energy for takeoff. In spite of the fact that I could not agree to all points of the regulations (the weight of the energy accumulator of 20 lb had to be carried in the aircraft and the flight path had to go around two marks 1700 ft apart) the aircraft was designed to meet the regulations as far as possible.

In preparation for the takeoff the airplane was anchored to the ground by a pair of anchor-pins at the centre of the fuselage, and the pilot stretched several rubber cables, one after another, from the fuselage to a second anchor at a certain distance in front of the aircraft. Then he entered the cockpit and released the anchor at the fuselage. The aircraft accelerated and climbed to a height of about 10 ft. At this point the pilot put his power into two pedals connected to the propeller and continued to fly horizontally for a distance of about 400 ft. When his peak power output was over he relaxed and finished his flight in a normal glide.

The total distance covered from takeoff point to standstill was 780 ft and was checked by a committee consisting of members of the Physikalische Gesellschaft and other officials. After consideration of all circumstances, this committee pronounced this flight as the first flight over a horizontal airfield accomplished by the unaided power of the pilot.

Later calculations and tests showed that on this flight at least 420 ft were covered in horizontal flight under the power of the pilot applied to the propeller, and not more than 360 ft resulted from the stored energy. Since the storing ability of the accumulator changed due to hysteresis in the rubber, and friction factors between the skid and ground changed, the distance of 360 ft is an optimal figure. Test flights without using the propeller covered distances between 280 and 360 ft, comprising the acceleration path on the ground, the climb path until the stored energy was used up, and the glide path without power (Figure 3).

When the news of this first flight went out, people said that such a short flight with the aircraft launched by a rubber bungee, could have been done with any good glider without man-power. When it was pointed out that a glide of such a distance could not be made from a launching height of 10 ft, unless the aircraft had a glide ratio of at least 1:62, it was argued that the launch had been done at excess speed, so that the glide distance could be attributed to kinetic energy. A calculation of this condition shows that launching at excess speed with a given amount of stored energy is less efficient and results in shorter flight distances than those actually flown. Besides that, the aircraft in question was not capable of storing the necessary energy in excess speed, according to its lift/drag diagram and its flight envelope, since it would have fallen apart before that point could be reached[1].

This illustrates the situation at that time, when a clear definition of man-powered flight had not been established. The committee should have said that for the first time a horizontal flight had been achieved under the direct power of the pilot, for a distance of at least 420 ft; the total flight of 780 ft included a takeoff and climb for a distance of 120 ft, using the pilot's energy (stored in an accumulator), and a glide of not more than 240 ft. We will see later that elongation of the glide path by continuing to apply cruising power was not feasible.

Subsequent flights

After several improvements to the aircraft (in particular, controls) and changing the pilot for a stronger one, further flight tests were made in August 1936 at the airport at Frankfurt and a total distance of 1300 ft was covered. The horizontal flight path was at least 940 ft compared with 420 ft of the year before.

A few months later on the 21st November, 1936, the aircraft was flown at Hamburg before members of the Lilienthal Gesellschaft. A short movie strip from a newsreel which shows one of these flights is still in existence and shows a horizontal flight path of more than 1060 ft, of a total distance of 1420 ft. From Figure 4, taken from this strip, it can be seen that, after recovering the normal height of about 10 ft, the pilot maintains this height for the length of the man-powered flight.

In the following year we demonstrated the aircraft at three air shows at Schleusingen, Schwarza and Leipzig, each time covering distances from 1400 to 2000 ft. We would not have agreed to undertake these scheduled demonstrations if we had not been confident of achieving this performance regularly even in poor weather conditions. At Schleusingen, the flights had to be done in the rain.

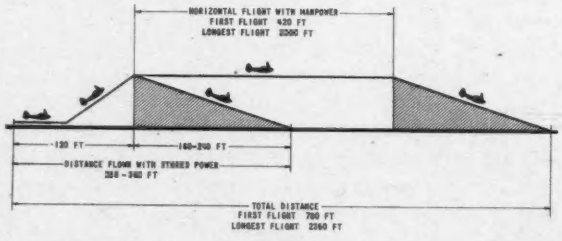

Figure 3

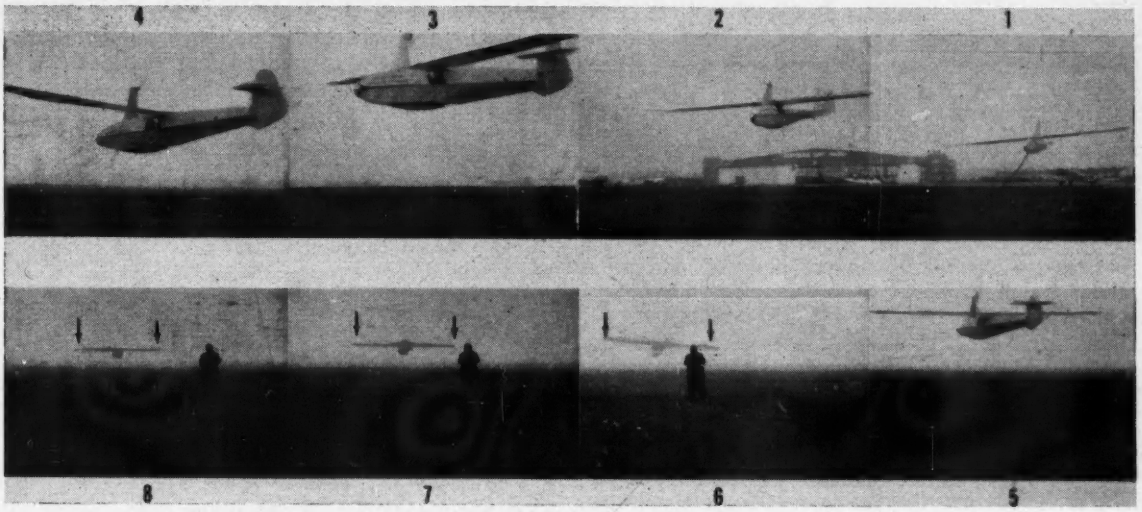

Figure 4

Taken from a movie strip made at Hamburg in November 1936

On the 4th July, 1937, at the airport at Meiningen, a distance of 2350 ft was attained and measured by airport officials. This included a horizontal flight of 2000 ft flown in 1 min 12 sec at a height of 10 ft. The horizontal part of this flight was five times longer than that of the first flight in 1935. These results were reported in the newspapers, but they are apparently not known in aviation circles today.

A weight of 20 lb, equal to the weight of the rubber bungee and the winding equipment, was carried at all times in the nose of the fuselage and could not be removed without seriously affecting the position of the centre of gravity – especially not after the alteration of the tail surfaces in the second year, which resulted in higher tail weight. In all cases the stored takeoff energy was the same; the accumulator system was not changed.

These results were the best we could expect with this aircraft and with this pilot. We had no intention of looking for another pilot, although this could have led to flights of 2 minutes with this aircraft. In the end we could not afford the experiments any longer and gave the aircraft to the Luftfahrt Museum in Berlin, in February 1938.

Between July 1935 and February 1938 a total of about 120 flights were made with this aircraft. About 80 flights were made with man-power; the others were done for testing changes in trim and controls and training two pilots to the peculiarities of man-powered flight. Of the 80 man-powered flights at least 15 were of a duration of 1 minute or more.

Other flights

There were other man-powered flights before and after ours. In 1927 an airplane with flapping wings was designed by Mr. Lippisch and flown at the Wasserkuppe Soaring Centre. Several of its flights were stretched glides up to double the normal distance, on a not horizontal terrain. Takeoff was accomplished with rubber bungee and teams.

In Italy a man-powered aircraft was built by Bossi-Bonomi in 1936. Takeoffs were made with teams[8] and the results were stretched glides. The longest flight, with assistance by team to a height of 25 ft, was ⅜ of a mile. In some cases, takeoffs were made under the power of the pilot alone, through a driven wheel and the propellers. The flying distance after this type of takeoff is reported by Mr. Bossi to have been 300 ft.

Today in 1961, 26 years after our first man-powered flight, another prize is being offered, by Mr. Kremer, and the competition will be conducted by the Royal Aero Club of the U.K.[8] The regulations do not allow the use of stored energy and specify a flight in a figure of eight around two marks half a mile apart, which will require a flying time of between 3 and 4 minutes. It seems that the regulation banning stored energy was made because of the recording difficulties which could arise from its use.

PERFORMANCE LEVELS IN MAN-POWERED FLIGHT

Now it would be appropriate to establish definitions of the different performance levels in man-powered flight.

When we consider a glide elongated by applying man-power, the lower limit is the normal glide with zero power, the upper limit horizontal flight. The range between these limits can only be considered as an intermediate state, which I will call "the man-powered glide". The aircraft of Lippisch belongs to this category and most of the flights with the Bossi-Bonomi aircraft were done in this regime.

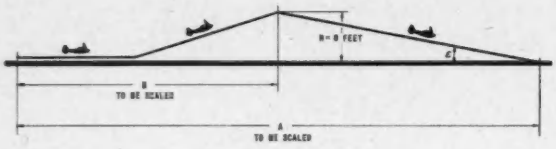

Figure 5
Scheme for calculation of takeoff height

Only the horizontal part of a flight with man-power can be considered as "man-powered flight." If stored or external energy is used for takeoff, the amount of this energy has to be checked and the part of the flight attributable to it has to be deducted from the whole. Another way would be to record the height of the flight-path by photography and to time only that part of the flight which is above release level. This leads to practical difficulties when the release level is not at the eye level of the recording person. The ideal case is the takeoff under the direct power of the pilot, since here the whole flight is above take-off level, if the airfield is level.

I want here to inject a proposal for defining assisted takeoff for any particular aircraft by establishing, for that aircraft, a specific limited amount of stored energy used for takeoff and the best use, in terms of flying time, that can be made of that energy.

The aircraft should be launched on a level airfield so that the height at power shut-off is near zero – let us set an arbitrary maximum of 8 ft on this release height, sufficient to give the pilot a margin for the correction of slight deviations from the horizontal flight path.

Release height H (Figure 5), defined as the distance between the lowest point of the aircraft and the ground, is to be calculated from the total distance A flown with the stored energy, the glide ratio ($\tan \epsilon$) of the aircraft under conditions of ground effect, and the horizontal distance B from start to power shut-off. The best flying time from start to finish (the distance A) must be established by a series of test flights, all done with the same amount of stored energy.

The time so established must be deducted from the times of subsequent flights using man-power and launched with the same amount of stored energy. The result in each case would be the time of the horizontal part of the flight, achieved under pilot-power applied to the propeller.

Once the figure for the duration of that part of the flight attributable to stored energy has been established, no distances would have to be scaled and a stop watch would be sufficient for recording the man-powered element. Under this arrangement the energy storing equipment would never have to be carried in the aircraft; in fact all considerations affecting the takeoff would be standardized and established as a datum, from which the "man-powered flight" can be measured.

Figure 6 shows the performance characteristics of a professional racing cyclist. We know that a man has a certain power level which he can maintain for a long time, up to several hours. By working at this cruising power level, at which the lungs are capable of maintaining the oxygen supply required by the body, no energy reserves are used up. Man has a certain capability of storing oxygen in his blood, which enables him to do a certain amount of work without adding new oxygen by breathing. This reserve of energy is of the order of 1100 m kg. This energy can be used in a very short time, e.g. 10 seconds, or it can be spread over hours. If the total power output is distributed over more than 5 minutes, the expenditure of reserve energy becomes very little compared with the cruising power. We will consider the power up to 5 minutes as the short-time power and over 5 minutes as the long-time power.

Performance Level 1

The horizontal flights 25 years ago were short-time flights and done at heights of less than the wing span, that is within ground effect. This will be considered as Performance Level 1 (Figure 7). The Haessler-Villinger aircraft is typical of this group with assisted takeoff and Bossi-Bonomi with unassisted takeoff.

Performance Level 2

If a man-powered aircraft is to be built today, its level of performance should be an improvement on that of 25 years ago. Horizontal flights of 1 minute duration have already been made. If a new aircraft could fly for say 2 minutes, it would be an improvement but it would not be a significant advance in the art of man-powered flight, and would scarcely be a sufficient reward for the effort entailed.

To achieve real progress the power necessary to maintain horizontal flight must be equal to or less than the power output of a man for 5 minutes or more. We will see later that it seems to be possible today to fly for several hours at low heights, with the help of ground effect, using stored energy for takeoff in the manner described above. That will be Performance Level 2. To be realistic, the regulations of any competition today should conform to this level.

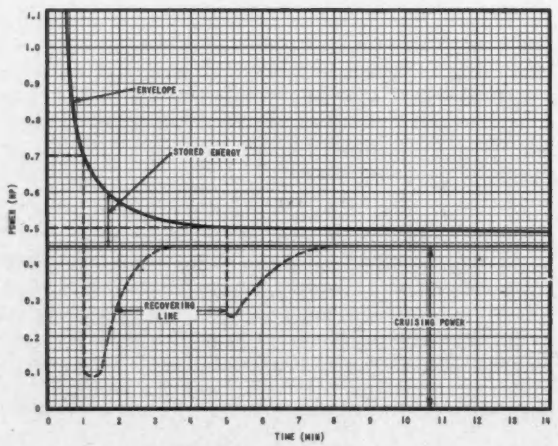

Figure 6
Typical man-power envelope

	PERFORMANCE LEVEL	PERFORMANCE	GROUND EFFECT	TAKE OFF	AIRCRAFT	FLYING TIME	
						ACT	PROPOSED
RESTRICTED MAN-POWERED FLIGHT	INTERMEDIATE	GLIDE RATIO IMPROVED		UNLIMITED ASSIST	LIPPISCH DOSSI – BONOMI		
	1	SHORT-TIME HORIZONTAL FLIGHT (BELOW 5 MIN)	YES	LIMITED ASSIST	HAESSLER – VILLINGER	72 SEC	
				NO ASSIST	DOSSI – BONOMI PROPOSAL NORMEILER	10 SEC	90 SEC
	2	LONG TIME HORIZONTAL FLIGHT (ABOVE 5 MIN)	YES	LIMITED ASSIST	PROPOSAL NYA, B		1 HR
	3	LONG TIME HORIZONTAL FLIGHT (ABOVE 5 MIN)	NO	NO ASSIST	PROPOSAL NYA		1 HR
UNRESTRICTED FLIGHT	4	SOARING WITH AVERAGE PILOT GLIDE RATIO ABOVE 1:75	NO	UNLIMITED ASSIST	PROPOSAL NYB & C		

Figure 7

Performance Level 3

If the drag of the aircraft can be reduced to the point where the power necessary to maintain horizontal flight at a height equal to or greater than the span of the aircraft, i.e. out of ground effect, is no greater than the cruising power output of a man, we would come to Performance Level 3. This performance looks feasible today for a limited number of pilots. If it can be accomplished, the takeoff problem will be automatically solved, since the power necessary for horizontal flight at ground level will be lower than that for cruising out of ground effect; the pilot will be able to take off without using up his reserves and climb to a height equal to the span, where he can continue to fly for several hours.

Some hold the view that only flight with unassisted takeoff should be considered as man-powered flight. However, if that part of a flight which is directly attributable to stored energy or other assistance is checked in a reliable way and deducted from the whole distance flown, there can be no reason why the remainder should not be considered as a man-powered flight. It seems to be unreasonable to limit a man-powered aircraft to short-time flights by a premature requirement that it should take off under direct pilot-power, when man-powered flights lasting for a respectable time could be made with assisted takeoff as described. During a takeoff run, the pilot would use a great part of his reserve energy, limiting his time of actual flight, whereas, with assisted takeoff, he would fly on cruising power alone. Takeoff under direct pilot-power will come into its own as soon as it is possible to fly at cruising power without ground effect.

Performance Level 4

If it were feasible to fulfill strength and weight requirements for a combination of soaring and man-powered flight, then we would get Performance Level 4 for unrestricted flights. To perform at this level a glide ratio of 1:75 with man-power should be considered as a minimum.

MAN-POWER

I made my first tests on available man-power, with cyclists in 1933. The cyclist to be tested had to pull a second cyclist of the same weight and in the same attitude and position, giving the same conditions for both (Figure 8). The second cyclist did no work and had only to watch a scale indicating the tension in the connecting cable. A rubber damper was included in the connection, to absorb shocks caused by roughness of the road. A third person with a stop watch checked the time taken to cover a measured distance. Since the power used to pull the second cyclist was equal to the power to move the first, the total power output was twice the amount shown by the scale and stop watch. The whole setup was simple and worked very satisfactorily.

Finding a pilot

I tested first myself, then some friends, then every available member of my gliding club, and the results were discouraging for use in man-powered flight. Then I went to a camp of professional racing cyclists; and that made ends meet. I found a fellow who was willing to work with me, who developed a power output of 1.3 hp for 30 seconds. I made arrangements with my gliding club that this man should be taught to fly as quickly as possible. When I started designing the aircraft for him, I laid it out in such a way that I would get as wide a power margin as possible, to allow for still unknown losses. I realize now how near I was, theoretically, to achieving flights up to 5 minutes with this design and this cyclist.

The first difficulty came when I filed an entry for the competition and the committee insisted that the accumulator for takeoff power should be carried in the aircraft; this meant an additional weight of 20 lb. I had to decide whether to drop the project altogether or to add the weight, which would make the chances of complete success very marginal. Success meant not the fulfillment of the requirements of the competition – this could not be done – but rather the achievement of the first horizontal flight by man-power; time and distance were of secondary importance. Here my friend, Franz Villinger, came to my assistance and we decided to continue together. All the work was done at night and on week-ends.

When the aircraft began to take shape, I found out that our pilot was not making sufficient progress with his flying lessons; as a professional cyclist, he was more interested in cycling than in flying and, because of his profession, he was out of town most of the time. Finally I had to look for another pilot with gliding experience. Since I could not find the right man in my own club, I went to other clubs and eventually settled on a Mr. Duennebeil. His power output was far too low for our purpose (60% of the professional cyclist) but he was the best man available. It was he who made the first man-powered flight at Frankfurt in 1935. The fact that we were able to do this even with this low level of power output proves that the design was based on reliable data, though in his Mitchell Memorial Lecture at Southampton[4] Mr. B. S. Shenstone is reported as saying "The Haessler-Villinger design . . . was based on quite false data on

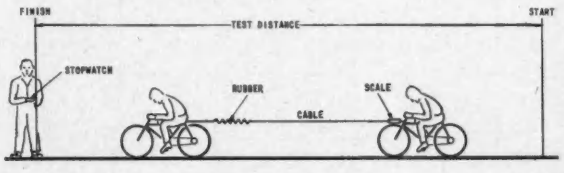

Figure 8
Power test with cyclists

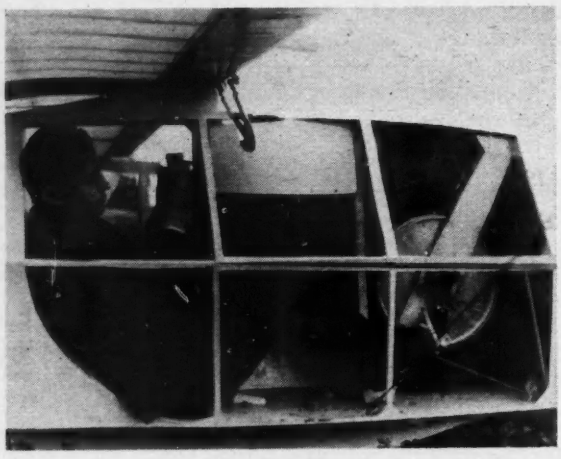

Figure 9

the power a man could produce", without any supporting figures. After the first flight we started testing again, in search of a better man. Since the glider pilots did not look promising and the professional cyclists were too hard to get, we looked for amateur racing cyclists in different towns and selected a Mr. Hofmann as our next pilot. His power output was about halfway between those of Duennebeil and our first professional. Hofmann was unemployed at this time and we sent him to a flying school at our expense; then we looked for a job for him in Dessau, where Villinger and I were living.

Altogether we tested about 50 cyclists. In the first year, we ran our tests from 20 seconds to 40 seconds, but in the next year we extended them up to 5 minutes. Our discovery of the sharp power drop in the first few minutes was discussed with Mr. Ursinus and he arranged to carry out some further tests in the "Muskelflug Institute" which he had founded in 1935.

At the time of our first man-powered flights, doubts were expressed about our pilot seating arrangement and many considered the rowing movement to be more efficient than cycling. Mr. Ursinus investigated the different types of possible movements and seating arrangements and concluded that the rowing movement was less efficient than cycling and that our seating arrangement was superior both to the normal bicycle arrangement and to a prone position of the pilot. In addition, the position of the pilot in our aircraft was unique in not requiring the pilot to use his hands to balance himself, so that no reaction loads due to balancing were conducted into the control system (Figure 9).

Mr. Ursinus also found out that a combination of cycling with the legs and hand-cranking gave a significantly higher power output for periods of less than 2 minutes.

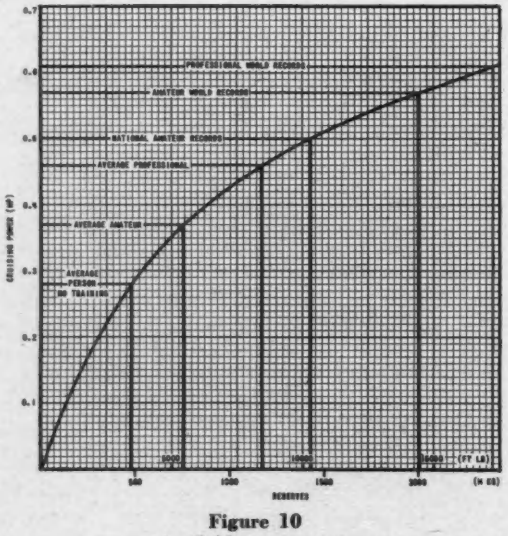

Figure 10
Available man-power

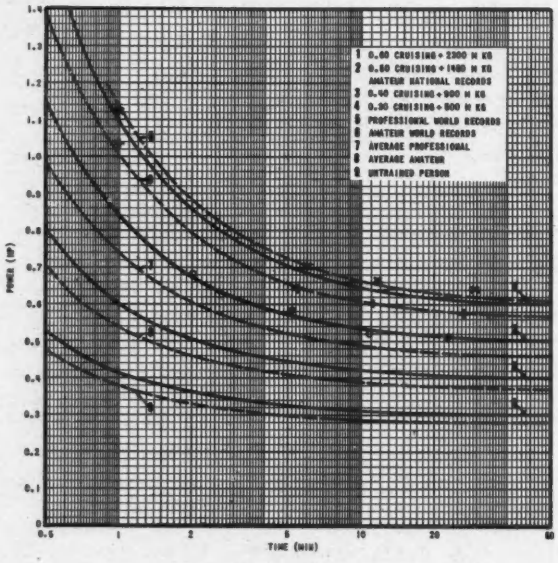

Figure 11
Available man-power

Summing up my own results, I found that, according to his state of training, every person has a certain cruising power level where oxygen exchange is balanced and no reserves are used up. For a professional cyclist, the energy reserves of the body, above cruising power, are of the order of 1100 m kg or 8000 ft lb and his cruising power is about 0.46 hp; a trained amateur cyclist has a cruising power of 0.37 hp and an average cyclist about 0.28 hp. This refers to an average pilot weighing 65 kg. I was the first to publish these figures, in 1937[5].

Cruising power and reserve energy

The energy reserves above cruising power level can be used at different short-time power levels (Figure 6). The envelope of these short-time power levels is a hyperbola. When a cyclist has maintained a certain level of power output until it reaches this envelope, he is exhausted and has to relax; he cannot continue following the envelope line; his power output drops sharply and then, as his oxygen level is restored, it returns gradually to cruising power level. In flights of less than 5 minutes this recovery would not be possible before the aircraft had lost height and

AVAILABLE MANPOWER FOR PILOT - WEIGHT 143 LB (65 KG)						
LEVEL OF TRAINING	POWER FOR MINUTES (HP)					
	1	2	5	10	20	60
UNTRAINED AVERAGE	0.38	0.33	0.30	0.29	0.28	0.28
AMATEUR RACER	0.55	0.46	0.41	0.39	0.38	0.37
PROFESSIONAL RACER	0.79	0.60	0.52	0.48	0.47	0.46
RECORD NATIONAL AMATEUR	0.83	0.67	0.57	0.53	0.51	0.50
RECORD WORLD AMATEUR	1.03	0.80	0.66	0.61	0.59	0.57
RECORD WORLD PROFESSIONAL	1.16	0.89	0.72	0.66	0.63	0.61

Figure 12

landed. The recovery line is difficult to establish, but experience shows the trend.

At the beginning, I did not know the nature of this power decay and, when I found that the power drop in the first two or three minutes was greater than expected, the tests with the two cyclists were extended up to 5 minutes. Beyond 5 minutes the recording of the tension in the tow cable became less and less reliable and I had to extrapolate the results to one hour after repeated tests to establish the reliability of the figures below 5 minutes.

Mr. Nonweiler has given the power used by cyclists in establishing national and world records[6]. In Figure 10 I have plotted cruising power against energy reserves from zero to world record performance. The results show a close relationship between these two factors so that it is now possible to calculate the power decay against time for each cruising power level (Figures 11 and 12). To find the performance of a cyclist, only one test of over 1 minute is necessary, and the power decay against time can then be read from the graph.

Figure 13 shows available cruising power against weight of cyclist. This is based on the experience that persons weighing about 140 lb have the best power/weight ratio. Above and below this weight this ratio becomes less favourable.

All the tests referred to were done with cyclists. The efficiency of the chain drive of the bicycle was not checked and separated from the results, so that the actual man-power was in fact higher than indicated, by the amount of the frictional losses. This must be borne in mind when calculating the efficiency of an aircraft drive system.

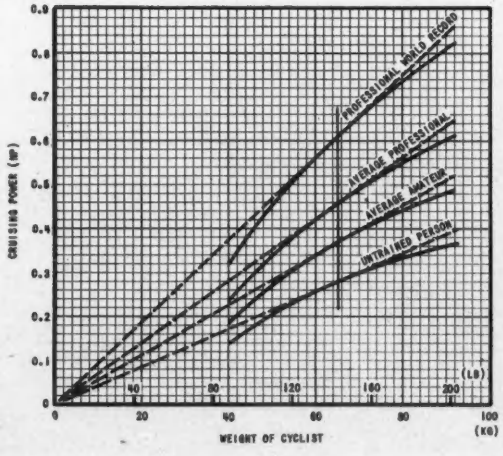

Figure 13
Power/weight ratio for cyclists

EFFICIENCY OF THE PROPULSION SYSTEM

I want here to comment upon a remark attributed to Mr. Shenstone, in his Henson and Springfellow Lecture entitled *Man-powered Flight*[7], that the power transmission in the Haessler-Villinger aircraft was inefficient because it incorporated a belt drive. He claimed that a chain drive would be more efficient, were it not for the twist in the chain necessitated by the two axes of the power drive having to be arranged at right angles to each other (Figure 14).

The efficiency of belt drives depends in the first place on the desired lifetime of the belt. When a belt is to be used for 40 hours a week in commercial work, it should have a lifetime of several months without

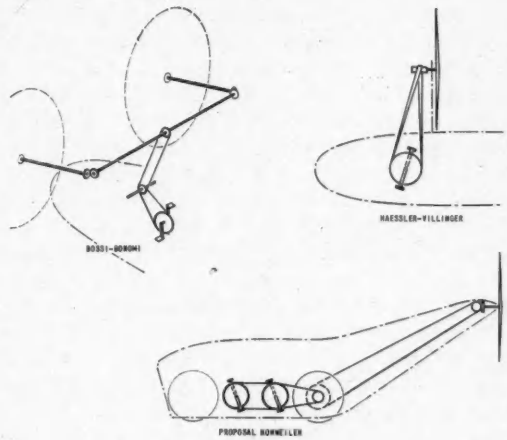

Figure 14
Propulsion systems

maintenance. The materials used to meet this requirement are limited in flexibility and give efficiency coefficients below those of a straight chain drive. In a drive for a man-powered aircraft conditions are quite different; its life is counted in minutes and it is under constant maintenance. We tried to find a material with the highest flexibility and good surface friction, and were not interested in long life. First we tested all available commercial belt materials, none of which were satisfactory. Then we started to develop our own, using fabric belting of different gauges, different widths and different types of weaving, which we rubberized with a special solution to get less slip and better contact with the pulley. The pulleys were covered with a layer of rubber on a metal base. In this way we evolved a belt drive of an efficiency better than that of a straight chain drive. The only trouble we experienced was stretching after several flights, due to the fabric base being made of a natural fibre. We changed the belt after every six flights. Today materials like nylon would make this unnecessary.

The efficiency of the propulsion system of our aircraft has been unjustly criticized and in defence I

		HAESSLER - VILLINGER		BOSSI - BONOMI		PROP. NONWEILER	
WEIGHT PROPULSION SYSTEM	DIRECT WEIGHT (LB)	4.0		25.0		25.0	
	INDIRECT WEIGHT (LB)	3.2		20.0		18.0*	
	TOTAL (LB)	7.2		64.4		83.0	
	POWER REQ'D (0.005 HP/LB)	0.036		0.322		0.415	
		EFFICIENCY	LOSS (%)	EFFICIENCY	LOSS (%)	EFFICIENCY	LOSS (%)
EFFICIENCY SHORT DURATION (1.0 HP)	PROPELLER	0.82	18.0	0.87	13.0	0.88	12.0
	POWER DRIVE ∮	1.00	0	0.94	6.0	0.94	6.0
	WEIGHT		3.6		32.2		20.8**
	TOTAL	0.786	21.6	0.488	51.2	0.612	38.8
EFFICIENCY LONG DURATION (0.5 HP)	PROPELLER	0.82	18.0	0.87	13.0	0.88	12.0
	POWER DRIVE ∮	1.00	0	0.94	6.0	0.94	6.0
	WEIGHT		7.2		64.4		41.6***
	TOTAL	0.748	25.2	0.186	83.4	0.404	59.6

* INCLUDES 80% FIN WEIGHT (20 LB)
** LOSS RELATED TO 2 HP (2 SEATER)
*** LOSS RELATED TO 1 HP (2 SEATER)
∮ EFFICIENCY OF BICYCLE CHAIN DRIVE ASSUMED 1.00

Figure 15
Efficiency of propulsion systems

would compare our arrangement with the unconventional systems of the Bossi-Bonomi aircraft and the Nonweiler proposal.

To determine the total efficiency of a propulsion system we must consider not only propeller efficiency and frictional losses in the drive system (for which only the part above the level of the losses in a bicycle are significant) but also the power necessary to keep the propulsion system aloft; this amounts to about 0.005 hp/lb. We should not overlook the fact that the propulsion system is not a part of the structure of the airframe and, to support and accommodate it, the structural weight of the aircraft is increased by some 80% of the weight of the propulsion system itself. We will call this part the indirect weight of the propulsion system. This weight factor is so important that, if we are to fly at cruising power, the direct weight of the propulsion system, comprising the whole drive system, bearings, fittings, fillers, doublers and propeller should be limited to 6 lb, since the loss due to the combined weight, direct and indirect, should not exceed 10% of the power available.

At 1 hp the total efficiency of the Haessler-Villinger drive system was 78%, compared with 49% for the Bossi-Bonomi system (Figures 15 and 16). At cruising power (0.5 hp), we get for the Haessler-Villinger 75% and for the Bossi-Bonomi 17%. In the latter the power loss due to weight alone amounts to 64%, compared with 7% for the Haessler-Villinger. This shows clearly that the influence of the weight of the propulsion system can easily offset any efforts to increase propeller efficiency.

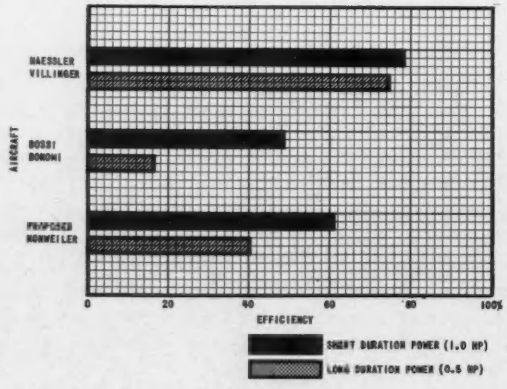

Figure 16
Total efficiency of propulsion systems

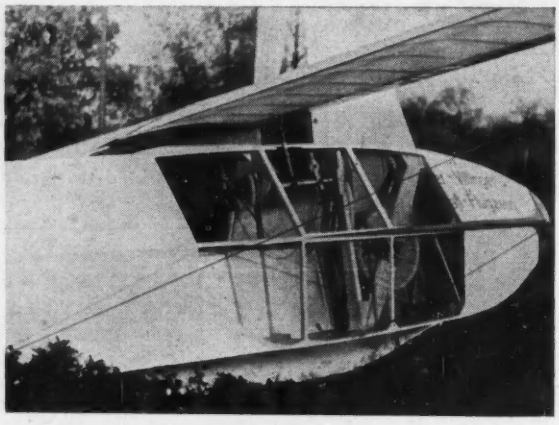

Figure 17

CONTROLS

In controlling a man-powered aircraft the feet, which normally move the rudder, cannot be used for this purpose. In the Haessler-Villinger aircraft, movements of the control wheel were normal for longitudinal and lateral control. For moving the rudder, the wheel rotated about a vertical axis (Figure 17). After some training this arrangement did not cause any trouble to the pilot.

To save weight, we did not use the conventional control surfaces for lateral and longitudinal control. For lateral control, the angle of incidence of the two halves of the wing could be changed differentially in opposite directions and, for longitudinal control, the angle of incidence was changed symmetrically. The stabilizer was fixed.

This arrangement was used in the first year of our experiments. Lateral control was satisfactory as long as the aircraft did not get into extreme positions; there is a danger of unsymmetrical stall and I would not use this device again. Longitudinal control was not satisfactory; it caused over-controlled takeoffs, with too steep climbs and consequent loss of speed, and resulted in some hard landings and repairs. In the second year we changed back to a normal stabilizer and elevator arrangement with far better results. At the same time the size of the rudder was increased.

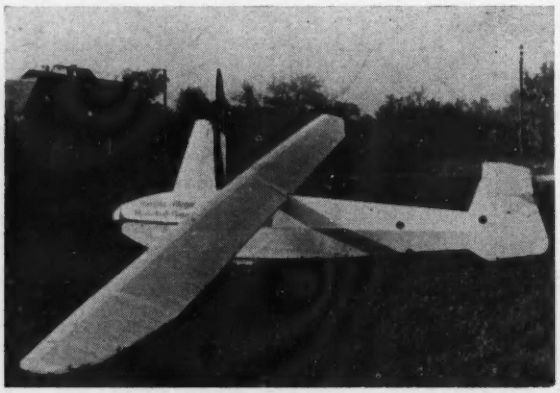

Figure 18
Control surfaces — 1935

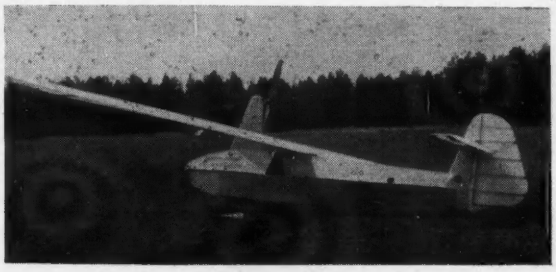

Figure 19
Control surfaces — 1936

The difference in the tailplane design and rudder arrangement in 1935 and 1936 can be seen in Figures 18 and 19.

The use of spoilers for lateral control, as used on the Bossi-Bonomi aircraft, cannot be recommended, since the response of the aircraft to control movements is too slow.

As a result of these experiences, I think that the control system of a man-powered aircraft should be completely conventional. Any deviation will cause delays arising from incorrect takeoffs, damage from hard landings, changes found necessary from flying experience and so on.

WEIGHT OF THE HAESSLER-VILLINGER AIRCRAFT

Many designers assume that the natural way to achieve minimum weight in a man-powered aircraft would be to reduce the strength – which seems to be justifiable in this special case, since no flying would be done at heights greater than 50 ft. When we designed the Haessler-Villinger aircraft, we started out with an ultimate load factor of 2.5. A check of the wing deflections, however, showed that the strength in bending had to be increased until deflections could be considered normal. In this way we ended up with an ultimate load factor of about 6.

We placed a restriction on diving speed to limit the torsion loads. Takeoff and landing loads could not be reduced. Our aircraft was only a quarter of the weight of a similar sailplane but still had almost full strength (Figures 20 and 21).

The rough breakdown in Table 2 indicates how the weight goes down when a sailplane design is converted to suit the conditions of man-powered flight.

It is important to stress every part of the aircraft carefully and keep a strict weight control during design and actual building (Figures 22 and 23).

Some pounds can be saved by selecting materials of lower specific weight and gauges below usual limits.

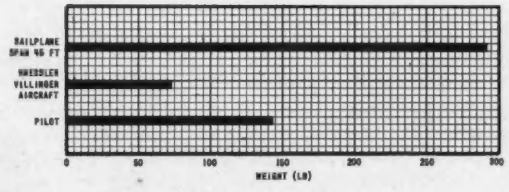

Figure 20
Weight comparison

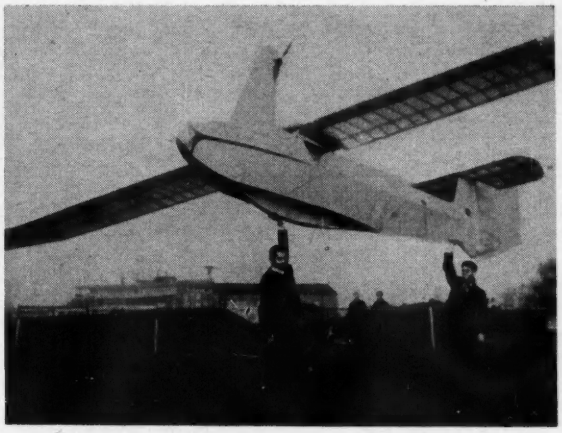

Figure 21

Instead of using birch plywood with a minimum gauge of 0.8 mm (0.032 in), on many parts we used cedar plywood with lower specific weight and a minimum gauge of 0.6 mm (0.024 in). For covering the wing and tail surfaces, we used silk with a special type of impregnation. The weight of the fabric covering after impregnating was 160 gr/sq m, compared with the normal 300 gr/sq m on sailplanes. Special care has to be taken with the use of paints, lacquer and dope. No brush should be used, only spraying by a skilled painter.

With reduction of cross-sections to a minimum the usual methods of gluing cannot be used. Special supports have to be made for use during the gluing process, so that clamping pressures can be safely applied, and the weight of these supports and clamps must itself be supported, since it cannot be carried by the airplane structure.

The fuselage was covered with 0.6 mm cedar plywood to give a sufficiently stiff structure. Plywood gauges around the pilot's seat and skidbox were normal. At first we thought to save weight with a fabric-covered fuselage, but calculations of deflections soon showed the advantages of the plywood covering without sacrificing weight.

TABLE 2
SCHEME FOR REDUCTION OF A/C WEIGHT TO MINIMUM

Sailplane single-seater with cantilever wing of 13.5m span		150 kg
1) Remove instruments	10 kg	
2) Reduce payload from 110 to 65 kg (Diff. payload = 41% at a rate of 0.8 = 33%)	46 kg	
3) Convert cantilever wing to one with wire bracing	19 kg	
4) Reduce wing area to min weight/span	10 kg	
5) Limit diving speed	5 kg	
6) Limit ability to withstand handling for parts with low stress	15 kg	105 kg
		45 kg
7) Co-ordinate all factors in original min layout		10 kg
Weight of man-powered aircraft		35 kg

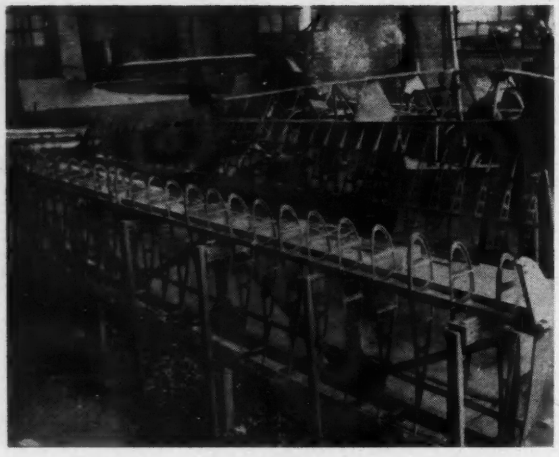

Figure 22

Aerodynamic efficiency

In his lecture mentioned above[7], Mr. Shenstone is reported to have criticized the Haessler-Villinger aircraft as aerodynamically inefficient. Since our aircraft with 13.5 m span had a glide ratio of 1:24, better than other sailplanes of the same span, and a sinking speed of 0.52 m/sec, which is below that of any comparable sailplane even today, I cannot see the grounds for this assertion. Probably the unusual wing design, with wire bracing, does not fit the normal concept of an aerodynamically efficient aircraft. The drag of the bracing wires was 3.5% of the whole drag, demanding 3.5% of the whole power. With 0.9 hp total, this amounted to 0.031 hp. This power requirement could be offset by a weight saving of 6.2 lb, since the power requirement to keep 1 lb aloft with this aircraft was 0.005 hp, and the actual weight saving with our wing design, in comparison with a similar cantilever wing, was of the order of 30 lb. Thus we effected a saving of 17% of the available power and demonstrated the superiority of a braced wing over a cantilever wing.

Our aspect ratio was 18.8. In modern sailplanes the limit for the aspect ratio of cantilever wings is about 20. Man-powered aircraft will have to go to aspect ratios of 30 and over and this will not be feasible with any cantilever wing; we shall have to resort to other arrangements.

Figure 23

Table 3 gives the weights for the main components of the Haessler-Villinger aircraft, which will be used as a basis for the calculations that follow.

LIST OF SYMBOLS

P = Required power – hp
W = Weight – kg or lb
V_{sink} = Sinking speed – m/sec or ft/sec
η = Efficiency of propulsion system
b = Span – m or ft
λ = Aspect ratio
C_D = Drag coefficient
C_L = Lift coefficient
D_i = Induced drag
L = Lift
Q = Dynamic pressure
S = Wing area – sq m or sq ft

POWER, WEIGHT AND SPAN

After taking stock, I will now try to demonstrate what we can expect today of a new man-powered aircraft. Since in man-powered flight the available power is a minimum, we will have to search for an aircraft where the required power becomes a minimum.

TABLE 3

WEIGHT BREAKDOWN OF THE HAESSLER-VILLINGER AIRCRAFT

1) Wing			
a) Main Spar			
Spar caps	2.910 kg		
Spar web	1.115		
Uprights & fillers	0.456	4.481 kg	
b) Rear Spar			
Spar cap	0.325		
Web	0.471	0.796	
c) D-Nose skin	4.850	4.850	
d) Etc.			
Trailing edge	0.465		
Tip edge	0.100		
Qty 70 Main ribs 50 gr	3.500		
Qty 60 Skin stiffeners 15 gr	0.900		
14.3 sq m Impregnated fabric covering	2.280		
Fittings	0.400		
Lacquer & glue	1.238	8.883	19.010 kg
2) Fuselage			
Frame 1	0.045		
" 2	0.150		
" 3	0.250		
" 4	0.593		
" 5	0.327		
" 6	0.280		
" 7	0.220		
" 8	0.180		
" 9	0.140		
" 10	0.120		
" 11	0.110		
" 12	0.085	2.500	
Longerons	2.520	2.520	
Skid	0.600		
Skidbox—Skin	0.900		
Skidbox—Formers	0.160		
Seat & Floor	0.800	2.460	
Outer-skin 0.6 mm plywood	2.800	2.800	10.280 kg
3) Empennage		4.000	
4) Controls in fuselage		0.500	
5) Wire bracing		0.600	5.100 kg
EMPTY WEIGHT OF AIRCRAFT			34.380 kg

Empty weight	34.380 kg
Propulsion system	2.000 kg
Energy accumulator (Rubber bungee = 7.00 kg)	9.700 kg
Weight of aircraft	46.080 kg
Pilot	65.000 kg
TOTAL WEIGHT	111.080 kg

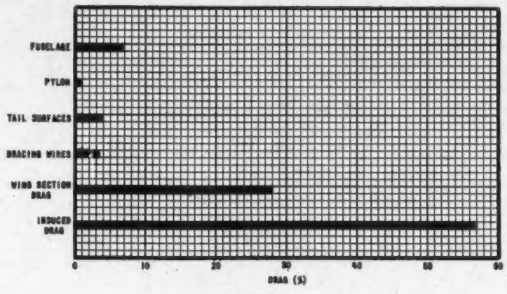

Figure 24
Drag breakdown — Haessler-Villinger aircraft

The power required for horizontal flight is –

$$P = \frac{W\,V_{sink}}{75\eta} \text{ m kg/sec} \quad \text{or} \quad \frac{W\,V_{sink}}{550\eta} \text{ ft lb/sec} \qquad (1)$$

The efficiency of the propulsion system, η, was discussed earlier. We will now have a closer look at the factors which affect the sinking speed –

$$V_{sink} = 4\sqrt{W/b^2}\,\sqrt{\lambda}\,C_{D_{tot}}/C_L^{1.5} \text{ m/sec}$$
$$\text{or } 29\sqrt{W/b^2}\,\sqrt{\lambda}\,C_{D_{tot}}/C_L^{1.5} \text{ ft/sec} \qquad (2)$$

at sea level.

W/b^2 is known as the span loading and is the main factor affecting the sinking speed. λ in the formula calls for low aspect ratios. And the last element, $C_{Dtot}/C_L^{1.5}$, requires the total drag of the aircraft to be as small as possible and the lift near the stalling value.

Since $\lambda = b^2/S$, one could write $\sqrt{W/b^2}\,\sqrt{\lambda}$ as $\sqrt{W/b^2}\,\sqrt{b^2/S}$ i.e. $\sqrt{W/S}$, indicating the primary importance of low wing loading. This misled several designers of man-powered aircraft into building wings of tremendous areas, which resulted in the aircraft becoming too heavy (1930 Zaschka aircraft – 475 sq ft; Bossi-Bonomi – 226 sq ft; Haessler-Villinger – 107 sq ft).

This sinking speed formula contains about every possible factor affecting the performance of the aircraft and the examination of each to find the design with minimum power requirements is a very time consuming business.

Many possible ways of achieving aerodynamic improvements have been discussed in other papers on man-powered aircraft. I will try to approach the power problem in another way. We have to decide which factors have the greatest influence on performance, so that we can concentrate on them; all other factors must be packed into one constant and the upper and lower limits of this constant considered in the light of existing experience.

When we take a look at Figure 24 showing the relative sizes of the different components of the total drag of the Haessler-Villinger aircraft, we see that the induced drag is 57% of the total. Reduction of the induced drag is the greatest problem in designing a man-powered aircraft. The profile drag is of next importance, but presents no design problem provided we confine ourselves to airfoils already used on modern sailplanes, the drag coefficients of which are well established. All other components of the total drag are so small that any improvement in this area will have a negligible effect on the performance of the aircraft. The induced drag is

$$D_i = \frac{L^2}{Q\pi b^2} = \frac{W^2}{Q\pi b^2} \text{ kg} \qquad (3)$$

Since the lift equals the weight, we see the importance of weight and span.

Figure 25 shows the span loading against sinking speed for a random assortment of well known gliders. The upper and lower limits of these values give lines going to zero in the shape of a parabola. For these lines we can now write

$$V_{sink} = \begin{matrix}0.66\\0.59\end{matrix}\sqrt{\frac{W}{b^2}} \text{ m/sec} \qquad (4)$$

This formula will give reliable results provided the design approximates to the conventional shape of gliders. Final performance calculations will have to be done in the usual way.

Using this formula, Eq. (1) giving the power necessary for horizontal flight can be written

$$P = \begin{matrix}0.0089\\0.0078\end{matrix}\frac{W\sqrt{W}}{b}\frac{1}{\eta} \quad \text{or} \quad \frac{c}{\eta}\frac{W\sqrt{W}}{b} \text{ hp} \qquad (5)$$

(For the Haessler-Villinger $c = 0.0089$: for Proposal H4 $c = 0.0078$ metric).

This formula shows that the main problem is to design a wing of maximum span and minimum weight. All other points are of secondary importance. That means that designing a man-powered aircraft is strictly a structural problem and not an aerodynamic one. Of course, the aerodynamic design has to be of a high order but it must not interfere with the weight problem. It is not necessary to break fresh ground

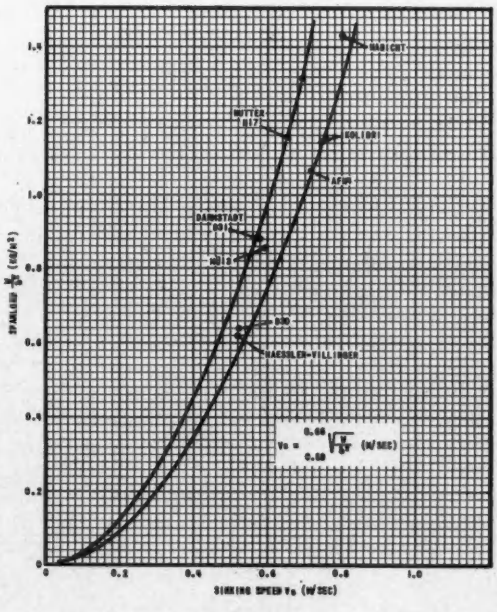

Figure 25

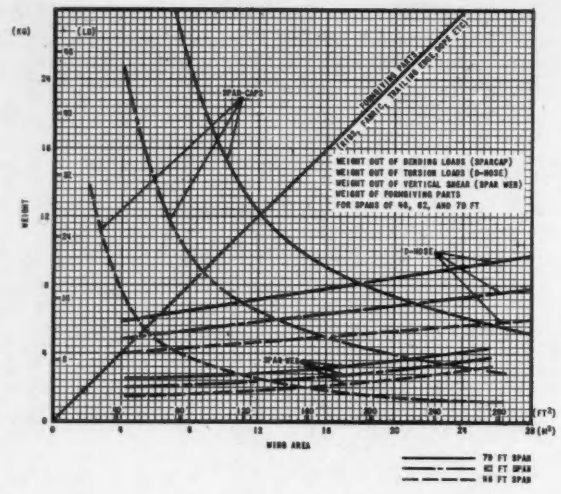

Figure 26

in aerodynamics: on the other hand, on the structural side, new design techniques will have to be used.

WING WITH MINIMUM WEIGHT

Now we will try to find the wing having minimum weight, for a given span and a given load. I will use the actual weights of the Haessler-Villinger aircraft as a basis and calculate the changes in weight for a range of wing areas from 4 to 28 sq m (40 to 300 sq ft) and for three different spans. In Figure 26 the weight of the bending material is plotted against wing area for spans of 46, 62, and 79 ft. For a given airfoil section, increase in wing area results in corresponding increase in wing thickness and consequently the weight of the bending material goes down; and vice versa.

In the graph showing the weight of the spar web, we see the influence of span. Theoretically, for a given span and a given load, the weight of the web should not change with changing spar depth (i.e. wing thickness), but in practice changes arise from limit gauges of materials and the changing weight of the necessary stiffening.

In the graph showing the weight of the D-nose, which handles the torsion loads, the influence of limit gauges and increasing stiffening requirements with increasing wing area is also apparent.

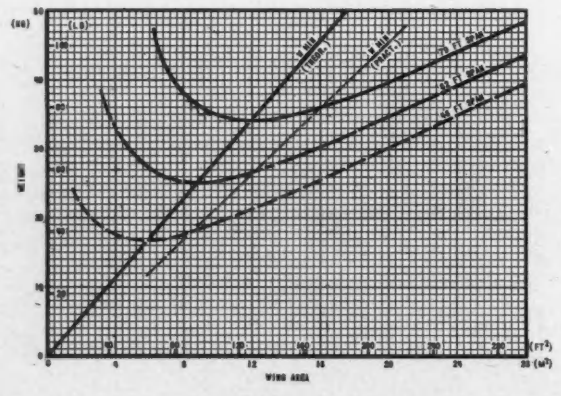

Figure 27
Wing weight against area for a single seater

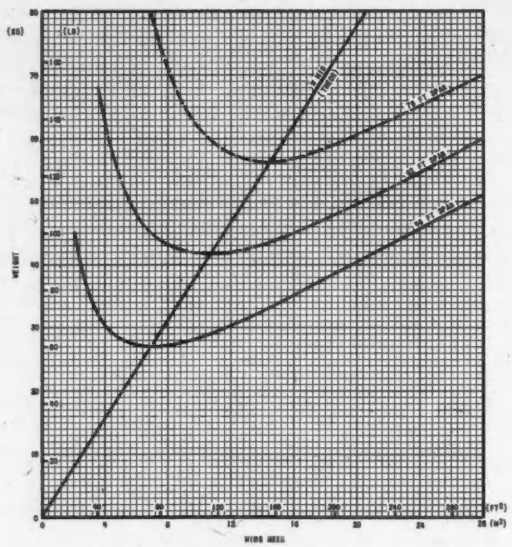

Figure 28
Wing weight against area for a two seater

The total weight for all other parts of the wing of the Haessler-Villinger aircraft, such as ribs, trailing edge, fabric covering etc, amounted to 0.21 lb/sq ft (1 kg/sq m) of wing area, and this figure is assumed to be unaffected by changing area.

When we add the weight of these four structural groups together we can plot the weight of the wing against wing area for the three chosen spans (Figure 27). Each curve has a clearly marked minimum, which lies on a straight line going to zero. This gives the theoretical minimum weight of wing at each span. For a practical design, I would choose a point at a greater wing area, say, on the dotted line. The weight difference would be small and, since the aspect ratio of the theoretical minimum is very high and accordingly gives high deflections, a wing at the dotted line, with lower aspect ratio, would be stiffer. The

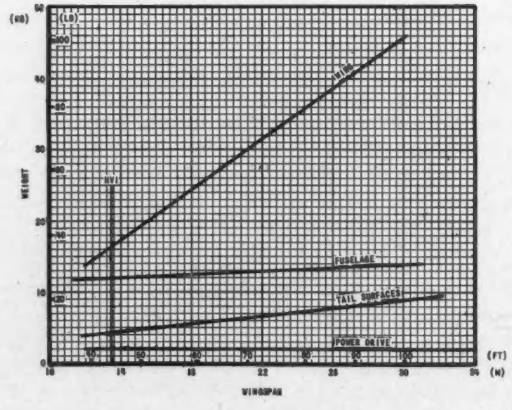

Figure 29
Weight of wing, fuselage, tailsurface and power drive for a single seater

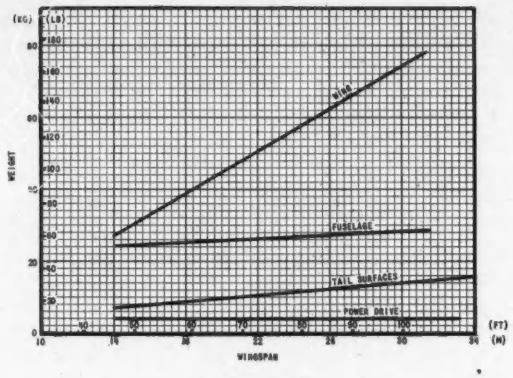

Figure 30
Weight of wing, fuselage, tailsurface and power drive for a two seater

best compromise, to locate this point for an actual wing, can only be determined by calculation of deflections. A wing of 14 m span would certainly be satisfactory and the Haessler-Villinger wing had such dimensions.

In Figure 28, I have repeated this process for the higher wing loading of a two seater aircraft. In this case, the theoretical minimum weights occur at slightly greater wing areas than in the first case, but not in proportion to the increased loads. The minimum weight of the two seater wing of 24 m span exceeds the minimum weight of the single seater wing by only 65%.

AIRCRAFT WITH MINIMUM WEIGHT AND ITS PERFORMANCE

Having found the optimum weight for a wing of given span, we can now draw a graph combining these results with the weights of the other components of the aircraft (Figures 29 and 30). The weights of the Haessler-Villinger aircraft will again serve as a basis, at 13.5 m span. The weight of the tail surfaces goes up in the same way as the wing. The propulsion system is not affected by the span and stays constant. The length of the fuselage changes with increasing span and this adds slightly to its weight. Adding up the weights of these components we can get, as the final result, the minimum weight of the whole aircraft for any given span, for the single seater and the two seater. For the 14 m span in each case, the two seater is heavier by 85%; for 30 m span a two seater would be heavier by only 71% of the single seater.

I have shown the above results in Figure 31 and drawn lines indicating the empty weight against payload for spans from 40 to 100 ft; these will be useful later for checking other cases.

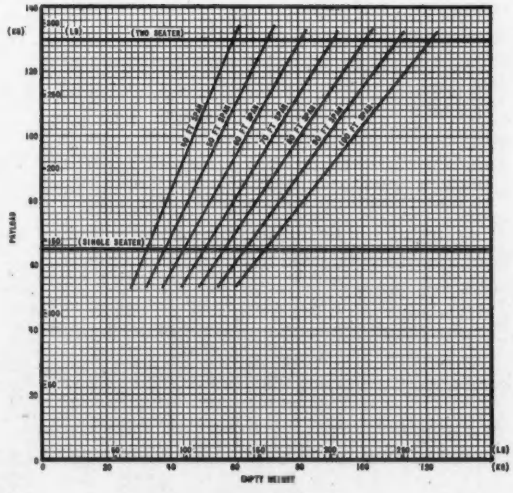

Figure 31
Minimum empty weight against payload for spans of 40 ft to 100 ft (wing with bracing wires)

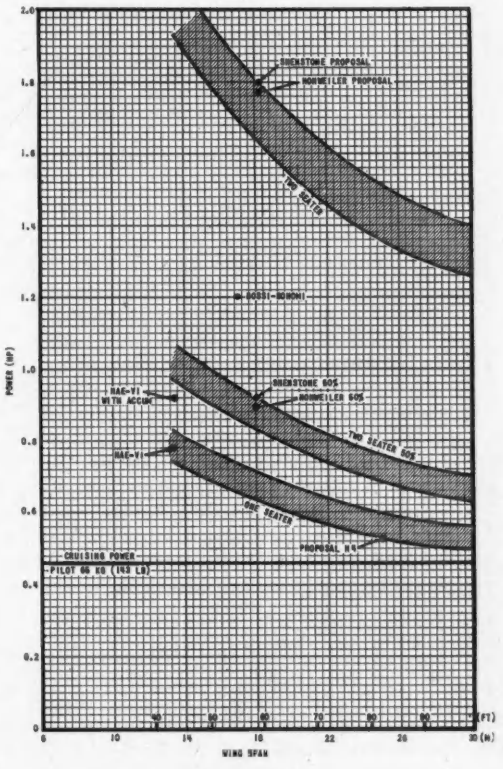

Figure 32
Required man-power against span

Now we can calculate by Eq. (1) the required power for horizontal flight at any given weight and span. The results for both the single and two seater are shown in Figure 32. For better comparison between single and two seater, I have added a curve showing the 50% power requirement of the two seater, which should correspond to the full power requirement of the single seater if performances were equal. This graph indicates clearly the superiority of the single seater, since in a two seater the power requirement for each man is 30% higher. This is again in conflict with Mr. Shenstone who is reported[7] to have said that the Haessler-Villinger aircraft failed to achieve better results, because being a single seater the optimum power was not available – the optimum size of crew is considerably more than one.

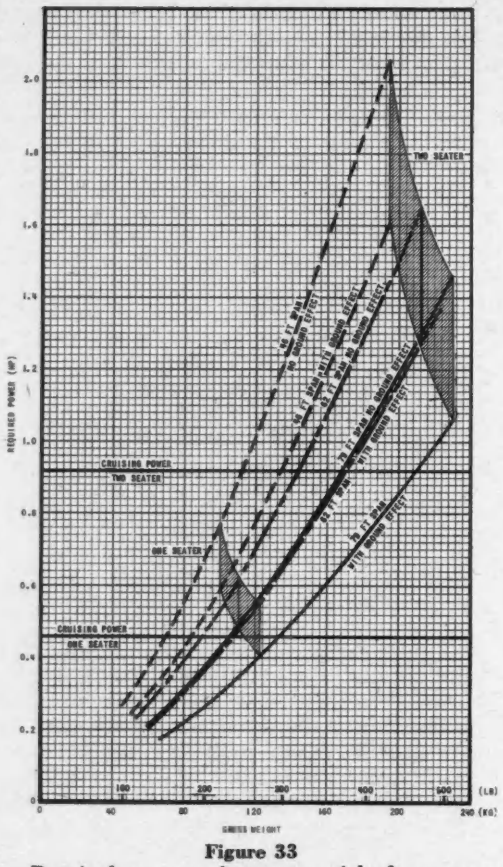

Figure 33
Required power against gross weight for a one and two seater

The point is borne out by Figure 33, which shows the relationship between required power and gross weight. Since the required power is proportional to the 1.5th power of the weight, only the lightest single seater structure has scope for future development. This does not mean that flying a two seater would not be possible. By using short-time power, flights could be achieved in a two seater up to 1.5 minutes, even without takeoff assistance. Under the same conditions, long-time flights of 1 hour could be made in a single seater, by using ground effect, as indicated in the graph.

Since the level of the required power is directly related to the time for which this power is available, we are now able to plot possible flying time against gross weight (Figure 34). As a basis for this calculation I have used the power of a professional racing cyclist weighing 65 kg, having a cruising power of 0.46 hp and reserve energy of 1100 m kg. Although the Haessler-Villinger aircraft is shown on the graph as having a possible flying time of 2 minutes with ground effect – when we actually achieved only 1 minute – it must be remembered that we did not actually use a pilot of this power level. If the aircraft could have been built without the weight penalty of the energy accumulator, the possible flying time with the professional cyclist would have gone up to 5 minutes. On the other hand, for the Bossi-Bonomi aircraft on the same power basis we get a possible horizontal flying time of 38 seconds with ground effect (assuming the same efficiency of the power drive).

It would be helpful in giving a clearer picture of the actual quality of an aircraft if other authors would use the same "standard pilot" as a basis for comparison.

The Haessler-Villinger aircraft, without the weight of the energy accumulator, had a performance similar to our calculated aircraft of 46 ft span. The aircraft of 62 ft span has a possible flying time of 1.5 minutes without ground effect and could make long-time flights of over 1 hour with ground effect at a height of 10 ft. The aircraft of 79 ft span would be capable of a flight of 2.2 minutes without ground effect, and a flight of over 1 hour with ground effect at heights of more than 10 ft.

INFLUENCE OF PILOT WEIGHT ON AIRCRAFT PERFORMANCE

These calculations have been based on the standard pilot with a weight of 65 kg. Now we will check what influence a change in the weight of the pilot has on the performance of the aircraft. The empty weight of the aircraft differs according to the payload for which it is designed. We will assume that, for each pilot weight, an aircraft with the corresponding empty weight is available, giving us the line relating gross weight to pilot weight in Figure 35.

In Figure 36 the required power, with and without ground effect, plotted against gross weight and pilot weight, is compared with various available powers. We see that the feasibility of long-time horizontal flights is increased by selecting pilots of lower weights. If it were possible to find a professional racing cyclist weighing 120 lb, long-time flights without ground effect would be possible with aircraft weights calculated on the basis of that of the Haessler-Villinger.

Since the cruising power of national record breaking amateurs would be 10% higher, and of world record breaking professionals 30% higher than that of the average professional cyclist shown in the graph, we see that the chosen power level has little hope of attainment: the average amateur cyclist has no hope

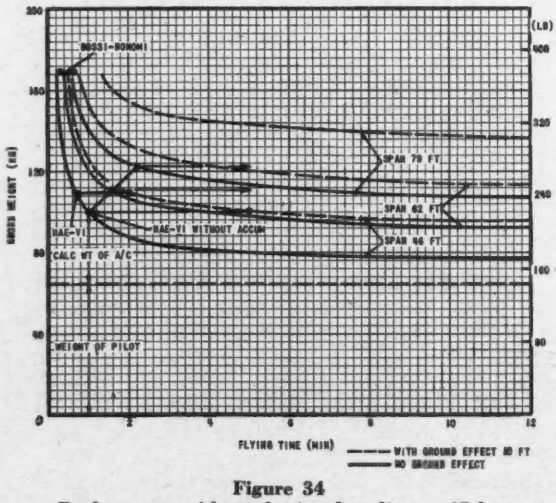

Figure 34
Performance with professional cyclist — 65 kg

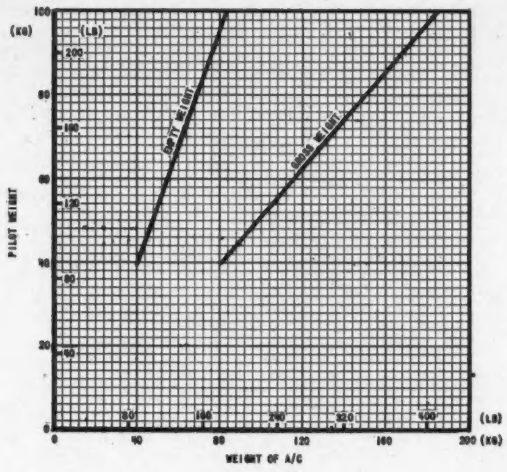

Figure 35
Pilot weight against aircraft weight for a span of 79 ft

of achieving long-time horizontal flights. The power which was available for my tests with the pilots Duennebeil and Hofmann would be insufficient even today, with better aircraft, for flights of over 5 minutes. Bossi was lucky in finding a pilot with the right power level, and with flying experience at the same time.

PROPOSAL

Having reviewed possibilities of designing a successful man-powered aircraft, we should now select a performance goal which would justify the necessary work and expense. Then the aircraft should be designed for this performance, leaving a good margin for unforeseen losses, to minimize the risk of failure.

Performance for restricted flights

This goal should be a flight of 1 hour, at cruising power, at a height equal to the span i.e. just out of ground effect. Takeoff should be unassisted, since at

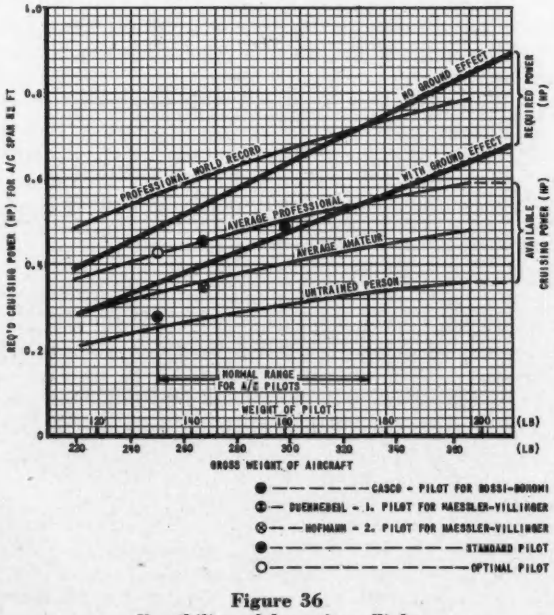

Figure 36
Feasibility of long-time flight

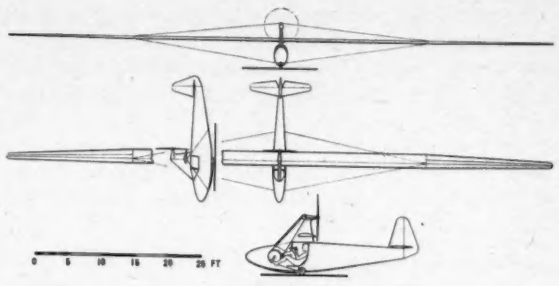

Figure 37
Man-powered aircraft — Proposal Haessler H4

ground level the ground effect helps to bridge the power gap between takeoff and ceiling height.

The lowest acceptable performance would be a flight of 1 hour, at cruising power with the ground effect, at a height of 10 ft. Takeoff could be done with limited assistance. The aircraft would have to be designed in such a way that either a skid or a power-driven wheel could be used. Testing would begin with the skid and takeoff assistance, and, when the performance has increased with training and growing experience – which could take a month or a year – to the point at which the pilot is able to get near to the ceiling height, the skid should be replaced by the power-driven wheel and the pilot can take off by himself.

If the weight of the aircraft cannot be reduced sufficiently or the pilot fails to come up to specification or both, then discarding the weight of the wheel, saving the pilot the effort of takeoff and allowing him to fly in the ground effect still makes it possible to accomplish a 1 hour flight, with these limitations.

An alternative lowest acceptable performance would be a takeoff using the power-driven wheel, the pilot using up his energy reserves in a short-time flight of less than 5 minutes. This could be accomplished at the same weight and pilot-power as the restricted 1 hour flight with ground effect.

Performance for unrestricted flights

If we want to fly an aircraft without the above-mentioned restrictions, the structure must conform to normal strength requirements for a load comprising the average pilot, parachute and instruments. However, the application of man-power might still influence the performance sufficiently to justify the attempt. If we assume that a glide ratio of 1:75, with man-power, could be considered as the lower limit for unrestricted flight, by leaving out instruments and parachute and using a professional cyclist, such an aircraft would still be able to fly, with ground effect, for 5 minutes or more in restricted flight.

It is not within the scope of this paper to speculate how a combination of soaring and man-power could improve performance. Experience will show the actual advantages and disadvantages of such a combination. Only the feasibility will be checked here.

The increase in weight to meet normal strength requirements would be small, since only the weight of the D-nose will go up for greater torsion loads. Since the weight level achieved with the Haessler-

Villinger aircraft cannot be considered as an absolute minimum, further improvements may well be possible, and we will make the assumption that, as a limit case, any increase in the weight of the D-nose can be offset by other weight savings. In the following Proposal H4, I use the already calculated weights as a basis, and show the percentage by which the weight could go up in certain areas without materially affecting the performance of the aircraft.

Specifications for Proposal H4

The dimensions of the aircraft (Figure 37) are given in Table 4.

TABLE 4
PROPOSAL H4

Span	25.00 m	82 ft
Wing area	16.75 sq m	180 sq ft
Wing loading	6.6–12.0 kg/sq m	1.35–2.44 lb/sq ft
Aspect ratio	37.3	37.3
Chord	0.67 m	26.4 in
Glide ratio	1:44	1:44
Fuselage cross-section	0.35 sq m	3.77 sq ft
Prop dia.	1.70 m	67 in
Prop eff.	0.84	0.84
Wing section	NACA 633–618	

An aircraft with these dimensions can be built for different payloads at correspondingly different empty weights. Three possible weight cases, A, B, and C, are shown in Figures 38 and 39.

Case A would be an aircraft for restricted flights with man-power only. Pilot weight would be between 132 and 141 lb and power requirements call for an average professional racing cyclist or top notch amateur. Empty weight should be between 110 and 152 lb (10% below and 17% above calculated weight). Flights could be made for 1 hour, up to heights of 60 ft at the lower weight limit and at 10 ft at the upper weight limit.

Case B is an aircraft for restricted and unrestricted flight. Without parachute and instruments a professional cyclist could fly this aircraft for 1 hour at a height of 10 ft.

An average amateur racing cyclist, with a weight between 132 and 145 lb, could fly unrestricted with parachute and instruments and improve the glide ratio to 1:90 with his cruising power and to 1:100 with 5 minute power. The empty weight of 186 lb can be 17% above the calculated weight.

Case C is the upper weight limit for the aircraft, where a glide ratio of 1:75 can still be achieved in unrestricted flight at the 5 minute power level of the average amateur. The highest acceptable weight of the empty aircraft could be 238 lb, which would be 40% above calculated weight. With 11 lb less the glide ratio of 1:75 could be held with cruising power for 1 hour.

We see that the wide range of acceptable performances allows sufficiently wide weight tolerances to enable an aircraft to be built without too much difficulty. The main factor in these wide limits is the full strength of the aircraft. In building man-powered aircraft reduction of strength does not give the hoped for weight reductions and limits the use of the aircraft. If the man-powered aircraft is to have any future, it will probably have to be built to normal strength requirements.

PROPOSAL H4
(SPAN 82FT – 25M)

CASE		WEIGHT									**CALC KG
		MINIMUM (RESTRICTED FLIGHT)			MINIMUM (UNRESTRICTED FLIGHT)			MAXIMUM			
		LB	KG		LB	KG		LB	KG		
A	PILOT	132	60					141	64		
	EMPTY WEIGHT	110	50	*–10%				152	69	*+17%	56/59
	GROSS WEIGHT	242	110					293	133		
	PERFORMANCE	ONE HOUR 60 FT HEIGHT PROF. CYCLIST						ONE HOUR 30FT HEIGHT PROF. CYCLIST			
B	PILOT	132	60		132	60		145	70		
	'CHUTE & INST				26	12		26	12		
	EMPTY WEIGHT	154	70	*+3%	154	70	*+3%	186	80	*+17%	68
	GROSS WEIGHT	286	130		312	142		357	162		
	PERFORMANCE	5 MIN – ONE HOUR WITH G.E. (10FT) PROF. CYCLIST			GLIDE RATIO 1:100 WITH AV. AMATEUR 1:75 WITH UNTRAINED PILOT						
C	PILOT				132	60		176	80		
	'CHUTE & INST				26	12		26	12		
	EMPTY WEIGHT				226	103	*+34%	238	108	*+40%	77
	GROSS WEIGHT				384	175		440	200		
	PERFORMANCE	GLIDE RATIO 1:75 AVERAGE AMATEUR									

*DIFFERENCE IN % BETWEEN WEIGHT FOR PROP #4 AND **CALC WEIGHT
**EMPTY WEIGHT CALCULATED ON BASIS OF HAESSLER-VILLINGER A/C WEIGHTS

Figure 38

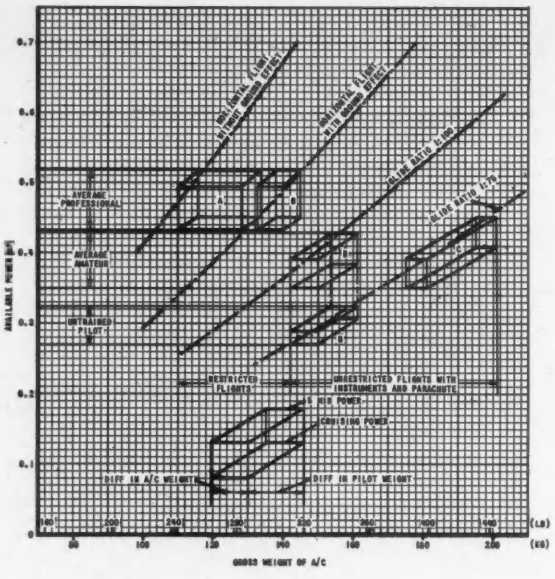

Figure 39
Performance of Proposal H4 (span of 82 ft) with cases A, B and C

REFERENCES

(1) *Kraftspeicher für Muskelflug*, FLUGSPORT, 19TH FEBRUARY, 1936.

(2) *Muskelkraft Flugzeug Bossi-Bonomi*, FLUGSPORT, 28TH APRIL, 1937.

(3) *Regulations and Conditions for the Kremer Competition*, JOURNAL OF THE ROYAL AERONAUTICAL SOCIETY, P XII, FEBRUARY, 1960.

(4) *Manpowered Flight at Southampton*, THE AEROPLANE, 16TH DECEMBER, 1960.

(5) Haessler, H. – *Muskelkraftflug*, SPORTFLIEGER, FEBRUARY, 1937.

(6) Nonweiler, T. R. F. – *The Man-Powered Aircraft*, JOURNAL OF THE ROYAL AERONAUTICAL SOCIETY, VOL. 62, NO. 574, OCTBER, 1958.

(7) *Prospects for Skycycles*, AERONAUTICS, FEBRUARY, 1959.

FALLING PROBE ELECTRON DENSITY MEASUREMENTS†

by Professor P. A. Forsyth* and A. Kavadas**

Institute of Upper Atmospheric Physics, University of Saskatchewan

One of the more fundamental measurements that can be carried out in the ionosphere is a determination of the electron content. For that part of the ionosphere that is accessible to ground based sounders, the vertical electron density profile of the undisturbed ionosphere is fairly well known. For many years regular measurements have been carried out by ionospheric sounders at stations located all over the world. Before the advent of the research rocket there remained certain ambiguities in the sounder results, but these have been resolved by means of the rocket measurements of Seddon, Jackson and others. The method used in these early rocket experiments is shown in Figure 1, and depends upon the differential retardation suffered by radio waves of different frequencies when passing through an ionized medium. The usual method involves the use of two harmonically related frequencies, one near the critical frequency of the region to be investigated, the other being the sixth or seventh harmonic of the first. These two frequencies are transmitted simultaneously from the rocket as it proceeds upward into the ionosphere. Due to the retardation suffered by the lower frequency, the received signals on the ground change their relative phases.

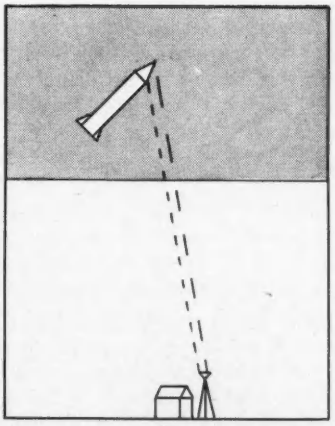

Figure 1

Illustrating the principle of the propagation experiment of Seddon and Jackson for measuring ionospheric electron densities.

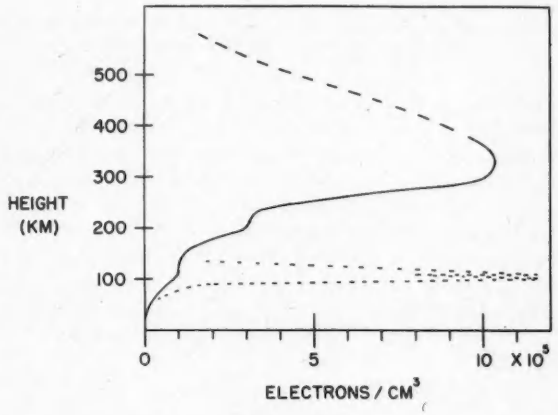

Figure 2

A typical electron density profile for the undisturbed ionosphere. The broken line suggests a modification that might occur during an auroral disturbance.

The phase comparison is made on the ground by first producing the appropriate harmonic of the lower of the two received signals and then comparing this harmonic with the signal received at the higher frequency. By measuring the relative phase change of the two signals as the rocket goes into the ionosphere, it is possible to deduce the total electron content of the ionosphere between the rocket and the ground station. It is the variation with height of this electron density, integrated along the line of sight from the ground station to the rocket, that provides the distribution of electron density as a function of height in the ionosphere. Clearly the sensitivity of this method to local variations is very limited. A typical electron density profile for the undisturbed ionosphere is shown in Figure 2.

When the ionosphere is disturbed the electron density can be expected to vary considerably from point to point, and under these conditions the propagational type of experiment, using either a ground based or a rocket borne transmitter, will be subject to considerable error. This was recognized several years ago and various attempts have been made to overcome the difficulty. The problem becomes most severe in the case of auroral measurements, because it is believed that the ionization associated with an auroral display is very inhomogeneous and that the electron density varies through wide limits in distances of the order of a few meters. The radio evidence concerning this

---

†Paper read at the Canadian High Altitude Research Symposium in Ottawa on the 21st October, 1960.

*Professor of Physics

**Assistant Professor of Physics

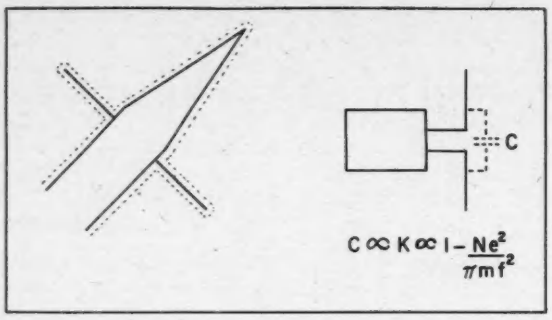

Figure 3

Illustrating the principle of operation of the RF impedance probe method of measuring the electron density.

ionization, obtained by means of propagation experiments, is still incomplete and poorly understood. A rocket experiment that would measure the electron density in relatively small volumes of the ionosphere during an auroral display would be of great value. It would also enhance considerably the value of the information if it could be obtained simultaneously for two or three separate trajectories in the ionosphere. This additional information would help to distinguish between the temporal variations and the spatial variations.

In an attempt to study the various methods that could be used for electron density measurements in the disturbed or auroral ionosphere, a NASA team, consisting of Bourdeau, Jackson, Kane and Serbu, flew a specially instrumented rocket from Churchill in September 1959. This rocket carried a conventional propagation experiment and, in addition, an RF probe experiment. The principle of the RF probe is shown in Figure 3. The probe consists essentially of an antenna driven by a relatively weak source of constant RF energy. The impedance of this antenna changes when it is immersed in an ionized medium, and this change in impedance can be used to measure the electron density in the surrounding medium. This type of experiment gives great promise for measurements that must be made in inhomogeneous media such as the auroral atmosphere. Figure 4 shows a comparison of the electron density results from the two experiments in the same rocket (the propagation experiment and the impedance probe experiment), from which it may be seen that the propagation experiment gave a value which was some 1.5 times as great as that obtained from the impedance probe experiment near the peak of the trajectory. Because this flight was a test of the two methods, it was flown during a period of quiet ionospheric conditions, and so it is believed that the propagation experiment gave the best results. Fortunately, the experimental team had also put into the same rocket a Langmuir probe and an electric meter, from which it was possible to deduce that the rocket acquired a negative potential in the ionosphere and that the RF probe measurements were, therefore, in error, because of an ion sheath that formed about the probe antenna. The effect of this positive ion sheath of a few centimeters thickness forming about the RF probe antenna is to decrease the electron density in the immediate vicinity of the probe and therefore to decrease the effect of the ionized medium on the impedance of the probe. In spite of this sheath formation, the RF probe method is likely to be of great value in investigations of the inhomogeneities in the ionosphere.

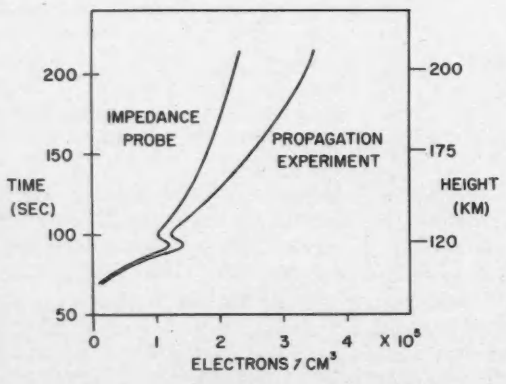

Figure 4

Comparison of the results obtained in a single rocket using both the RF impedance probe and the propagational method of measurement. (After Bourdeau, Jackson, Kane and Serbu, International Space Science Symposium, Nice, 1960.)

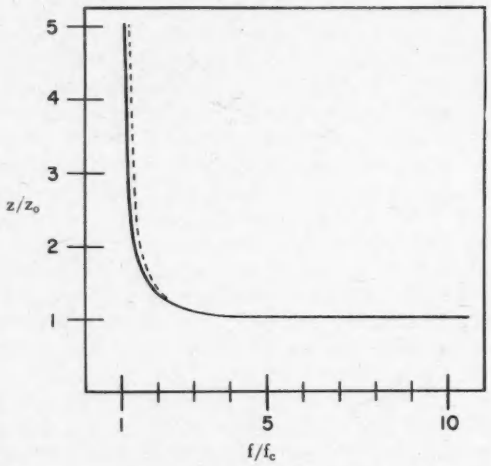

Figure 5

Illustrating the variation of impedance (Z) of an antenna in an ionized medium, as a function of electron density and frequency (f). Z_o is the free space antenna impedance and f_c is the critical frequency of the medium.

With this as background, we are now describing another electron density experiment which we hope to try next year. The experiment is a modification of the RF impedance probe, and is intended to investigate the structure of the ionization in an auroral display. The basic difference in the new experiment is that the RF source is not fixed in frequency. The frequency is made variable and caused to track the critical frequency of the surrounding medium continuously. It is hoped in this way to overcome the difficulties introduced by sheath formation. Figure 5 shows the variations of impedance of an RF probe as a function of electron density (f_c^2) and frequency (f). Just at the

Figure 6
Illustrating the approximate trajectories of the three ejected packages.

critical frequency ($f/f_c = 1$) a large change of impedance takes place and, in particular, the radiation resistance of the antenna becomes infinite. The so-called critical frequency at which these sudden changes take place is determined by the electron density according to the expression $f^2 = Ne^2/\pi m$, where N, e and m are the electronic density, charge and mass, respectively. The effective volume surrounding the probe has a radius of the order of a wavelength, and the measurement should not be significantly affected by the presence of a very thin layer surrounding the probe, particularly if this layer is one that is deficient in electrons.

It has already been mentioned that it would be desirable in studying the auroral ionization to make the measurement at two or three points simultaneously. In our experiment we plan to eject simultaneously from the rocket three separate instrumented packages, each of which will carry out continuous measurements of the local electron density along its particular trajectory. A sketch of these trajectories is shown in Figure 6. The ejection of a small instrumented package from the parent vehicle also has the very considerable advantage of removing the measuring device from the contaminating influence of the rocket body and its surroundings.

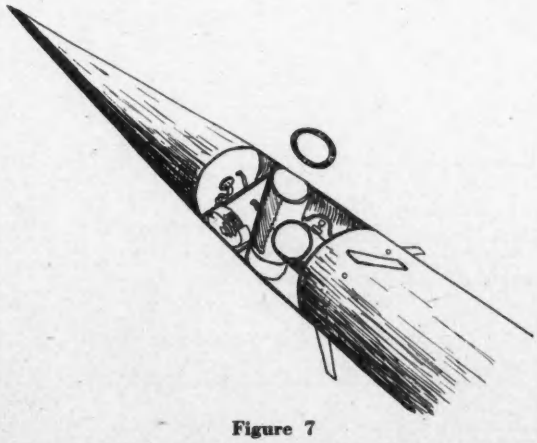

Figure 7
A sketch of the rocket nose cone showing the location of the packages before ejection.

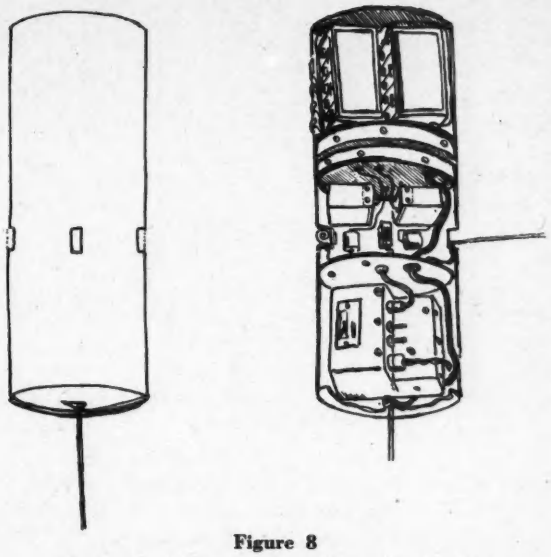

Figure 8
A sketch of the ejected package showing the internal construction.

Figure 7 shows a sketch of the rocket nose cone with the three packages in position. As soon as the rocket is well clear of the lower atmosphere, these three packages are simultaneously ejected approximately in the horizontal plane but in directions separated by 120° in azimuth. They then travel on their individual trajectories which continue to separate farther and farther apart until impact. Each package is, of course, equipped with its own telemetry transmitter so that the three sets of measurements can be continuously monitored from the ground.

Figure 8 shows a sketch of the ejected package. The four short antennas are for the telemetry transmitter, but also serve as a ground plane for the long antenna which is the sensing probe. Internally, the package consists only of the telemetry transmitter, a suitable modulator, the sensing circuit and battery pack. In addition, of course, facilities have to be provided for the monitoring of the operation of the internal circuits up until the time of firing.

Figure 9 shows the measuring or sensing circuit. The measurement is performed with the aid of a vari-

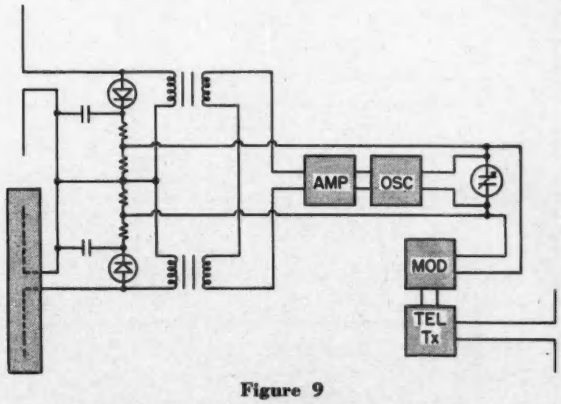

Figure 9
Block diagram of the probe instrumentation.

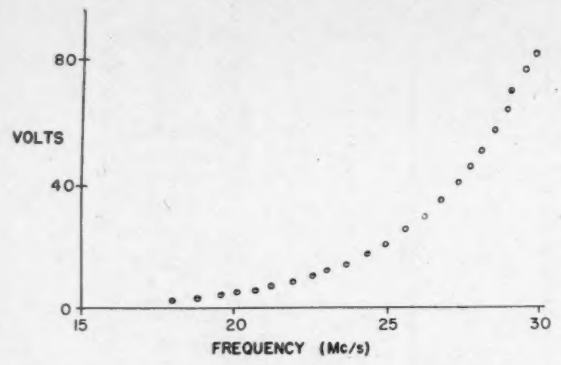

Figure 10

Graph of the variation of probing frequency with bridge unbalance voltage.

able frequency oscillator and an impedance bridge, which remains approximately balanced as long as the radiation resistance of the antenna maintains a value close to that experienced in free space. The external sensing antenna is in one of the arms of the impedance bridge and in the other is a network having the same impedance variation with frequency as that of the antenna. Thus, as long as the antenna is in free space, the bridge is balanced for all frequencies and the oscillator seeks its lowest permitted frequency. If the local electron density increases so that the plasma frequency (or local critical frequency) exceeds the oscillator frequency, then the sudden sharp change in the antenna impedance will unbalance the bridge and cause the oscillator frequency to increase until it exceeds the local plasma frequency and the bridge balance is again restored. This feed-back action keeps the oscillator frequency just above the plasma frequency. The actual frequency controlling element is a varicap, a device which changes its capacity in response to an applied dc potential. In order to monitor the local electron density it is only necessary to monitor the frequency of oscillation of the sensing oscillator. This is done by a separate circuit and the resulting signal is applied to the telemetry transmitter. In Figure 10 is shown the variation of frequency of the oscillator as a function of applied voltage. The choice of a frequency range for the experiment is not easy because so little is known about the auroral ionization, but we have finally settled on that shown in Figure 10.

CONCLUSION

This experiment is the first endeavour in the rocket field undertaken by our University group. As a result, we are learning as we go along and there have already been several false starts. We have completely revised the package layout and shape several times, but we feel that we are now close to the final design layout. We have not yet solved all of the problems connected with the ejections of the packages from the rocket although we do have the design of an ejection package which we hope we will be able to fit into the rocket nose cone. In any case, the project is going forward quite rapidly and we hope that all our problems will be solved in time to permit the firing of the rocket early next spring.

AERODYNAMICS OF BLASTS†

by Dr. I. I. Glass,* A.F.C.A.I.

Institute of Aerophysics, University of Toronto

SUMMARY

For the past decade theoretical and experimental investigations have been conducted at the Institute of Aerophysics on shock tube flows. Recently, this work was extended to include the analogous flows generated by spherical and cylindrical explosions. Glass spheres and cylinders are pressurized by means of compressed gases or combustible mixtures and are shattered to generate an explosion. Similar methods can be used for implosions, underwater explosions and wave interactions. The finite mass, strength and breaking time of the glass diaphragms impose some limitations on certain experiments, where this technique is used to generate a blast wave. Nevertheless, the method has proved very valuable in the study of many basic properties of spherical and cylindrical blast phenomena that have been investigated, using piezo-pressure gauges and several schlieren and shadowgraph techniques. Some consideration is given to intense explosions from concentrated energy sources for spherical, cylindrical and planar blasts, and explosions and implosions generated from finite sources with the same geometries. Blast wave simulators for aerodynamic tests and the dynamic testing of structural components are briefly discussed.

LIST OF SYMBOLS

a	sound speed (ft/sec, mm/μ sec)
$\alpha(\gamma)$	function of γ
C_v	specific heat at constant volume (ft lb/slug°R, cal/gm°C)
C_p	specific heat at constant pressure (as above)
E_o	total energy in spherical flows (ft lb, equivalent gm of TNT) energy per unit length in cylindrical flows energy per unit area in planar flows
E	E is proportional to E_o, $E = E_o/\alpha(\gamma)$
ϵ'	E_o/p_1, an energy parameter (ft^3, ft^2, ft depending on ν)
ϵ	$\sqrt[3]{E_o/p_1}$ ft, for spherical flows
f	flow quantity at a given radial distance r or R
G	$G(r/R)$ a function of the reduced radial distance
γ	C_p/C_v specific heat ratio
λ	r/ϵ non-dimensional energy reduced distance
$\mathscr{L}$	$\dfrac{r}{(E/\rho_1)^{1/(3+\nu)} t^{2/(3+\nu)}}$ non-dimensional distance
M_s	(S/a_1) shock Mach number
N	number of grid zones in shock transition
n	a power index
ν	1, 2, 3 for planar, cylindrical, spherical flows
p	pressure (lb/ft^2, dynes/cm^2, or atm)
ΔP_s	peak overpressure at the shock front (atm)
π	3.1416, also non-dimensional parameters
q	artificial viscosity [non-dimensional form Eq. (17)]
R	shock wave radius (in, ft)
r	radial distance (in, ft)
r_i	Lagrangian or initial radius (in, ft)
r_o	diaphragm radius (in)
ρ	density (slugs/ft^3, gm/cm^3)
S	shock velocity (ft/sec, mm/μ sec)
t	time (sec)
τ	$a_1 t/\epsilon$ non-dimensional energy reduced time
T	temperature (°K)
$\mathscr{T}$	$\dfrac{p_1^{5/6} t}{E_o^{1/3} \rho_1^{1/2}}$ non-dimensional time
u	particle velocity (ft/sec)
U_1	free stream velocity in steady flow (ft/sec)
V	volume (ft^3, cm^3)
X	$\frac{1}{3}(r_i/\epsilon)^3$, a non-dimensional Lagrangian variable in spherical flows
ΔX	grid spacing in numerical computation

Subscripts

0	a reference atmosphere 14.7 psi, 0°C
1	ambient or atmospheric conditions
2	conditions immediately behind the shock wave
3	conditions immediately behind the rarefaction wave
4	conditions in the diaphragm
P_{21}	p_2/p_1 shock pressure ratio
P_{41}	p_4/p_1 diaphragm pressure ratio
T_{21}	T_2/T_1 shock temperature ratio
T_{41}	T_4/T_1 diaphragm temperature ratio
$\overrightarrow{S}\overleftarrow{S}$	forward and backward facing shock waves (particles enter from right and left, respectively)
$\overrightarrow{R}\overleftarrow{R}$	forward and backward facing rarefaction waves
C	contact surface
Air/Air	diaphragm separating interior air at high pressure (and temperature) from exterior air at low pressure; similarly for HE/Air

†Paper read at the Joint I.A.S./C.A.I. Meeting in Montreal on the 18th October, 1960.

*Professor of Aeronautical Engineering

INTRODUCTION

BLAST waves are familiar phenomena. They occur in nature in a relatively mild form during thunderstorms or they may become very intense during volcanic (steam) explosions. It is estimated that the Krakatao explosion of 1883 resulted in an energy release equivalent to 5000 megatons of TNT[1]. However, man was also able to generate controlled or uncontrolled shock waves of increasing intensity when he learned how to crack a whip[2], discovered propellants and explosives, made use of coal mines and grain elevators and, finally, when he invented nuclear weapons[3].

The aerodynamics of blasts is not only of interest in itself, but it is also closely related to supersonic and hypersonic flight, and its now familiar shock wave patterns and sonic booms. It is of interest to note, for example, that a pound mass, at the earth's escape speed of 7 miles/sec, possesses a kinetic energy equivalent to over 14 lb of TNT (Figure 1). Consequently, a ballistic re-entry at such speeds is very much like a powerful explosion. It is fortunate that most of this energy is absorbed through the bow shock in the denser layers of the atmosphere, by heating the air which is left behind in the wake of the vehicle. Only a very small percentage of this energy is finally transferred to the vehicle itself, otherwise it would quickly vaporize. In a similar manner, the finite amount of energy in an explosion spends itself through shock wave heating of an ever increasing mass of air until the shock becomes vanishingly weak.

Mechanical, chemical, electrical or nuclear blasts all dissipate their energy through shock waves. In the latter, however, about half of the energy is dissipated through thermal and nuclear radiation, although at very early times the thermal energy leakage is small[3]. Large flow velocities, temperatures and pressures are induced behind a shock wave and it is the pressure and drag forces that cause the structural damage. The flow quantities decay in value with time and distance, and when the shock wave is far enough away from the point of explosion it has attenuated to a sound wave, and the physical quantities behind the wave are then only vanishingly different from those in the ambient atmosphere. A similar type of decay applies to the shock system surrounding a supersonic aircraft so that when it flies at a sufficiently high altitude its effects on the ground are negligibly small.

The properties of both idealized intense explosions from concentrated constant energy sources and very weak explosions can be predicted analytically[4, 5, 6]. On the other hand, the analysis of actual explosions from finite sources must be treated by numerical methods[7, 8]. Such analyses have only become possible in recent years with the advent of high speed electronic computers and the increased knowledge of the thermodynamic properties of explosives and of the air itself.

Some of the analytical solutions for intense explosions can also be applied to steady hypersonic flight

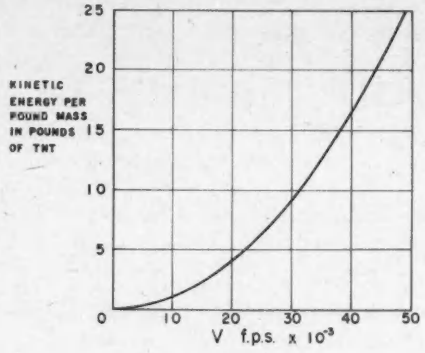

Figure 1

Variation of kinetic energy per pound mass (TNT equivalent) with re-entry velocity

through the so-called blast wave theory. For example, the solution for the intense cylindrical blast wave carries over to steady hypersonic flow over axisymmetric blunt-nosed slender bodies, and the planar blast to two-dimensional flows[9, 10, 11, 12].

The method of generating cylindrical and spherical explosions, implosions and wave interactions that has been developed at UTIA, consists of bursting glass spheres or cylinders from 1 to 6 inches diameter. For explosion studies these glass "diaphragms" are pressurized by means of compressed gases or combustible mixtures and exploded in a facility which consists of a 3 ft diameter steel sphere whose ambient atmosphere can also be varied. For implosion experiments the steel sphere is pressurized and the glass spheres and cylinders are evacuated and implode owing to the existing pressure differential or they can be broken mechanically. In the case of an underwater blast the sphere is exploded through overpressure in a small tank filled with water. A few preliminary experiments of exploding spheres in a supersonic flow at $M = 2.5$ have also been tried[13]. The head-on collision of relatively weak spherical shock waves has been successfully investigated[14].

An explosion generated from a 2 inch diameter glass sphere pressurized to 400 psi is driven by a blast energy equivalent to about 50 milligrams of TNT. Although the scaling of strong explosions in a facility of this type is aerodynamically quite possible it would only apply to very small models and at relatively small overpressures (up to several atmospheres). Consequently, shock tubes, sector tubes and other devices that are driven by TNT, or other chemical explosives, must be used to produce high pressure pulses of long duration (fractions of a second), which are required for the proper simulation of the flow over large models with relatively long structural response times. The present facility is best suited to basic studies of the gasdynamics or the aerodynamics of the blast itself or the flows induced over small models by explosions.

INTENSE EXPLOSIONS FROM CONCENTRATED ENERGY SOURCES — SPHERICAL, CYLINDRICAL AND PLANAR BLASTS

The instantaneous release of a finite amount of energy in a concentrated form at a point, line or plane gives rise to an intense blast wave in a spherical, cylindrical or one-dimensional geometry, respectively. All of these blast waves possess the property that the profiles of any thermodynamic and dynamic flow quantity f (pressure, temperature, density and flow velocity) relative to the corresponding value immediately behind the shock front remain invariant with time t, when the distances r are expressed as fractions of the shock wave radius from the point of the explosion, r/R. That is, as the decaying blast wave engulfs an ever greater mass of gas, at a given fractional distance, the physical quantities possess the same ratio, or $f(r,t)/f(R,t) = G(r/R)$. This similarity is predicted on the assumption that the shock wave is so strong that the ambient pressure and temperature are negligibly small in comparison with those behind the shock wave. Consequently, the similarity solution applies to the intermediate region between the origin of the explosion, where $\rho \to 0$ and $T \to \infty$, and that radius of the shock front where the shock wave has attenuated to an extent that the strong-shock assumption is invalid.

This type of problem was considered independently and almost simultaneously for the spherical case by Taylor[4], Sedov[5] and von Neumann[6]. The cylindrical case was considered later by Lin[10], who also noted that his solution should be applicable to the analysis of a steady flow over an axisymmetric, blunt-nosed slender body at zero angle of attack at hypersonic speeds (where r is equivalent to y and t is equivalent to x/U_1)[11]. An observer viewing a passing hypersonic body through a slit normal to the flight velocity will see very significant changes in the radial flow velocity as the body appears to drive the shock wave in a piston-like manner. Consequently, the flow in the (y,x)-plane appears like a cylindrical explosion in the (r,t)-plane. The flow in transverse planes exhibits a self-similarity in both cases when the shock wave is very intense and can be treated as having one independent variable. In a hypersonic axisymmetric flow the total drag is related to the energy per unit length in a cylindrical explosion. The planar, cylindrical and spherical blast waves were treated by Sedov[5] and later by Sakurai[12].

In solving this type of problem it may be seen that the solution will depend on the following six quantities: γ, p_1, ρ_1, E_o, r and t. The first three quantities describe the gas, E_o is the instantaneous energy release, and r and t are the independent variables in the space-time plane of interest. From dimensional analysis (using length, mass and time as the three basic quantities), it is known that five minus three or two non-dimensional (π) functions can be formed that will describe the subsequent motion (γ is already dimensionless). In the spherical case, for example, these functions are, $\mathscr{L} = \left(\frac{\rho_1}{E_o}\right)^{1/5} \frac{r}{t^{2/5}}$ and $\mathscr{T} = \frac{p_1^{5/6}\, t}{E_o^{1/3}\, \rho_1^{1/2}}$. Since it is assumed that for the strong blast wave $p_2 \gg p_1 \sim 0$, the non-dimensional time parameter $\mathscr{T}$ becomes zero and the motion is independent of time and is self-similar as noted above, and only two-dimensional constants E_o and ρ_1 are essential for a solution of the problem.

If we assume that the gas is perfect and inviscid, the equations of continuity, motion and energy (particle isentropic) which are valid in the region bounded by the blast wave are given by:

$$\frac{\partial \rho}{\partial t} + \frac{\partial (\rho u)}{\partial r} + (\nu - 1)\frac{\rho u}{r} = 0 \tag{1}$$

$$\frac{\partial u}{\partial t} + u\frac{\partial u}{\partial r} + \frac{1}{\rho}\frac{\partial p}{\partial r} = 0 \tag{2}$$

$$\frac{\partial}{\partial t}\left(\frac{p}{\rho^\gamma}\right) + u\frac{\partial}{\partial r}\left(\frac{p}{\rho^\gamma}\right) = 0 \tag{3}$$

where, $\nu = 1$, 2 and 3 for planar, cylindrical and spherical flows, respectively.

In general, this set of nonlinear, partial differential equations is too difficult to solve and recourse must be made to numerical techniques. However, in the case of intense blasts where only two dimensional quantities E_o and ρ_1 affect the motion, the two independent variables r and t are so related that the equations can be reduced to ordinary differential equations and exact self-similar solutions are possible[5]. The boundary conditions that have to be satisfied are that the particle velocity at the origin is zero and that the following Rankine-Hugoniot equations are satisfied across the shock wave at a radius equal to R:

$$u_2 = \frac{2}{\gamma + 1} S\left[1 - \frac{1}{M_S^2}\right] \tag{4}$$

$$\rho_2 = \frac{\gamma + 1}{\gamma - 1}\rho_1\left[1 + \frac{2}{\gamma - 1}\frac{1}{M_S^2}\right] \tag{5}$$

$$p_2 = \frac{2}{\gamma + 1}\rho_1 S^2\left[1 - \frac{\gamma - 1}{2\gamma}\frac{1}{M_S^2}\right] \tag{6}$$

For intense blasts, M_s is very large and the above relations reduce to

$$u_2 = \frac{2}{\gamma + 1} S \tag{4a}$$

$$\rho_2 = \frac{\gamma + 1}{\gamma - 1}\rho_1 \tag{5a}$$

$$p_2 = \frac{2}{\gamma + 1}\rho_1 S^2 \tag{6a}$$

The solution of Eqs. (1) to (3), subject to the above boundary conditions, are given in detail in Reference 5 for planar, cylindrical and spherical flows, and the results are illustrated in Figure 2. It is seen that the pressure behind the shock wave is a maximum and falls off quite rapidly near the shock wave to level off to a nearly constant value for radial positions $r/R < 0.5$. As expected, the fall-off in pressure is greatest for the spherical case, with its greatest free-

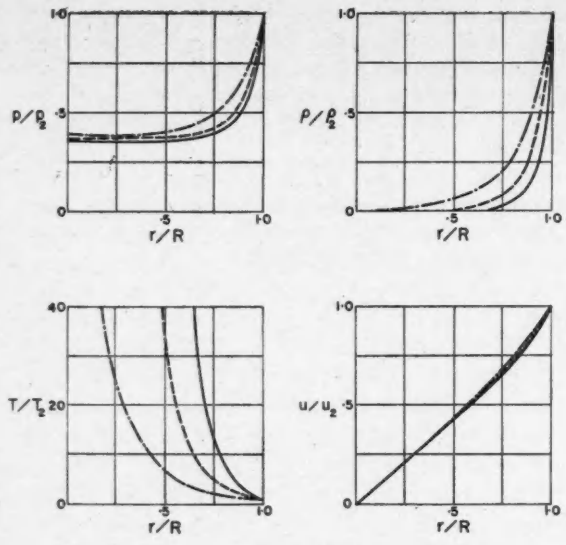

Figure 2

Self similar profiles for intense planar (— · —), cylindrical (— — — —) and spherical blast waves (————)[5]

dom for expansion, and least for the planar case. The same tendency is even more accentuated in the density profiles, where it is seen that nearly all of the mass of gas engulfed by the blast is concentrated close to the shock front itself. The pressure and density profiles are reflected in the temperature profiles where it is seen that, subject to the assumption of an inviscid non-conducting gas, enormous temperatures are developed towards the centre of the blast, as a result of the prevailing vanishingly small densities and finite pressures. This is particularly marked in the spherical case. The particle velocities decrease from their maximum value behind the shock front to zero at the origin of the blast. It is seen that the curves differ only slightly in the range $0.5 < r/R < 1$, but here at a given r/R, the spherical flow velocity is the lowest and the planar velocity the largest.

The motion of the shock wave is, of course, also found from the solution. However, an insight into this can be obtained from the dimensional considerations noted above. Since E_o represents the total energy released in the spherical case, per unit length in the cylindrical case and per unit area in the planar case, it has dimensions of $ML^{\nu-1}T^{-2}$, where M, L and T represent the usual basic quantities of mass, length and time. Consequently, the non-dimensional distance noted above can be expressed as

$$\mathscr{L} = \frac{r}{\left(\frac{E}{\rho_1}\right)^{1/(3+\nu)} t^{2/(3+\nu)}} \tag{7}$$

where $E = E_o/\alpha(\gamma)$

The function $\alpha(\gamma)$ is a constant and is determined from the solution of the equations of motion. With the above notation the shock wave path can be obtained from Eq. (7) as

$$R = \left(\frac{E}{\rho_1}\right)^{1/(3+\nu)} t^{2/(3+\nu)} \tag{8}$$

where, for convenience, $\mathscr{L}$ was set equal to unity. Using Eqs. (8) and (6a), the quantities in Table 1 can be derived. From the shock radius R, shock speed S, the pressure behind the shock p_2 or the overpressure ΔP_s, it can be seen that the spherical blast wave decays most rapidly with time or shock radius.

It is worthwhile considering some actual applications of the above equations. Eq. (8) was used by Taylor[4] to deduce the energy yield of the atomic explosion in New Mexico. Measurements of shock radii with time from high speed photographs gave the points shown in Figure 3, which is a plot of Eq. (8) for the spherical case; that is

$$5/2 \log R(\text{cm}) - \log t(\text{sec}) = 11.915 \tag{9}$$

The value 11.915 is the intercept of the 45° line with the ordinate axis at $\log t = 0$, and equals ½ $\log E/\rho_1$. For $\rho_1 = 1.25 \times 10^{-3}$ gm/cm^3, $E = 6.76 \times 10^{23} \times \rho_1$ ergs $= 8.45 \times 10^{20}$ ergs. For $\gamma = 1.4$, the solution for the spherical blast yields $\alpha(\gamma) = 0.851$ or $E_o = 7.19 \times 10^{20}$ ergs, or, using a value of the energy content of TNT as 1000 cal/gm, this is equivalent to a yield of

TABLE 1

SOME PROPERTIES OF INTENSE BLAST WAVES

Geometry	R, (Eq. (8))	$S = dR/dt$	ΔP_s or $p_2 \propto S^2$
Spherical	$\left(\frac{E}{\rho_1}\right)^{1/5} t^{2/5}$	$\frac{2}{5}\left(\frac{E}{\rho_1}\right)^{1/5} t^{-3/5} = \frac{2}{5}\left(\frac{E}{\rho_1}\right)^{1/2} R^{-3/2}$	$\frac{1}{R^3}$
Cylindrical	$\left(\frac{E}{\rho_1}\right)^{1/4} t^{1/2}$	$\frac{1}{2}\left(\frac{E}{\rho_1}\right)^{1/4} t^{-1/2} = \frac{1}{2}\left(\frac{E}{\rho_1}\right)^{1/2} R^{-1}$	$\frac{1}{R^2}$
Planar	$\left(\frac{E}{\rho_1}\right)^{1/3} t^{2/3}$	$\frac{2}{3}\left(\frac{E}{\rho_1}\right)^{1/3} t^{-1/3} = \frac{2}{3}\left(\frac{E}{\rho_1}\right)^{1/2} R^{-1/2}$	$\frac{1}{R}$

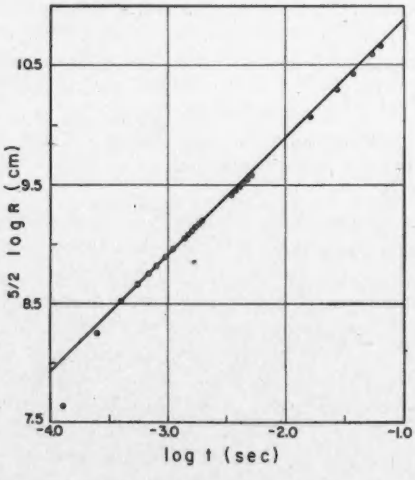

Figure 3

Velocity of the spherical blast wave from an intense explosion[4]

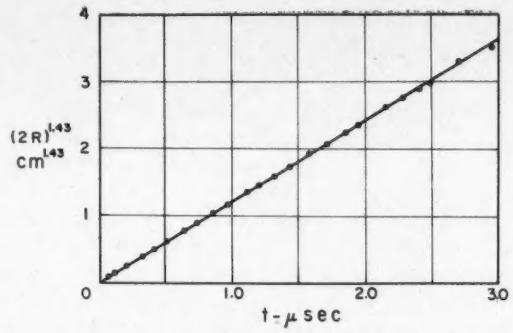

Figure 4
Shock path from an exploding wire[15]

17 kilotons of TNT. It should be noted that an upward translation of the straight line in Figure 3 would be indicative of a stronger or higher energy yield spherical blast and vice versa. The answer obtained in this manner is only approximate considering the simplifying assumptions of a point source, constant energy and a perfect inviscid gas. In an actual case a significant portion of the energy is dissipated through thermal radiation at later times[8]. Nevertheless, the method shows that a great deal of insight can be obtained from this type of analysis.

An example of an intense cylindrical blast wave is the sudden explosion of a fine cylindrical metal wire, caused by the sudden input of a heavy electrical current pulse. The analysis of the motion of the shock wave is made more difficult by the complex manner in which energy is added, and the change of phase of the wire from a solid to a vapour that occurs at very small times. In addition, the imperfect equations of state for the metal and the ambient gas into which the blast propagates must be taken into account. In fact, the exploding wire becomes analogous to a hot, pressurized cylinder that is suddenly ruptured, rather than a line source. Consequently, imploding shock waves and wave interactions occur that invalidate the similarity assumptions.

A recent survey of exploding wires is given in Reference 15, where Bennett's experimental results indicate a variation favouring $R \propto t^{0.6}$, rather than $t^{0.5}$ as given by Eq. (8). For this case $\alpha(\gamma) \simeq 1$ (see References 5 and 10). One of the best results for a 5 mil exploding copper wire with a rated energy of 60 joules/cm (~ 15 milligram TNT/cm) is shown in Figure 4. Here, the shock wave is advancing into air at 0.5 atm at a rate of $R \propto t^{0.7}$. However, in the range of ⅕ to 1 atm, a single plot of $R \propto t^{0.6}$ appeared to fit the remaining results even better. The fact that all of these experiments at different ambient densities gave an apparently constant E/ρ_1, or that a decreasing ρ_1 could apparently decrease the energy added to the copper wire is surprising. However, when this result is considered from the viewpoint of the cylindrical analogue to the shock tube noted above, it might be explained by the fact that a diaphragm pressure ratio that changes by a factor of 5 (as in this case) would hardly affect the strength of a strong shock wave[16]. Some critical comments regarding this problem by Bennett and Rouse can be found in Reference 15.

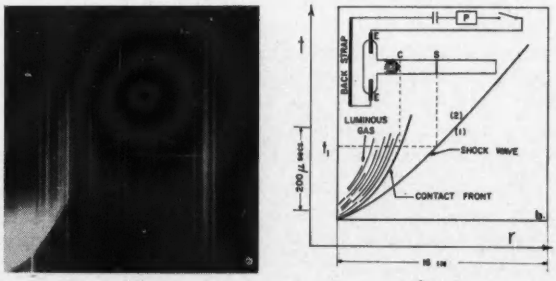

Figure 5
Blast wave produced in a T tube
(a) schlieren record of the (r, t)-plane
(b) explanatory sketch: air at 500 mm Hg and 300K°K, capacitors 2μf at 17.5 kv

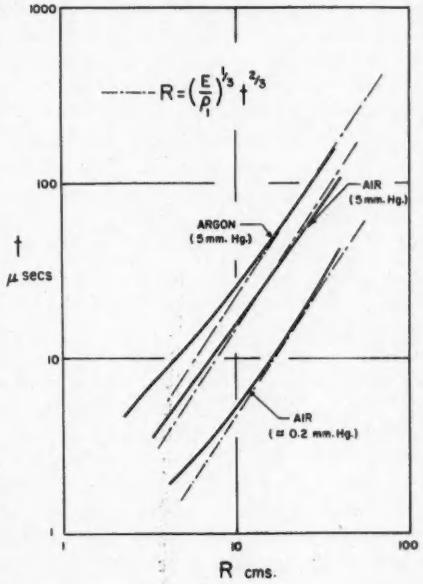

Figure 6
Shock wave paths in a T tube in air and argon

A planar type of blast wave may be generated by the sudden addition of electrical energy to a gas by means of an electrode or electrodeless discharge. The so-called T tube, developed by Fowler and Kolb, is a typical example (see Reference 16 for a brief survey). Such a device for adding energy to a gas in a plane (ideally), as investigated at UTIA, is shown schematically in an insert in Figure 5. Energy during a discharge is added to the gas across a gap from two 1.5 microfarad, 30 kv, low inductance capacitors by means of ohmic heating and through the magnetogasdynamic ponderomotive force applied as a consequence of the rigid back-strap. During an experiment the current, rate of current and voltage inputs are monitored across the gap by means of oscillograms. The energy input is therefore known as a function of time. The sudden addition of electrical energy coupled with the ponderomotive force generates a blast wave in the 22 mm pyrex tube, whose path is illustrated in Figure 5 in an (r, t)-plane schlieren record.

The initial conditions are noted in the figure, and from the oscillograms a computation has indicated that about 20, 8 and 5 joules/cm² were added to the gas in three damped half-cycles at about 3 μ sec intervals. The latter two probably did not contribute very much to driving the blast wave as there was no apparent strengthening of the shock wave after the first half-cycle. Figure 5 shows the hot, luminous expanding gas driving the shock wave in front of it. During the first 25 μ sec it is difficult to separate the shock front from the luminous gas on the schlieren record. Some typical shock paths are shown in Figure 6 as solid lines and the dashed lines show the planar blast wave decay given by Eq. (8). In this instance $\alpha(\gamma) \sim 1.08$, where $\gamma = 1.4$, and $\alpha(\gamma) \sim 0.60$, where $\gamma = 5/3$[5]. Also in this case, similarity is not achieved during the early phase of the flow because the assumption of energy addition at a plane is not met. A finite source is probably closer to reality. At higher pressures (5 mm Hg) and after about 20 μ sec, $R \propto t^{2/5}$ appears to be a reasonable approximation for subsequent small time intervals. Below 20 μ sec the shock waves are weaker than predicted by this power law. However, for the case of air at a pressure of 0.2 mm Hg, a power law profile appears to be entirely inadequate. The blast wave is considerably stronger at the low pressures, which would result from a higher effective diaphragm pressure ratio. Further details are given in Reference 17.

It is worthwhile to note at this point that, in the analysis of an intense blast, at times when shock wave attenuation no longer permits the assumption that the pressure in front of the shock wave may be neglected by comparison with that behind it, the exact Rankine-Hugoniot shock conditions must be satisfied and that the solution is no longer self-similar. Eqs. (1) to (3) must now be solved numerically. This has been done by Brode[7], who made use of the concept of an artificial viscosity in order to overcome the difficulty of flow discontinuities at the shock wave. The artificial viscosity spreads the shock front over about 6 mesh lengths and a continuous transition results, analogous to an actual shock transition. The results are shown in Figure 7 for air considered as a perfect gas and an imperfect gas. It is seen that for shock wave peak overpressures, in atmospheres, in the range $\Delta P_s > 10$ atm, $\Delta P_s \propto 1/\lambda_s^2$ (a slope of 72°) and at very low overpressures, $\Delta P_s \to 1/\lambda_s$, the acoustic result for a spherical wave (a slope of 45°). In the intermediate range ΔP_s can be fitted with a polynomial in $1/\lambda_s$[8].

The perfect gas solution lies above the imperfect gas case and is indicative of the energy that is bound in vibration, dissociation, electronic excitation and ionization, and is not available for driving the blast wave. Brode estimates that the imperfect point-source explosion is only about 50% as efficient as that in perfect air ($\gamma = 1.4$)[8].

Brode has reported three explosions from very hot spheres of gas, where the interior density is assumed as that at standard conditions but at pressures of 122, 2000 and 20,000 atm[7, 8]. In the latter case the required uniform temperature is about 386,000°K. The 122 atm sphere approaches the perfect gas point-source solution at $\Delta P_s \sim 20$ and $\lambda_s \sim 0.2$, and the 2000 atm sphere

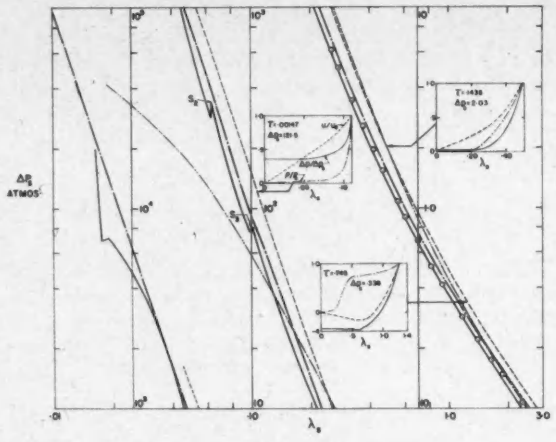

Figure 7

Variation of peak overpressures (ΔP_s) with shock radius (λ_s) for various explosions. Point source, air, perfect (— — — —), imperfect (— · — · —); hot sphere 2×10^4 atm and 3.86×10^5 °K (———); TNT (— · — · —)[8]

when $\Delta P_s \sim 300$ and $\lambda_s \sim 0.8$. The 20,000 atm sphere approaches the imperfect gas solution when $\Delta P_s \sim 2500$ atm and $\lambda_s \sim 0.035$, as shown in Figure 7. The latter then diverges somewhat from the imperfect point-source curve and is brought closer to it by the overtaking of the second shock and finally the third shock. After an overpressure of 10 atm the hot-sphere solution runs almost parallel to the imperfect gas point-source solution. The circled points are the data from a nuclear explosion, as reported in Reference 3, and are seen to agree very well with Brode's calculations, except at low overpressures when the explosion energy is small compared with the ambient energy of the air engulfed by the blast wave, and the accuracy in the calculation of maintaining a constant blast energy is reduced.

The TNT curve on Figure 7 exhibits a decay in $\Delta P_s \sim 1/\lambda_s$ initially[18]. Later, it cuts across the other three curves, and at low overpressures lies closest to the imperfect gas solution. As Brode points out, every explosion is affected by its initial history to some degree, and consequently they are difficult to compare or scale accurately. He indicates that a rough rule is that the peak overpressure in an explosion will decay in a manner similar to a point-source when the shock wave has engulfed a mass ten times the mass of the initial explosive. Furthermore, although the peak overpressure may be scalable the flow quantities within the blast interior may differ for each source, and identical scaling becomes very difficult[8].

Three profiles of overpressure to peak overpressure ratio $\Delta P/\Delta P_s$, density ratio ρ/ρ_2 and particle velocity u/u_2 from the blast centre to the shock front for the point-source, perfect gas explosion have been drawn on Figure 7, for $\tau = 0.00147$, 0.1436 and 0.745. These have been included to illustrate how, in time, the blast wave profiles depart from the similar solution for the strong shock wave[4, 5], and develop positive and negative phases when the overpressure

drops. A hot-spot remains near the origin even at late times, as indicated by the persistent near-zero densities and finite pressures.

An important conclusion that one might draw is that a finite source explosion will eventually decay very much like a point-source blast. The effects of the wave interactions appear to vanish quickly if the source is hot (high sound speed). Since the cube of the inverse radius type of shock-decay relation applies to the spherical-shock overpressures long after the strong shock conditions really cease to be accurate, the corresponding attenuation relations would also be expected to apply to the cylindrical and planar blasts. However, this is not entirely borne out by the exploding wire or T tube experiments noted above. In these cases it is possible that a modified type of similarity solution based on a decreasing energy input with time might yield a more realistic type of power profile for the shock path at early times. Later on the decay may well be represented by that from a finite source explosion in a manner exhibited by the nuclear blast points in Figure 7.

EXPLOSIONS AND IMPLOSIONS GENERATED FROM FINITE SOURCES

The foregoing results indicate that a realistic approach to the propagation of blast waves would be to consider an energy source of finite extent for spherical, cylindrical and planar explosions. Once a finite source is assumed then the complementary problem of implosions may be considered simultaneously. In order to simplify the analysis it is assumed that no energy is lost through radiation and that the flow is inviscid. The problem is then to determine the resulting flow properties when a plane, cylindrical or spherical diaphragm, which separates a gas at higher or lower pressure (and temperature) from that of the external atmosphere, is suddenly ruptured generating an explosion or an implosion, respectively (Figure 8). In the case of a planar flow one assumes a very small length of chamber r_0 relative to the channel in the case of an explosion. On the other hand, in the case of an implosion the channel is made very short.

For very small times, less than the time it takes for the head of the rarefaction wave or the shock wave to reach the origin in the case of an explosion and implosion, respectively, Eqs. (1) to (3) can be solved by using a power series solution or the method of characteristics[19, 20]. The results are illustrated schematically in Figure 8. The planar case is the familiar shock tube case, which has been treated in great detail by many authors[16]. Here state (4) is at high pressure (and temperature) and state (1) at low pressure. Since the flow is symmetrical about the origin, consider that the right diaphragm is ruptured. Immediately a shock front S moves into region (1), compressing and heating the gas in region (2) in an irreversible manner. At the same instant a rarefaction wave R moves into state (4) and isentropically expands and accelerates the particles in the opposite direction to form state (3). This gives rise to a contact surface C,

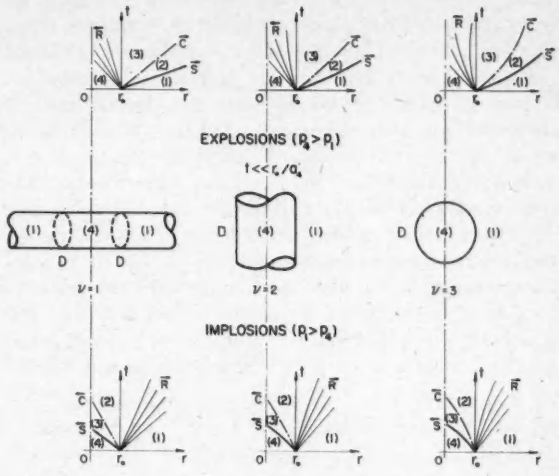

Figure 8
Spherical, cylindrical and planar explosions and implosions

which separates the uniform state (2) existing at a high entropy level from that of state (3).

For the cylindrical and spherical explosions the picture is changed. States (2) and (3) are no longer uniform. The shocks and contact surfaces decelerate. Consequently, state (2) is a region of decreasing entropy behind the shock path. The characteristic lines in the expansion fan accelerate towards the shock front[18], and it will be shown that the existence of an imploding shock wave turns state (3) into a non-isentropic region. These effects are even more pronounced in the spherical case than in the cylindrical case (Figure 8).

When an implosion occurs, the shock accelerates towards the origin and it is followed by an accelerating contact surface. The characteristic lines in the expansion wave decelerate in a direction opposite to the shock front. State (2) is now a region of increasing entropy behind the shock path. The effects are again accentuated for the spherical flow. As expected, for the same diaphragm pressure ratio P_{41}, a finite source explosion generates a stronger rarefaction wave for the spherical and cylindrical blasts than for the planar explosion, and vice versa for the implosion. Furthermore, it might have been anticipated that, since in cylindrical and spherical flows the contact surface decelerates and it also behaves as a massless piston, it would send expansion pulses to decay the main shock wave and compression pulses to form a second shock at the tail of the rarefaction wave, in the case of cylindrical and spherical explosions. In implosions the reverse takes place. Here the compression pulses reinforce the main shock and the expansion pulses reinforce the main rarefaction wave. Consequently, a second shock wave does not occur in an implosion. This will be verified subsequently.

Although the above approach for small times is of interest, it does not solve the problem. A solution has to be obtained from a numerical integration of a

set of stable, finite difference equations that approximate the nonlinear partial differential equations (Eqs. (1) to (3)). The boundary conditions of zero velocity at the origin and the Rankine-Hugoniot relations across shock waves must also be satisfied. It might be noted that although a solution is possible by using the method of characteristics for the planar case, it is complicated by the additional term in the continuity equation for the cylindrical and spherical cases. This term leads to a singularity at the origin and causes the planar Riemann invariants $[2a/(\gamma-1) \pm u]$ to vary along characteristic lines so that the method becomes complex, especially when unique values for the flow quantities no longer exist as a result of the formation of shock waves from steepening compression waves.

The method of numerically integrating Eqs. (1) to (3) has been developed by Brode[7] and successfully applied to a number of problems[8, 15, 21]. For convenience, Eqs. (1) to (3) are written in Lagrangian form[15]. The independent variables are time t and the initial radial position of a gas element r_1. The dependent thermodynamic and dynamic variables are made non-dimensional by using the ambient gas properties (for example, $\bar{p} = p/p_1$, $\bar{u} = u/a_1$ etc, and the bars can be omitted for simplicity). Similarily, the independent variables are made non-dimensional by using the pressure-reduced energy of the gas contained in the interior of the diaphragm.

For example,

$$\frac{E_0}{p_1} = \epsilon^\nu = \frac{V\rho_4 C_v T_4}{p_1} = V\frac{P_{41}}{\gamma_4 - 1} \tag{9}$$

where

$V = 4/3\,\pi r_0^3$ spherical flows, $\nu = 3$
$V = \pi r_0^2$ per unit length, cylindrical flows, $\nu = 2$
$V = 2r_0$ per unit area, planar flows, $\nu = 1$

For spherical flows in particular,

$$\frac{\epsilon^3}{4/3\,\pi r_0^3} = \frac{P_{41}}{\gamma_4 - 1} \tag{10}$$

From Eqs. (9) and (10) it is seen that the reduced energy per unit volume (reduced energy density) depends only on the diaphragm pressure ratio P_{41} and the specific heat ratio γ_4 in all blast cases, and approaches infinitely large values when $P_{41} \to \infty$ or $\gamma_4 \to 1$. The usefulness of Eq. (10) will be considered subsequently. The following dimensionless quantities are now formed:

$$\lambda = r/\epsilon$$
$$\tau = a_1 t/\epsilon \tag{11}$$

With the above notation, the Lagrangian equations of motion in non-dimensional form can be expressed for the spherically symmetric case, as follows[7]:

$$\frac{\partial \lambda}{\partial X} = \frac{1}{\rho\lambda^2} \tag{12}$$

$$\frac{\partial u}{\partial \tau} = -\frac{\lambda^2}{\gamma}\frac{\partial}{\partial X}(p + q) \tag{13}$$

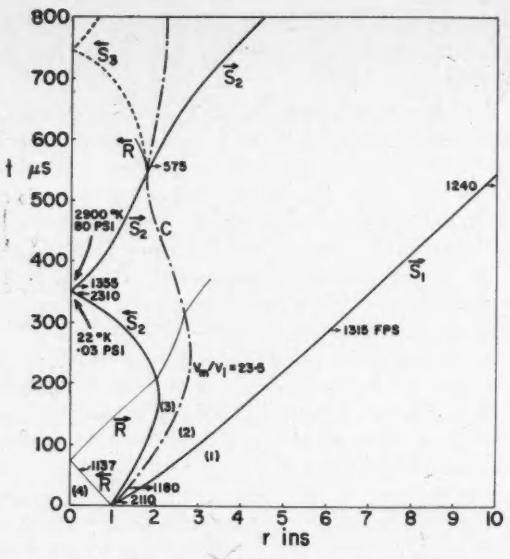

Figure 9

Computed wave system of a blast from a 2 inch diameter sphere case Air/Air, $p_4 = 22$ atm, $p_1 = 1$ atm, $T_4 = T_1 = 299$°K (shock tube flow reference: $S = 2110$ fps, $u_2 = 1250$ fps, $T_2 = 470$°K, $T_3 = 180$°K)

$$\frac{\partial p}{\partial \tau} = \frac{1}{\rho}\frac{\partial \rho}{\partial \tau}[\gamma p + (\gamma - 1)q] \tag{14}$$

$$u = \frac{\partial \lambda}{\partial \tau} \tag{15}$$

$$X = \frac{1}{3}\left(\frac{r_1}{\epsilon}\right)^3 \tag{16}$$

The quantity X is a Lagrangian variable expressing the non-dimensional volume per steradian for a spherical shell of radius r_1. The quantity q is the dimensionless form of the artificial viscosity that provides the means of automatically spreading the shock wave into a thin, continuous transition[22]. Brode has found that the following form of q produces the required results without significantly distorting the rest of the flow field:

$$q = \frac{9\gamma(\gamma+1)}{4}\left(\frac{N}{3\pi}\right)^2 \rho(\Delta X)^2 \frac{\partial u}{\partial X}\left[\frac{\partial u}{\partial X} - \left|\frac{\partial u}{\partial X}\right|\right] \tag{17}$$

Where, ΔX is the grid size ($\sim 1/100$ distance traversed by the shock wave), N is the number of grid zones in the shock front (~ 6) and $\partial u/\partial X$ is negative for shock waves so that $q \propto \left(\frac{\partial u}{\partial X}\right)^2$ for shocks and $q = 0$ for expansion waves or for contact surfaces. Eqs. (12) to (17) provide five equations for the five unknowns λ, p, ρ, u and q in terms of X and τ. A discussion of the finite difference equations that have been used by Brode to approximate the above partial differential equations and the required stability conditions in the time interval $\Delta\tau$ can be found in Reference 23.

Spherical explosions and implosions

Explosions have been produced by bursting 1 inch diameter to 5 inch diameter pressurized glass spheres.

Compressed air, helium, argon, sulfurhexafluoride and combustible mixtures of oxygen-hydrogen diluted with helium were used as driver gases. However, extensive numerical solutions by Brode were done only for the following two cases: 2 inch diameter spheres containing air at 22 atm and helium at 18¼ atm and 300°K. These cases were checked experimentally in some detail[24, 25]. It should perhaps be emphasized again that the shock-tube problem only has a simple analytical solution as long as the diaphragm separates chamber and channel sections of sufficient length to eliminate immediate wave interactions. The amount of work required to obtain a solution for a single spherical or cylindrical blast problem is rather extensive, and it is for this reason that the investigation was limited to the above two cases. Under the conditions noted above, the air and helium spheres contained an energy equivalent to 88 and 44 milligrams of TNT (1040 cal/gm), respectively. The nominal 50 mm diameter glass spheres were about 1 mm thick and weighed approximately 20 gm. The spheres were blown individually of pyrex or soda lime glass with stems about 65 mm long, 6 mm diameter and 1 mm thick.

The original computations, as previously described, for the Air/Air and He/Air blasts were done in the non-dimensional radius-time (λ, τ)-plane and on several graphs have been converted for convenience to units used in the experimental work. The conversion factors for the (r, t)-plane are: $\lambda = 0.2$ corresponds to $r = 1.1$ inches, $\tau = 0.2$ corresponds to $t = 90$ μsec for Air/Air, and $0.2\ \lambda \equiv 0.94$ inches and $0.2\ \tau \equiv 72$ μsec for He/Air. A standard atmosphere of 14.7 psi and 0°C (subscript 0) was used by Brode as a reference atmosphere rather than the ambient conditions.

The paths of the various wave elements are shown in the (r, t)-plane in Figure 9 for the case of Air/Air and in Figure 10 for He/Air. It is seen that when the sphere is ruptured, a decelerating shock wave S_1 moves into (1) followed by a decelerating contact front C. A rarefaction wave R propagates into (4) and a second shock wave S_2, which forms at the tail of the rarefaction wave but faces in the opposite direction to S_1, is swept outward by the expanding high pressure gas. However, as the second shock wave gains strength, it overcomes this flow velocity and finally implodes on the origin. Refractions at the contact front produce secondary waves (rarefaction and shock waves in the case of the air explosion, but only shocks for the case of the helium blast[16]) and cause it to oscillate as indicated, and after some time several shock waves S_1, S_2, S_3 move away from the explosion. Unlike similarly-facing shock waves in the plane case these waves do not overtake[26] at the times and distances considered here. For example, S_2 is caught in the negative-pressure phase of the primary shock wave where it encounters a low sound speed and opposing particle velocity that slows it up. In the case of the hot sphere, shown in Figure 7, S_2 does not encounter such conditions and does overtake to strengthen S_1, and this is repeated again by a third shock S_3. Unlike the planar flow, regions (2) and (3) are not uniform or isentropic owing to the existence of these shock waves of continuously varying strength.

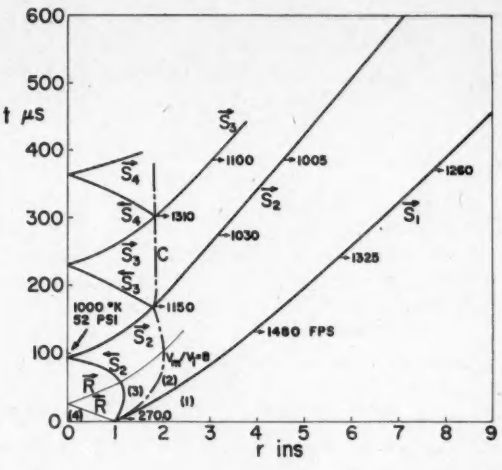

Figure 10

Computed wave system of a blast from a 2 inch diameter sphere case He/Air, $p_4 = 18¼$ atm, $p_1 = 1$ atm, $T_4 = T_1 = 301$°K (shock tube flow reference: $S = 2700$ fps, $u_2 = 1850$ fps, $T_2 = 600$°K, $T_3 = 197$°K)

It has been shown by Brode[7, 8, 24], that various types of blasts approach and have a decay rate like the limiting point-source solution for shock overpressure versus radius, after the primary shock S_1 has engulfed a mass of air of about tenfold that of the original explosive. For a hot or light gas this occurs much more rapidly than for a heavy gas for a given initial volume. Therefore, for the same size sphere r_0 and diaphragm pressure ratio P_{41}, the combination He/Air gives initially a much stronger shock than say, SF_6/Air (shock tube effect)[16]. However, SF_6 is a more efficient explosive when the point-source solution is finally reached and the scaling laws can be applied approximately (energy loading effect – Eq. (10)). That is, the same shock overpressure would take place at a larger physical radius for the case of SF_6. These effects are illustrated in Figure 11 for the cases of He/Air and Air/Air blasts used in the present experiments. It is seen that the He/Air case approaches the point-source solution faster, owing to the lower mass of helium, or since the sound speed in helium is much greater the effects produced by the wave interactions vanish sooner. Initially, the helium gives a larger peak overpressure ΔP_s at a given radius R than the air case. However, for the same initial diaphragm pressure ratio P_{41} the air sphere contains 5/3 as much energy as the helium sphere and, if both explosions would coincide with that of the point-source solution, ΔP_s at a given R would be larger for the air blast than for the helium blast. From Figure 11 it is seen that the initial history of a given blast is not "forgotten" and no curve is coincident with any other. Consequently, identical scaling using different sources is not possible, although as noted above for many purposes the close proximity of the curves may be quite sufficient for scaling.

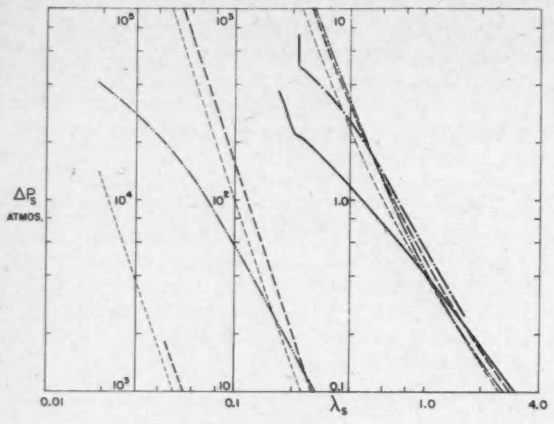

Figure 11
Shock overpressure (ΔP_s) for various explosions. Point source, perfect gas (— — — —), imperfect gas (- - - -); TNT, 1.5 gm/cm³, (— · · —); He/Air, 18¼ atm, (— · —); Air/Air, 22 atm, (———)

It is worth noting from Eq. (10) that once a spherical flow solution has been found for a given P_{s1} and γ_4 (this fixes the type of explosive), then it does not matter if r_0 or ϵ (mass of explosive) is increased or decreased. The same solution applies, as this only increases or decreases λ and the explosion is magnified or reduced in the physical (r, t)-plane.

The Air/Air and He/Air explosions approach the point-source curve at positions when ΔP_s decays in a more complex manner than $\Delta P_s \sim 1\,\lambda_s^3$ since the shock front is neither strong nor weak. The helium blast approximates the point-source, imperfect air attenuation when the shock is at $\lambda_s \sim 0.5$ or $R \sim 2.4$ inches, at a shock overpressure $\Delta P_s \sim 1.8$ atm. If one considered a 20 kiloton point-source blast, then applying the energy scaling relation such an overpressure would exist at a distance $R \sim (20 \times 10^6 \times 10^8 \times 10^9)^{1/3} (44)^{-1/3} (2.4/12) = 1540$ ft or 0.29 miles. The Air/Air blast cuts the point-source imperfect air solution when $\lambda_s \sim 1.1$ or $R \sim 6$ inches and $\Delta P_s \sim 0.35$ atm, but it has a more gradual attenuation. The equivalent scaled distance for a 20 kiloton blast when R is at the same overpressure occurs at $R \sim (2 \times 10^{13}/88)^{1/3} \times 6/12 = 3050$ ft or 0.58 miles. Consequently, only shock wave effects at large distances from very intense explosions with correspondingly small models could be simulated by using the present shock sphere apparatus.

In addition to the wave traces in the (r, t)-plane it is also possible to plot all the thermodynamic and dynamic properties of the explosions (see References 7, 8, 18, 21 and 24, for example) as functions of time or radial distance. Contours of constant particle velocity and density are shown in the (λ, τ)-plane in Figures 12 and 13, respectively. The decrease in density behind the incident and reflected rarefaction waves is quite apparent. The particle velocity however is increased through the incident rarefaction wave and decreased through the reflected rarefaction wave until it is zero at the origin. The density in front of the imploding shock wave near the origin is very small. The imploding shock also induces large negative velocities as it nears the origin. The effects are felt

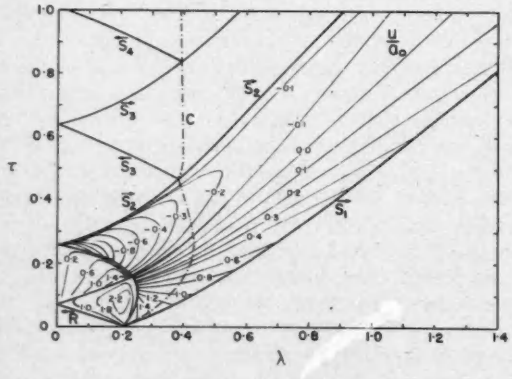

Figure 12
Lines of constant particle velocity in the (λ, τ)-plane. Case He/Air (see Figure 10)

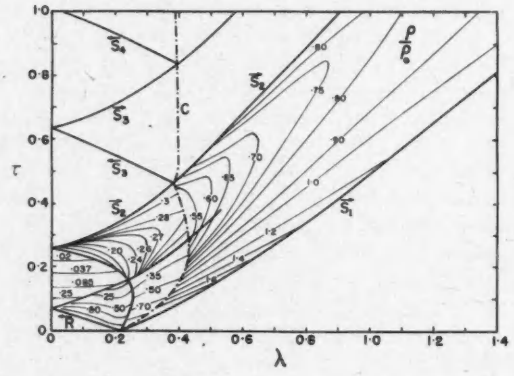

Figure 13
Lines of constant density in the (λ, τ)-plane. Case He/Air (see Figure 10)

over the entire flow field and it is seen that a line of zero particle velocity exists behind the exploding primary shock wave. This is the beginning of the negative phase, and the pressure becomes subatmospheric to the left of this contour. It is of interest to note that the constant density lines in the (τ, λ)-plane resemble their steady flow hypersonic counterpart in the (x, y)-plane, for a body whose axisymmetric shape is given approximately by the contact surface locus in the (t, r)-plane (the blast wave analogy would really apply to the cylindrical explosion, since the spherical blast involves four dimensions and it has no analogue in steady flow).

A second shock wave is also usually observed in the steady flow case. However, it always appears to be coupled with some overexpansion at the shoulder of a flat plate with a cylindrical nose, say, where the boundary layer thins and a recompression is necessary for the streamlines to match the body contour. Unlike an explosion, the second shock wave in supersonic flow appears to be caused by viscous effects, but this has not been verified analytically.

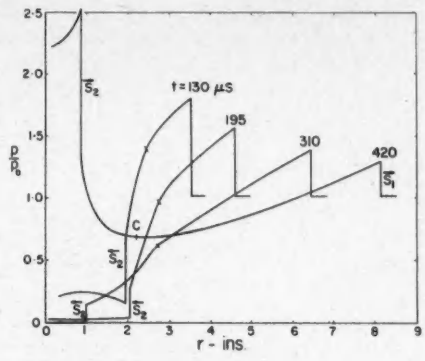

Figure 14
Pressure profiles at various times after an Air/Air explosion (see Figure 9)

As an example of a typical profile, the variation of pressure from the main shock front to the centre of the explosion is shown in Figure 14. (Any number of such profiles, or of density, temperature, particle velocity, dynamic pressure, and the static and dynamic pressure impulses, can be drawn from the detailed tabulated results.) The pressure profiles are shown for times of 130, 195, 310 and 420 μ sec. The contact surface is identified by a bar. At 130 μ sec the rarefaction wave has already reflected from the origin where the pressure is quite low. The second shock S_2 is imploding on the origin and the main shock S_1 has covered over 2 inches. As time goes on, the pressures behind the main shock and in front of the second shock are dropping, giving rise to a weaker first shock and a stronger second shock wave, respectively. At 420 μ sec, S_2 has reflected from the origin and is very much stronger than S_1, which it is now following.

The variation of temperature with time at the origin for the air blast is shown in Figure 15. It is seen that the temperature undergoes extreme changes from the reflected rarefaction wave to the reflected imploding shock wave (20°K to 3000°K). The origin is a singular point, and Guderley[26] has shown that the imploding shock wave in a perfect gas approaches infinite strength when it reaches the origin. For an imperfect gas (or perfect gas) considering viscosity and heat conduction this would hardly occur, furthermore the continuum equations may not apply very close to the origin. However, this is not the reason why the temperature (or any other thermodynamic quantity) remains finite on the present graph. It is due to the artificial viscosity that spreads the shock wave over about 6 mesh points and consequently it is not possible to approach the origin to within a few hundredths of an inch. For all practical purposes this is quite sufficient. The experiments conducted at UTIA indicate a finite shock velocity at the origin, within the limits of resolution of the (r, t)-plane schlieren records for cylindrical and spherical flows.

The question why the second or imploding shock wave occurs is often asked. It arises as a result of the spherical or cylindrical nature of the flow and can be understood by observing the path of the contact front, which indicates the manner in which the interior high pressure gas expands to its nearly stationary value at a pressure somewhat below the ambient atmosphere. As this front decelerates, it sends out ahead of itself rarefaction pulses that overtake and decay the primary shock. However, behind it compression pulses are sent out that steepen into the second shock wave. (The behaviour is qualitatively similar to the one-dimensional problem of impulsively accelerating a piston to a uniform velocity and then decelerating it instantaneously.) Such an effect does not occur in the planar case, where initially the contact front moves at a uniform velocity before it interacts with the shock or the rarefaction wave.

It might be noted that in the case of an implosion, the motion of the contact front is such as to generate in front of it compression pulses or Mach waves to further increase the strength of the imploding shock wave. However, behind it rarefaction pulses are produced. Consequently, a second shock cannot occur in an implosion. Furthermore, these rarefaction pulses make it possible to have a weaker initial rarefaction wave for a spherical implosion than in a shock tube flow. The inward motion of the contact front is stopped by the reflected imploding shock wave.

Although explosion experiments have been made using spheres from 1 inch to 5 inch diameter, the 2 inch diameter spheres have proven most satisfactory for the present 12 inch diameter field of view schlieren system. The 1 inch diameter sphere shrinks the phenomena at the origin while the 5 inch diameter magnifies it too much in many cases. Consequently, most of the blast effects will be illustrated with the results from the 2 inch diameter spheres.

Figure 16 shows a sequence of four shadowgrams that illustrate the bursting process of a 2 inch diameter glass sphere, pressurized at 300 psi, when it is hit with a ½ inch diameter mallet head and the subsequent development of the flow and the shock wave. The mallet head is attached to the slender rod which is part of a solenoid actuated breaker mechanism. At the top of the figures appears the rubber coupling that holds the stem through which the sphere is pressurized. The foil or wire at the right side forms part of the

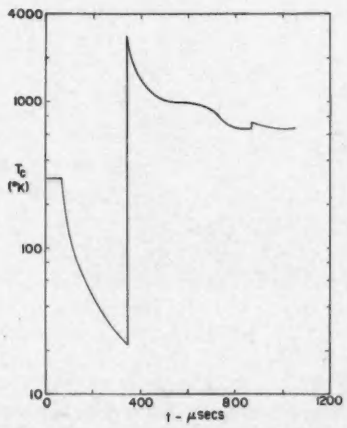

Figure 15
Temperature at the origin as a function of time after an Air/Air explosion (see Figure 9).

(a)

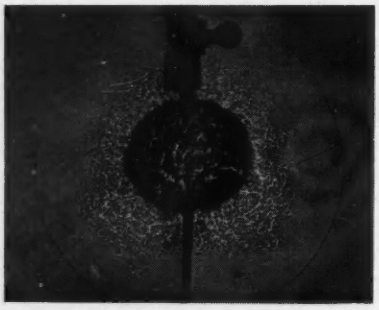

(b)

(c)

(d)

Figure 16

Spark shadowgrams of the explosions generated from a 22 inch diameter pressurized glass sphere. Case Air/Air $p_4 = 300$ psi, $p_1 = 14.7$ psi, $T_4 = T_1 = 300°K$, times after breaker struck the sphere, in μ sec: (a) 200, (b) 255, (c) 375, (d) 850

triggering circuit. It is seen that the gas rushes out through the fractured glass to generate compression waves which coalesce to form the shock wave. The contact region exhibits turbulence owing to its passage over the jagged glass fragments and its front is therefore irregular. Although this has an effect on the shape of the shock front at small times, the wave soon stabilizes and becomes perfectly spherical as shown in Figure 16c. The mallet blow affects the collective shape of the glass fragments so that they assume an ellipsoidal form as in Figure 16d, where the appearance and diffraction of the second shock wave can also be seen[24, 27]. The glass fragments are not small. It is only when they strike the wall of the steel sphere that they are pulverized.

Figure 17 is a schlieren record of the bursting of a 2 inch diameter glass sphere taken with a high speed, multi-source spark camera[28]. In this case the sphere was ruptured through overpressure alone. A band of conducting paint circled the sphere and when the paint was severed it supplied the pulse for triggering the spark sources. The central frame, which is on the optical axis, is circular (1 inch diameter) and is used for alignment purposes only. The remaining 8 frames are on a 2⅞ inch diameter pitch circle and undergo vignetting owing to the off-axis location of the spark light sources of the schlieren system[29], whose 12 inch diameter beams also transluminate viewing windows of identical size. All the 9 frames are taken on standard 4 inch × 5 inch Kodak Royal Pan cut film. The framing sequence is from 1 to 8, at intervals noted in Figure 17. The growth of the explosion is illustrated very well in this series. Especially noteworthy is the second shock wave in frame 6, and its disappearance in frame 7.

The same type of blast is shown in Figure 18, which is a schlieren photograph of the (r, t)-plane. The paths of the main shock wave, the second shock waves, the front of the contact region and the glass fragments are readily seen. From this and many other records it can be concluded that the imploding second shock and its reflection at the origin advance at finite speeds. The glass sphere breaks up in about 50 to 60 μ sec and the fragments accelerate to velocities of over 200 ft/sec. As a result, the shock front does not form instantly but as a consequence of coalescing compression waves as noted above. This can be seen in Figure 18 at small times and is similar to the formation process of plane shock waves in a shock tube[30].

A comparison of theory and experiment for the case of the air blast is shown in Figure 19. Owing to the finite duration of the breaking process of the glass sphere, the actual primary shock takes some time to form and to achieve full strength, and consequently it falls behind the theoretical wave. The glass fragments are quickly accelerated to a uniform velocity ($\sim$ 250 ft/sec) and represents an equivalent loss in energy available to drive the explosion ($\sim$ 20%). These effects cause the second shock to implode about 15 μ sec late. However, it races on and soon does match the theoretically predicted shock trace. The oscillations of the contact front are much milder than predicted by theory, and this no doubt arises from the

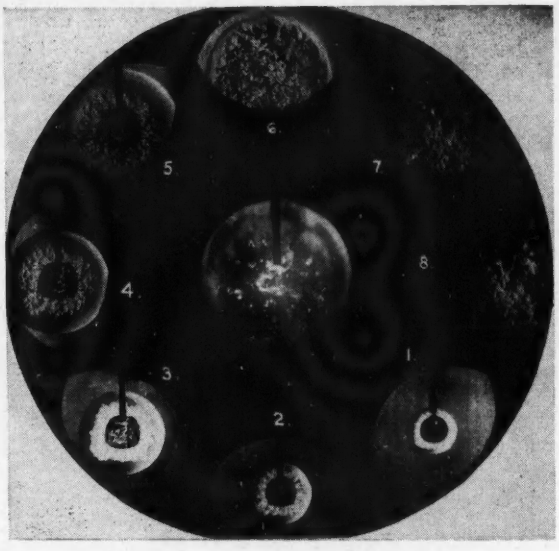

Figure 17

High speed schlieren photographs of an explosion generated from a 2 inch diameter pressurized glass sphere. Case Air/Air, $p_4 = 370$ psi, $p_1 = 14.5$ psi, $T_1 = 298°K$, times in μ sec from frame Nos. 1 to 8: 50, 100, 150, 200, 250, 800, 900, 1000

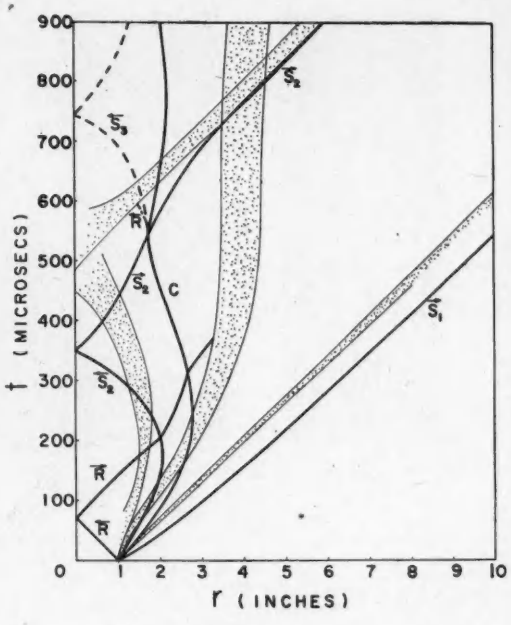

Figure 19

Comparison of theory and experiment of the wave system following the explosion from a pressurized glass sphere. Case Air/Air, $p_4 = 326$ psi, $p_1 = 15$ psi, $T_1 = T_4 = 300°K$. (Note that only the boundaries of the experimental results have been given for convenience)

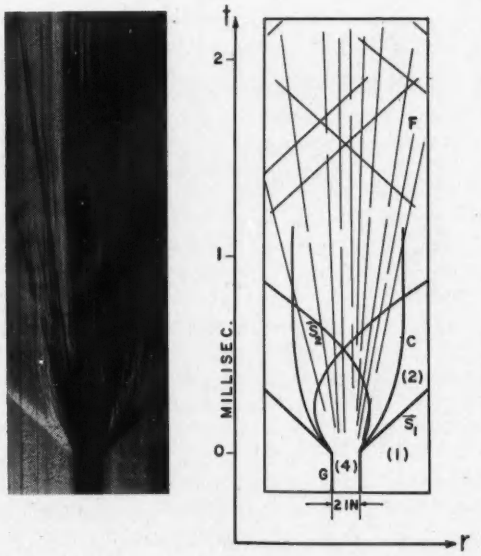

(a) (b)

Figure 18

Blast from a 2 inch diameter pressurized glass sphere
(a) schlieren record of the (r, t)-plane,
(b) explanatory sketch: G = glass sphere, F = glass fragments, S_1 = main shock, S_2 = second shock, C = contact surface.
Case Air/Air, $p_4 = 326$ psi, $p_1 = 14.4$ psi, $T_1 = T_4 = 297°K$

fact that the actual contact front becomes quite turbulent as it passes over the glass fragments. Consequently, the expected refraction process is more gradual. The large scale mixing at the contact front also causes the cold gas to occupy a larger (and asymmetrical) volume than predicted by theory. Some detailed discussions of the blast generated by an exploding glass sphere can be found in Reference 24, and more recently in Reference 25.

Two (r, t)-schlieren records for a He/Air explosion appear in Figure 20, where S_1, S_2 and S_3 are clearly seen. The implosion of S_2 is masked by the glass fragments since it occurs sooner than in air. The excellent reproducibility for the two runs for the 6 inch and 12 inch radii are shown in Figures 20a and 20b and is quite typical of all runs. The experimental results for the helium blast appear in Figure 21, and are seen to be qualitatively similar to those described for the air case. Owing to the initial formation delay, the second experimental shock wave appears where the calculated third shock occurs.

It is worth noting that the final results shown in Figures 19 and 21 were obtained in a very much improved apparatus[25], as illustrated in Figure 22, whereas the original explosion runs were made in a simple wooden box[24]. The glass spheres and cylinders were housed in a spherical shell of 3 ft diameter that could be pressurized or evacuated for explosions, implosions or wave interaction studies.

Some experiments were also conducted at the same diaphragm pressure ratio P_{41} but at half the absolute pressure level in order to verify Eq. (10), and to simu-

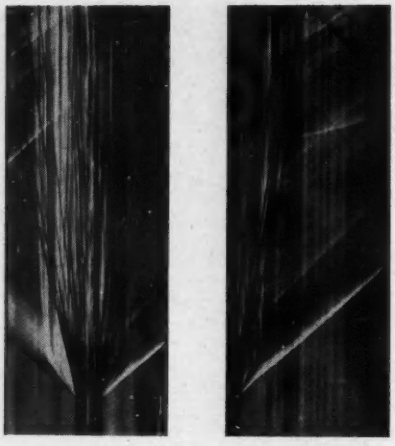

(a) (b)

Figure 20

Schlieren records of the (r, t)-plane showing the blast from a 2 inch diameter pressurized glass sphere. Case He/Air, $p_4 = 326$ psi, $p_1 = 14.7$ psi, $T_1 = T_4 = 300°K$ (a) symmetrical view; (b) view for maximum shock path

late an altitude explosion where the explosive energy density has been reduced in the same ratio as the ambient atmosphere. This is simple to do in the present case but is not so easily done with TNT, for example. The runs were in good agreement in every detail with those taken at ambient conditions (at sea level). However, this should not be misconstrued as a verification of scaling at high altitude, where sizeable excitation of internal modes can take place which are both density and temperature dependent. Under such conditions it is not possible to use the blast data obtained at sea level in order to extend it to high altitude by means of the energy parameter ϵ in a simple manner. It should be noted that TNT cannot be scaled identically at altitude, because by analogy with Eq. (10) the diaphragm pressure ratio P_a is changed as a result of the reduced ambient pressure p_1. To reproduce identical scaling, a solid explosive of lower energy density would have to be used to match the new pressure p_1 (see Reference 18).

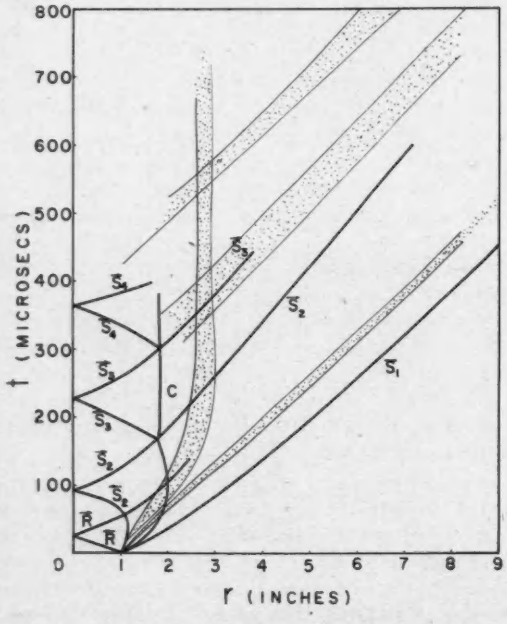

Figure 21

Comparison of theory and experiment of the wave system following the explosion from a pressurized glass sphere. Case He/Air, $p_4 = 264$ psi, $p_1 = 14.7$ psi, $T_1 = T_4 = 300°K$. (Note that only the boundaries of the experimental results have been given for convenience)

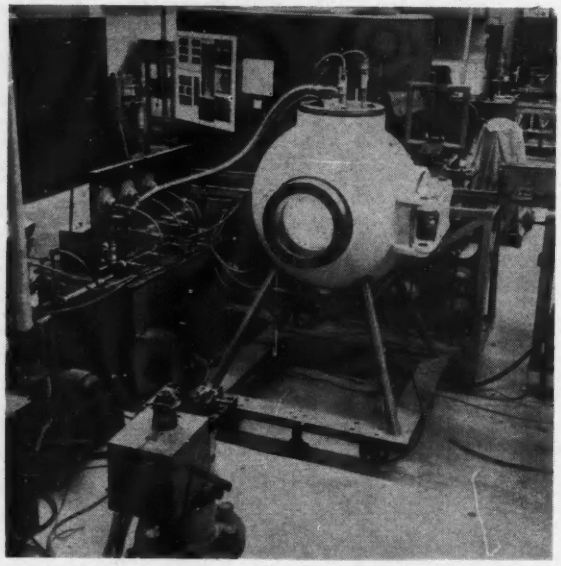

Figure 22

View of steel sphere, schlieren system, and ancillary equipment

Piezo-pressure records taken at given radii as a function of time for these types of explosions are discussed in some detail in Reference 25. As these gauges effectively measured the unsteady pitot pressure, they were useful for determining the instantaneous over-all Rankine-Hugoniot pressure jump across the incident and reflected shock waves. Miniature blast type gauges for measuring flow-pressure profiles have as yet not been developed. Two representative pressure records for Air/Air and He/Air explosions are shown in Figure 23. Good agreement was obtained between the pressure records and those of the (r, t)-plane schlieren photographs regarding shock arrival and shock strength.

It is worth noting that the head of the spherical rarefaction wave can also be seen when a gas with a high index of refraction, such as sulfurhexafluoride, is used in a large glass sphere which also helps to decrease the opacity, as shown in Figure 24. The imploding head moves at a constant sound speed of about 450 ft/sec until it reflects from the origin and then the speed decreases through the rarefaction wave. The second shock is also seen to implode and reflect from the origin about 1.3 millisec after the sphere breaks, and illustrates that the wave interaction effects

persist for a relatively long time in a low sound speed gas.

The effect of increasing the charge size or sphere diameter is well illustrated in Figure 25a when it is compared with Figure 18. For example, the corresponding distance between S_1 and S_2 is reduced by half in Figure 25a. Cranz[21] discovered that times and distances in spherical blasts of a given explosive, for example, scale directly with the radius of the charge. Consequently, if the charge radius is doubled or the mass increases eightfold, a given peak overpressure, say, will occur at twice the distance and time than those for the original charge. This property is already inherent in the present numerical solution because of the definition of τ and λ, which were made non-dimensional by the total explosion energy.

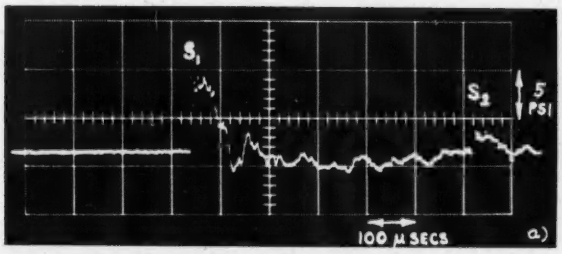

(a) Air/Air, $p_4 = 400$ psi, $p_1 = 14.7$ psi, $T_1 = T_4 = 300°K$

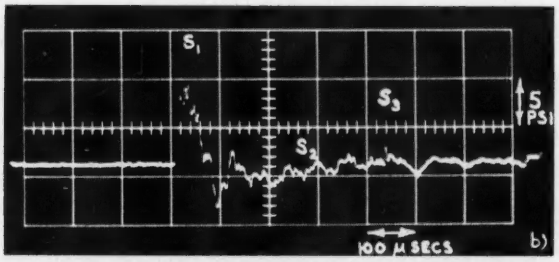

(b) He/Air, $p_4 = 326$ psi, $p_1 = 14.7$ psi, $T_1 = T_4 = 300°K$

Figure 23

Oscilloscope records of the response of an SLM piezo-pressure gauge to the blast from a 2 inch diameter glass sphere at a radius of 5.7 inches

The effect of a high diaphragm pressure ratio P_{41} is illustrated in Figure 25b, where the shock is propagating into the 10 mm Hg atmosphere at 2600 ft/sec with almost negligible attenuation. Consequently, very strong spherical shocks can be produced by using a hot, high pressure driver and a low ambient atmosphere. This result might have been expected since at the instant of rupture, conditions at a spherical or cylindrical diaphragm are as in an ordinary shock tube. That is, the planar solution applies at the instant of rupture but immediately after the cylindrical or spherical geometric decay takes effect. However, with combustion runs significant improvements in the production of strong shock waves should be possible if they are coupled with a low pressure atmosphere.

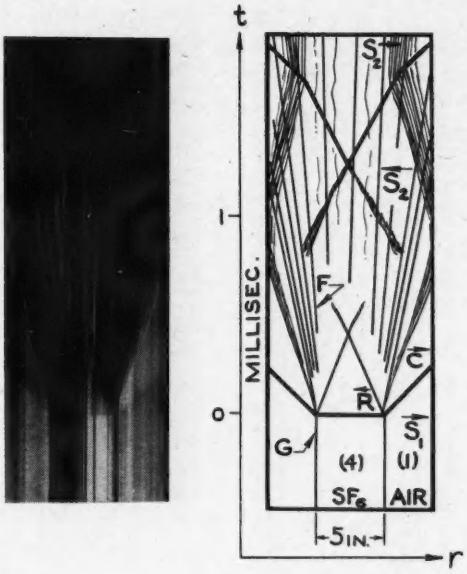

(a) (b)

Figure 24

Blast from a pressurized glass sphere containing sulfurhexafluoride
(a) schlieren record of (r, t)-plane,
(b) explanatory sketch: S_1 = main shock, S_2 = second shock, R = head of rarefaction wave, G = 5 inch diameter intact glass sphere, F = fragments of shattered sphere.
Case SF_6/Air, $p_4 = 70$ psi, $p_1 = 14.7$ psi, $T_1 = T_4 = 300°K$

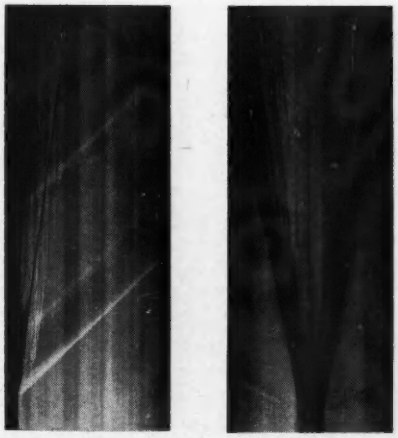

(a) (b)

Figure 25

Scaling properties of blast waves
(a) mass scaling effects of a blast from a 1.0 inch diameter pressurized glass sphere. Case Air/Air, $p_4 = 326$ psi, $p_1 = 14.7$ psi, $T_1 = T_4 = 297°K$,
(b) scaling properties at low pressure atmospheres for a 2 inch diameter glass sphere, $p_4 = 326$ psi, $p_1 = 0.013$ psi, $T_1 = T_4 = 295°K$

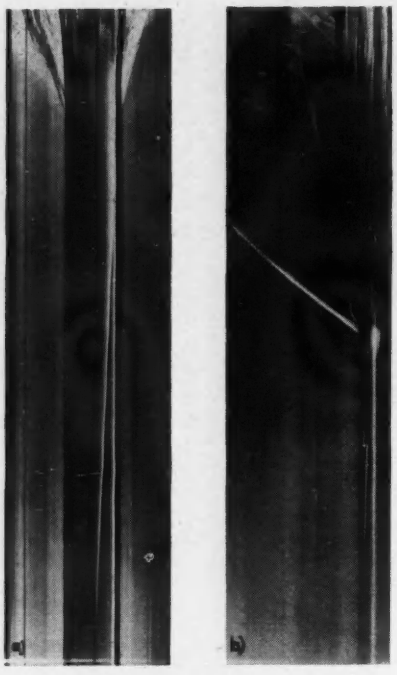

Figure 26

Combustion driven explosions

(a) spherical combustion in a 4 inch diameter × 4 inch long glass cylinder, $p_4 = 40$ psi (0.2 H_2 + 0.1 O_2 + 0.7 He) $p_1 = 14.7$ psi (Air), $T_1 = 300°K$

(b) 2 inch diameter glass sphere, $p_4 = 200$ psi (0.2 H_2 + 0.1 O_2 + 0.7 He), $p_1 = 14.5$ psi, $T_1 = 303°K$

Experiments using combustion drivers for 2 inch diameter to 5 inch diameter spheres have recently been performed at UTIA, using a stoichiometric mixture of oxygen and hydrogen diluted with 70% helium (partial pressures)[32]. The combustible gas was initially premixed in two stages, the hydrogen and helium from one tank was admitted first and oxygen from another was used to complete the charge. The three gases are now premixed (strict safety precautions must be taken) in a single high pressure cylinder to improve combustion through the homogeneity of the mixture. The mixtures are ignited at the centre of the sphere from a small spark obtained from a pulse transformer, using a 300 volt primary and 6000 volt secondary. The combustion process is illustrated in Figure 26a, where, for convenience, it is taking place in a 4 inch diameter cylinder, 4 inches long, so that it may be observed through the optically transparent end plates. The moment the spark occurred is shown by the horizontal light time. This timing marker was put on using another spark source. It is seen that the flame builds up in velocity during the first 200 μ sec and then maintains an almost constant speed of 50 ft/sec up to 1700 μ sec when it starts to decelerate[32], as a result of reflected compression waves generated by the piston-like flame front, and at 2800 μ sec the cylinder bursts. From these and other results it can be concluded that only a slow moving deflagration front occurs since the spark is very weak. The full pressure and temperature (theoretically nearly an order of magnitude greater than at ambient conditions)[16] is not realized in any of the present spheres (or cylinders) as they will normally not withstand more than about 600 psi. As a result, the spheres burst at each particular maximum strength and the combustion process is quickly extinguished by the incident and reflected rarefaction waves. Consequently, although a noticeable improvement in shock velocity is obtained the full benefit of combustion is not realized. Figure 26b illustrates this point. It is seen that the second shock wave reflects from the origin very early (less than 100 μ sec after rupture) owing to the predominantly hot helium in the driver gas mixture. An acceleration of the main shock wave occurs after about 50 μ sec and its maximum speed is only 2000 ft/sec. Therefore, the most significant improvement in shock strength would be obtained if the combustion drives were coupled with stronger spheres bursting in a low pressure atmosphere. Further details will be found in Reference 32.

Some earlier attempts to generate spherical implosions may be found in Reference 25. In the present experiments, the 3 ft diameter steel sphere was pressurized up to 125 psi, which is the limiting pressure of the existing windows in the sphere. The glass sphere, up to 5 inch diameter, was either evacuated and broken with the solenoid-operated breaker or the sphere failed automatically at its weakest section, owing to the crushing effect of the ambient atmosphere. Two representative results are shown in Figures 27 and 28.

Figure 27 is a high speed schlieren record taken at 50 μ sec intervals of an implosion from a 5 inch diameter glass sphere. It is seen that, when the mallet hit the sphere, the fragments that formed the lower cap

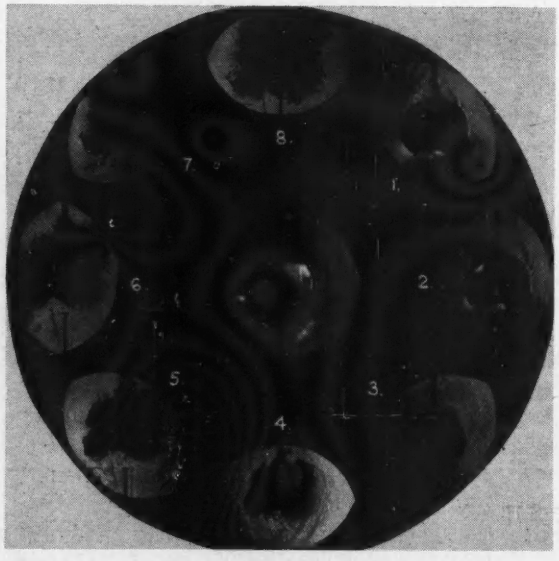

Figure 27

High speed schlieren record of an imploding 5 inch diameter sphere. Case Air/Air, $p_4 = 15$ psi, $p_1 = 100$ psi, $T_1 = T_4 = 300°K$. Times from 1 to 8 in μ sec, 900, 1100, 1300, 1600, 1900, 2200, 2500, 2800: mechanical break

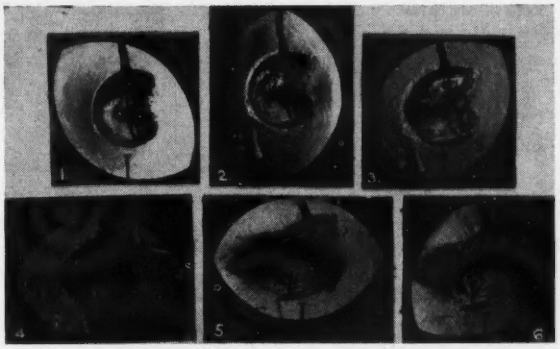

Figure 28

High speed schlieren record of an imploding 5 inch diameter glass sphere. Case Air/Air, $p_4 = 75$ psi, $p_1 = 125$ psi, $T_1 = T_4 = 300°K$. Times from 1 to 6 in μ sec, 600, 800, 1000, 1200, 1800: auto break

were carried inside the sphere by the inrush of high-pressure air. Unlike the explosion cases, the glass sphere did not fragment instantly, illustrating that a compressive load tends to keep it intact. The very interesting fringe pattern that covers the field consists of Mach waves that have been generated by the spherical rarefaction wave moving into the gas at rest. (The knife edge in the schlieren system was vertical and to the right looking from the camera. Therefore, light areas on the left of any frame are indicative of expansions and dark areas of compressions and vice versa on the right hand side.) The low pressure region around the periphery of the broken sphere caused by the inflow is clearly seen in frames 1 and 2 in the region of the lower cap. The shower of glass fragments soon impinged on the remainder of the sphere and broke it up, and then emerged through the upper cap of the sphere. The resulting flow was completely non-uniform.

Figure 28 illustrates a similar implosion run, but this time the sphere was broken by the crushing load of the external pressure. The painted conducting ring, which is clearly seen, supplied the trigger pulse for the camera. The right hand side of the sphere failed first as shown in frame 1. This time it is evident that the entire sphere has cracked since there is an efflux of gas from the sphere cracks on the left hand side. It must be concluded that compression or shock waves were formed by the piston action of the inrushing air, such that the pressure and temperature inside the broken glass sphere locally exceeded the ambient pressure. The density of the gas however is still lower than ambient (white). The glass fragments formed a "shaped charge" that completely penetrated and obliterated the left side of the sphere, as seen in the remaining frames.

A similar type of implosion is shown in Figure 29, which is a schlieren photograph of the (r, t)-plane. A 5 inch diameter sphere containing air at 300 mm Hg was used under an external pressure of 65 psi of 30% SF_6 and 70% air, in order to get a high index of refraction for the schlieren flow visualization. Rarefaction wave pulses are seen for about 800 μ sec to the left of the record (black lines) and when the glass fragments start moving towards the origin, the expansion appears stronger. About 400 μ sec later the fragments have reached their minimum collective apparent diameter and are then swept outward by the compression wave (broad black band on the right). The inner compressed air also is seen to be moving out at the left as a lower density (black) flow. Qualitatively therefore, the correct type of implosion record is obtained except that the shattering process does not take place instantly, and the waves form gradually. The interior flow is completely hidden by the opaque glass fragments so that it is not possible to tell whether any sharp imploding shock wave exists.

In view of the high speed schlieren records of the (x, y)-plane and those of the (r, t)-plane it must be concluded that this method of generating spherical implosions will not prove successful until a type of glass "diaphragm" is found that will shatter uniformly and very rapidly, and even then interior observations may prove impossible. The present results substantiate those obtained previously in Reference 25.

In summary, one can state that the use of pressurized glass spheres for generating spherical explosions has proved quite successful. The agreement with theory is satisfactory, considering the limitations that are imposed when a physical diaphragm, which has mass and takes a finite time to break up, is introduced. The motion of the second shock wave in the interior

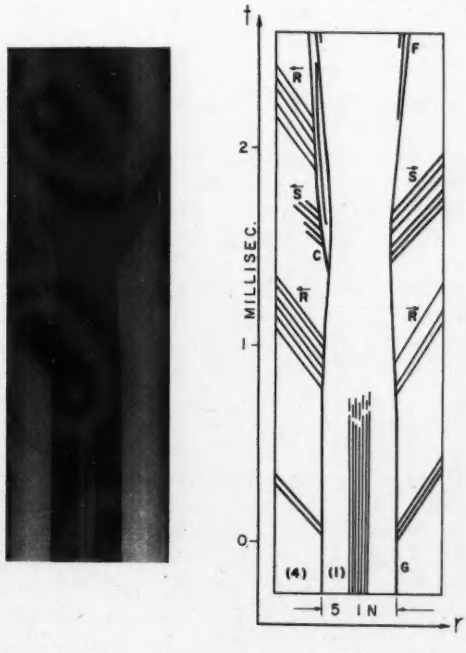

Figure 29

Spherical implosion

(a) schlieren record of the (r, t)-plane showing an imploding 5 inch diameter glass sphere

(b) explanatory sketch: G = glass sphere still intact, F = fragment of shattered sphere, $p_4 = 65$ psi (0.3 SF_6 + 0.7 Air), $p_1 = 5.8$ psi (Air), $T_1 = T_4 = 298°K$

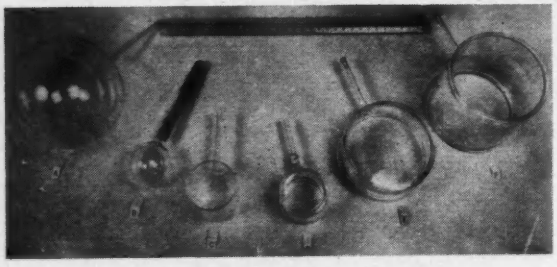

Figure 30

Types of glass spheres and cylinders used for explosion and implosion experiments

(a) 125 mm diameter × 1 mm wall, 60 gm,
(b) 50 mm diameter × 1 mm wall, 20 gm, in holder,
(c) 50 mm diameter × 65 mm long × 65 mm long × 1½ mm wall, 40 gm, open end,
(d) 50 mm diameter × 50 mm long × 1½ mm wall, 50 gm, closed end (3.2 mm wall),
(e) 100 mm diameter × 50 mm long × 3 mm wall, 200 gm, closed end (3.2 mm wall),
(f) 100 mm diameter × 100 mm long × 3 mm wall, 300 gm, closed end (3.2 mm wall)

and exterior gas has been established. There is little doubt from the schlieren records that the second shock wave does not reach infinite strength as it implodes and reflects at the origin as expected for a viscous, heat-conducting gas. Attempts were made to photograph the luminosity that might have been produced at the origin in argon and air but without success. This substantiates that even if strong imploding shocks were generated, the amount of gas affected by excitation at the origin is negligibly small.

Cylindrical explosions and implosions

During the past few months glass cylinders have been used to generate explosions and implosions[33, 34]. Open and sealed end cylinders have been used for this purpose (Figure 30). The sealed end cylinders were made by the Corning Glass Co., with glass end plates fused to the cylindrical body with a minimum of optical distortion. Both types of cylinders were held quite rigidly in a frame between two glass plates, approximately 12 inch × 12 inch × ¾ inch, in order to assure that a cylindrical flow geometry was maintained.

The cylinders were either pressurized and ruptured, using a solenoid-operated mallet, or they were ruptured by overpressure, when filled with a gas or combustible mixture of oxygen-hydrogen and helium (as for spheres), and an exploding wire was used for ignition in case of open end cylinders. Rubber gaskets and O-rings held the cylinders against the glass plates, which were drilled and fitted with two ⅛ inch diameter, copper electrodes. A 0.0025 inch diameter copper wire was stretched across the electrodes in the centre of the cylinder, and it was exploded by discharging an energy of 50 joules stored in a 25 μf capacitor at 2000 volts. The wire ignited the gas mixture and at a later time the cylinder ruptured and generated an explosion.

A blast from a 2 inch diameter closed end cylinder appears in Figure 31. It is seen that the wave system is very similar to the spherical explosion. The head of the rarefaction wave H is easily visible now through the flat end plates. The first shock S_1 and the imploding and exploding motion of the second shock S_2, as well as the path of the contact front C, can readily be distinguished.

Figure 32 shows a much stronger explosion from an open end cylinder. The rarefaction wave and the main shock wave are very clear in this record. The second shock wave is obscured by the internal flow and reflected shock waves. Sound pulses are seen in the interior of the pressurized cylinder (50 μ sec) prior to its complete collapse. The pulses which arise from the initial cracks in the cylinder are not seen in the exterior atmosphere, owing to its low density perhaps or the asymmetry of the break.

Figure 33 shows a cylindrical blast, using a stoichiometric mixture of oxygen and hydrogen diluted with 70% helium at a total pressure of 88 psi, which was initiated by an exploding wire. The moment the wire exploded is indicated by the luminous streak across the schlieren record. The shock wave from the exploding wire and its attached rarefaction wave move back and forth within the cylinder and distort the motion of the flame front. The burning mixture appears as a white region, and is finally extinguished by the expansion waves about 1100 μ sec after initiation. The black line through the centre is the position of the electrode. It can be seen that the shock wave was accelerating and finally was moving at 1700 ft/sec at a radius of about 5 inches from the centre of the explosion. Since every cylinder has its own bursting

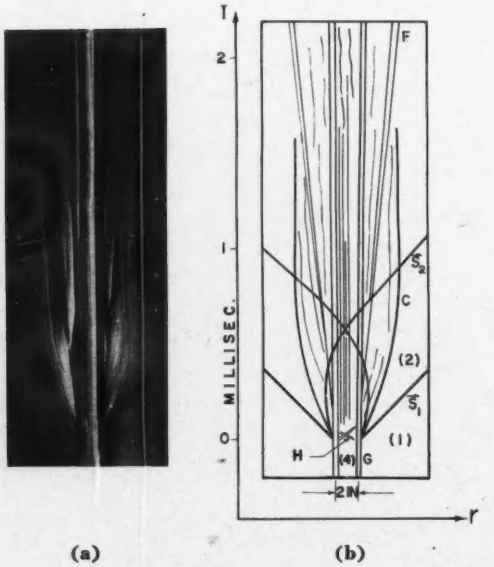

Figure 31

Blast from a 2 inch diameter pressurized glass cylinder (a) schlieren record of the (r, t)-plane, (b) explanatory sketch: G = sealed end glass cylinder 2 inch diameter × 2½ inch long: mechanical break F = glass fragments, S_1 = main shock, S_2 = second shock, H = head of rarefaction wave, C = contact surface. Case Air/Air, $p_4 = 115$ psi, $p_1 = 14.5$ psi, $T_1 = T_4 = 297°K$

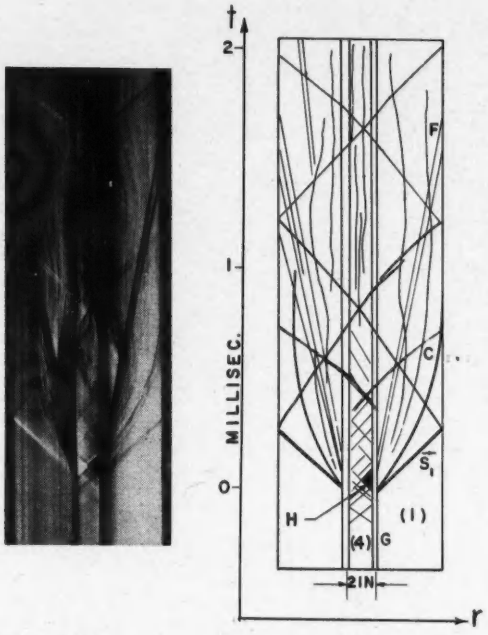

Figure 32

Cylindrical explosion from a pressurized open end glass cylinder 2 inch diameter × 2½ inch long
(a) schlieren record of the (r, t)-plane,
(b) explanatory sketch: G = open end glass cylinder, mechanical break, F = glass fragments, H = head of rarefaction wave, case Air/Air, $p_4 = 350$ psi, $p_1 = 14.7$ psi, $T_1 = T_4 = 300°K$

pressure, which is below the calculated constant volume pressure conditions, combustion will continue for a short time after rupture and will help to accelerate the shock front, but because the breaking strength of a cylinder is relatively low the full benefit of the high pressure and temperature due to combustion is not attained. The motion of the second shock is rather obscured in the combustion runs and it is difficult to distinguish.

From the above it can be concluded that it is quite feasible to generate cylindrical explosions using glass cylinders by any of the three methods noted. The combustion runs are more desirable when strong shock waves are required and for their reliability in obtaining a successful break. However, their initial conditions are not as well known as in explosions initiated with a mechanical breaker. Comparing the cylindrical and spherical explosions it can be stated that the spherical bursts are much more reliable and symmetrical. They do not suffer from gasket leaks and are much simpler to set up. In addition, the cylindrical explosions are not free from side-wall boundary layers.

For the analysis of the cylindrical explosions, Eqs. (12) to (17) may again be solved, employing the method developed by Brode. This has not yet been done, since it was felt necessary to establish first a successful method of generating such explosions prior to undertaking extensive calculations.

It was noted previously that a real difficulty with spherical implosions from ruptured glass spheres is that the interior flow is obscured by the opacity of the fragmented glass. To overcome this difficulty some cylindrical implosions were initiated using sealed end and open end cylinders[34]. The sealed end cylinders were not found to be useful for this work, as the end plates shattered and the net effect was an obstructed interior view nearly similar to the spherical implosions seen above. Large open end cylinders appear to offer some promise and their use is presently being investigated. Analyses also in this case will not be attempted until a feasible experimental method has been established. It should be noted that Payne[35] has numerically solved a number of cases for the cylindrical implosion. No second shock wave was found for the reasons given previously. Payne used a form for the artificial viscosity that did not prove as useful as the one employed by Brode (Eq. (17)), since it appeared to affect the entire flow field to some extent. It would be quite worthwhile to repeat this work using an equation of the form given by Eq. (17) for the artificial viscosity. Such calculations would be initiated at UTIA if a successful method of generating cylindrical implosions were developed.

Planar analogues of explosions and implosions

If a very short chamber relative to the channel is used to establish a shock tube flow, then the rare-

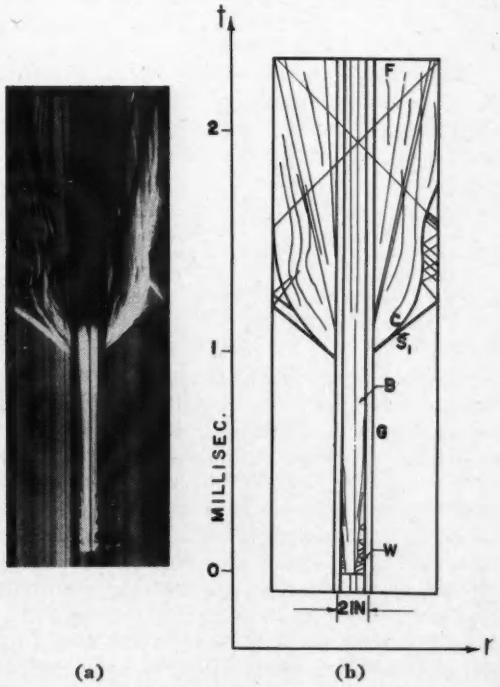

Figure 33

Combustion driven cylindrical explosion
(a) schlieren record of the (r, t)-plane,
(b) explanatory sketch: G = open end cylinder 2 inches × 2½ inches; auto break, F = glass fragments, E = exploding wire, W = wire generated shock, B = burning flame, $p_4 = 88$ psi (0.2 H_2 + 0.1 O_2 + 0.7 He), $p_1 = 14.7$ psi, $T_1 = 299°K$

faction wave will quickly reflect from the closed end, interact with the contact region, overtake the shock wave and establish a process of shock decay. A peaked type shock wave profile is then formed which resembles a blast wave. If the initial shock is very strong then the shock motion may perhaps have a type of strong planar blast wave decay similar to Eq. (8), after it had engulfed a certain mass of air corresponding to the spherical cases shown in Figures 7 and 11. In the planar case, a graphical or numerical solution using the method of characteristics would be quite feasible, especially since many of the interaction problems can be solved in closed form[16].

In a similar manner, when the channel of a shock tube is made very small compared with the chamber, then a flow analogous to an implosion can be generated. The shock wave "implodes" on the origin with uniform strength (end of channel), reflects from the closed end with an increased uniform strength, interacts with the contact surface and then with the rarefaction wave where it is decayed. Of course, it is only the attenuation of the shock wave that bears an analogy with the cylindrical and spherical blast waves in the explosion or implosion cases. Before that time the waves and states are uniform in the planar case and non-uniform in the cylindrical and spherical cases. It would be of some interest to investigate these two problems analytically and experimentally in a shock tube such as the Wave Interaction Tube at UTIA, which is well suited for this purpose.

BLAST WAVE SIMULATORS

The effects of blast waves can be simulated by different methods and to different degrees. Each method has its own inherent advantages and drawbacks. The following methods have been used:

(1) full scale tests[2],
(2) chemical explosions in open ranges[26, 27],
(3) chemical explosions in closed ranges[21],
(4) shock tubes,
(5) conical sector tubes[28], and
(6) explosively driven (Primacord) pressure vessels[29].

A full discussion of these facilities is beyond the scope of the present paper. However, it is worth noting that complete simulation can only be achieved in a full-scale test but with the inherent disadvantages of hazards, expense, and the lack of laboratory type of control and repeatability. The other facilities may simulate various properties of explosions and some of these better than others. For example, the blast from pressurized glass spheres or cylinders is most useful for the investigation of the shock wave and the flow properties, since the overpressures and their durations are comparatively small for significant size model tests. Shock tubes are very useful for the determination of aerodynamic loads on rigid models in a blast[40] and for proving structural components. Typical schlieren photographs of the flow over slender[41] and gable models with relatively short and long shock-transit times are shown in Figures 34a and 34b. In both cases the shock diffraction over the models gives rise to Mach-type shock reflection, which includes a vortex and a slipstream (contact surface). In Figure 34a the flow behind the shock wave is just supersonic and in Figure 34b it is subsonic and contains a series of Mach waves generated in the flow. For a slender solid model (Figure 34a), with a short shock-transit time or rapid pressure equalization, aerodynamic drag may be predominant. However, for a sizeable panelled structure (Figure 34b) with a long transit time, then peak pressures and the pressure impulse may cause the most severe damage.

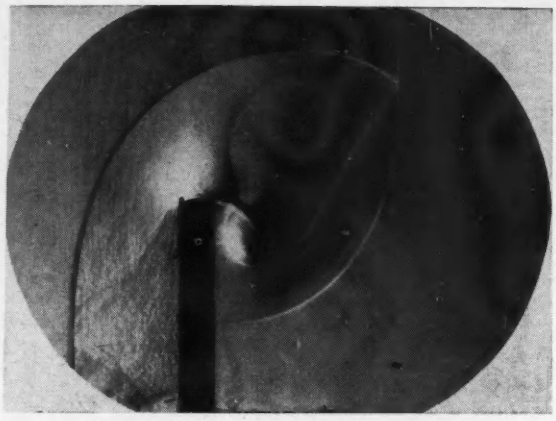

(a) diffraction of a plane shock wave over a slender model. Model thickness ½ inch, $p_1 = 185$ mm Hg, $P_{21} = 5.20$, $M_s = 1.04$, 2 inch × 7 inch shock tube, primary shock moves from left to right

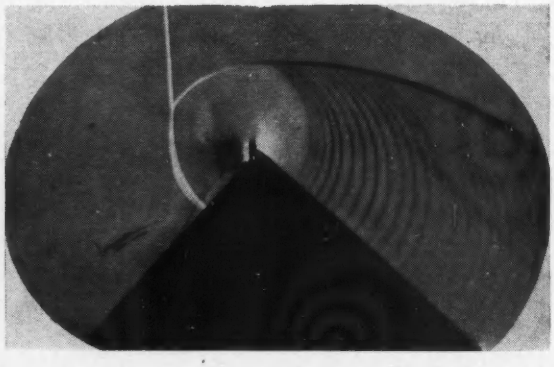

(b) diffraction of a plane shock wave over a gable model. Primary shock wave moves from right to left and has a subsonic flow behind it

Figure 34

For dynamic testing of sizeable structural components, a shock tube facility would become enormously large and expensive. For such tests high overpressures and long flow durations (of the order of the response time of the structure) are required, and explosively driven simulators, such as specially designed high pressure vessels[29] or sector tubes[28], appear to be very useful. It is worth noting that since all of the blast energy in a sector tube can be concentrated over a small solid angle rather than over 4π steradians, very large amplification factors are theoretically possible for very small cone angles [$(4/d\theta)^2$, or 5.25×10^4

for a 1° cone angle]. Consequently, relatively small charges can be used to produce effectively large explosions. In practice, such high magnification factors are not obtained owing to losses that arise from elastic and viscous effects. However, the experimentally obtained gain is still very impressive[28].

A blast from relatively small hemispherical TNT charges exploded in a steel hemisphere of about 50 to 100 ft in diameter, for example, would only have a magnification factor of two for the same charge weight. However, it would be more versatile than a narrow sector tube with regard to the number of models that might be tested per run at different radii, and it would have the advantage of simulation of terrain and water surfaces as well as the possibility of testing at low pressure (high altitude) testing. With a 7 lb hemisphere of TNT (1060 cal/gm) it would be possible to obtain an overpressure of 25 psi at 11 ft from the origin, about 3.4 millisec after the initiation of the blast. The positive phase would last about 2.2 millisec and the negative phase about 5.6 millisec. At a 50 ft radius, the overpressure behind the blast wave is down to 1.5 psi and should not present any structural difficulty. On the other hand, a pressure of 25 psi is reached at about 1560 ft in a 20 kiloton TNT blast, giving pressure profile durations of about 140 times as great as for the 7 lb hemisphere. Consequently, for dynamic structural tests, flow times of several hundred milliseconds would be required.

SOME RESEARCH APPLICATIONS OF EXPLOSIONS GENERATED FROM PRESSURIZED GLASS SPHERES AND CYLINDERS

It was noted previously that successful explosions can be generated from pressurized glass spheres and cylinders. Blasts produced in this manner are relatively safe in comparison with chemical sources, and the initial conditions are well known. The spherical explosions have the added advantage of the absence of any viscous boundary layer effects, and are even simpler to generate than cylindrical blasts. Consequently, spherical explosions produced in this manner can be applied to a variety of interesting research problems, such as underwater explosions, blasts in a supersonic flow[18], shock wave collisions[14], shock wave diffractions over various models, shock wave refraction at gaseous and liquid interfaces and shock waves at extremely low densities without boundary layer interference. Properties of cylindrical and spherical deflagration and detonation waves may well be investigated using the same techniques.

In the following subsections a few of the problems noted previously will be considered. As soon as the flow loses complete spherical symmetry, the analysis becomes very complex. It is necessary to introduce an additional space variable and more difficult boundary conditions. Consequently, problems on spherical shock wave collision, diffraction and refraction have as yet not been solved numerically, using the methods developed by Brode, as they tax the capabilities of present day high speed computers. It is hoped that such solutions will become possible in the near future. In the meantime experimental feasibility studies have been made of some of the problems outlined previously.

Underwater explosions

It is quite feasible to study underwater blasts generated from pressurized glass spheres, using compressed gases or combustible mixtures as drivers. Some preliminary runs have just been conducted in a commercial aquarium (8 inches × 16 inches × 10 inches deep) filled to a depth of about 8½ inches of water. Distilled water is most satisfactory as it reduces light absorption and scattering. Pressurized glass spheres 2 inch diameter containing air over 300 psi were used to produce the blasts, which were recorded with the high speed schlieren camera. One run containing 200 psi of a combustible mixture ($0.2\ H_2 + 0.1\ O_2 + 0.7$ He) was also photographed and a schlieren record of the (r, t)-plane was obtained. All the runs were self-breaks due to overpressurization. A trigger pulse to the spark light sources was provided by a painted circuit circling the glass sphere which was severed when the sphere burst.

High speed schlieren photographs of an underwater explosion generated from a 2 inch diameter glass sphere at 310 psi are shown in Figure 35a. In this experiment the schlieren system was not perfectly adjusted for the water, but rather for the air as the working medium. The record also suffers from a slight accidental double exposure which accounts for the flake-like background in some frames. Nevertheless, it does illustrate the blast phenomena quite well. In frame 1, the air-water contact surface appears as a black band and above it is the wider band of the aquarium metal framework. The sphere and its metal pipe holder are also seen. Tap water was used in the tank for this run. Frame 1 was taken 15 μ sec after the sphere ruptured. The hydrodynamic blast wave appears well formed but somewhat displaced below the ruptured sphere, which still appears intact. Unlike an air burst the glass fragments are constrained by the water from flying off. Taking half of the difference between the shock and glass sphere diameters, for a distance base line, gives the shock wave an average velocity of 1.84 inches in 15 μ sec or 12,300 ft/sec. Using a sound speed in water of 4800 ft/sec results in an apparent shock Mach number $M_s \sim 2.12$. Employing the calculated shock wave properties in water given in Reference 42, a corresponding pressure of nearly 35,000 atm would exist behind a blast wave at this shock velocity. Consequently, it must be concluded that the electronic timing, any optical refraction effects that might produce an enlarged shock wave image, and the encasement effect of the glass sphere will have to be carefully investigated before the actual velocities of the shock wave are accurately established.

Since vertical knife edges (to the right, looking from the camera) were used, the upper and lower portion of the shock do not appear so well defined. The left portion of the shock also suffers from the removal of light from an already weakly illuminated

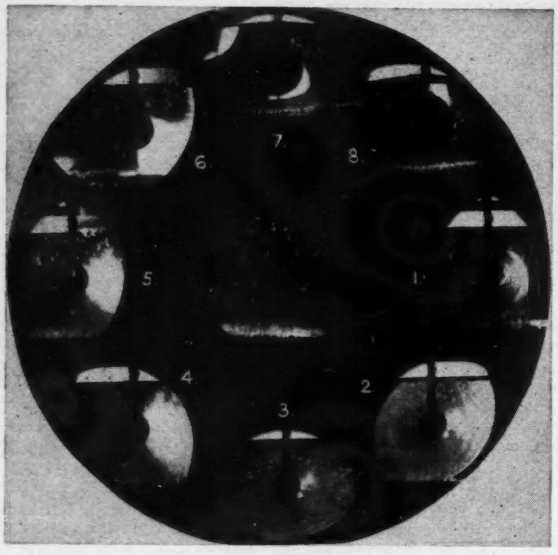

(a) High speed schlieren photograph of an underwater explosion generated from a pressurized glass sphere. Aquarium 8 inches × 16 inches × 10 inches, water depth 8½ inches, 2 inch diameter glass sphere pressurized at 310 psi, surrounding conditions atmospheric, framing rate from 1 to 8 in μ sec, 15, 60, 100, 200, 350, 700, 1300, 2000

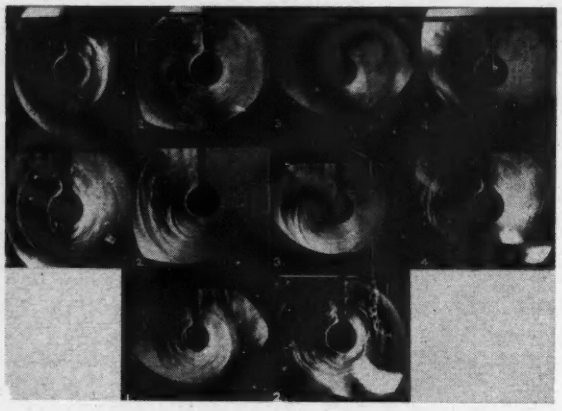

(b) High speed schlieren records of underwater explosions generated from pressurized glass spheres. Aquariums: 8 inches × 16 inches × 10 inches, water depth 8½ inches. Row No. 1: 2.1 inch diameter sphere, bursting pressure 300 psi, framing rate from 1 to 4 in μ sec, 11, 30⅜, 50, 70. Row No. 2: 2.1 inch diameter sphere, bursting pressure 365 psi, framing rate as above. Row No. 3: 2 inch diameter sphere, bursting pressure 330 psi, framing rate 20⅛ and 50 μ sec. Ambient, temperature 300°K at 1 atm

Figure 35

background. Many overtaking compression waves are seen behind the shock wave in the white area (compression) to the right of the frame. Unlike an air burst, the characteristic change from a white to a black area, as the gradients from the rarefaction zone of the peaked profile take effect behind the shock wave, is not seen here. The reflected rarefaction pulses, generated at the air-water contact surface as the main blast wave and overtaking compression or Mach waves refract at the contact surface, are seen in frame 2. These waves do travel with the sound speed in water at about 4800 fps, as will be noted later.

The compressed air bubble is seen to emerge in frame 4 and does not appear to have changed in frame 5. In frame 6 it has grown to a 3.0 inch diameter, in frame 7 to a 3.9 inch diameter and in frame 8 to a 4.6 inch diameter, giving an average velocity of about 60 ft/sec and 40 ft/sec, respectively. The air bubble appears effectively opaque, as a result of the spherical lens action of the surrounding water, which deflects the light rays very much like the glass sphere itself. In frame 7 the expanding bubble is now raising the water surface and in frame 8 this effect is still more apparent. Even in this last frame, after a flow duration of 2 millisec, the glass sphere still appears intact and its diameter is almost unchanged.

Figure 35b contains frames from three additional underwater explosions taken in similar aquariums (the glass side plates invariably broke during a run) all filled with distilled water. The schlieren system was adjusted for the water as the working medium. The improved quality of the schlieren photographs is quite noticeable. The advance of the blast wave and its refraction at the contact surface are well illustrated in row No. 1. The apparent average shock speed from frame 1 is 2 inches in 11 μ sec or 15,200 ft/sec; from frame 2, 3.1 inches in 30.4 μ sec or 8500 ft/sec. The difference between frames 2 and 3 gives 1.16 inches in 19.4 μ sec or a rapid decay to nearly 5000 ft/sec. The advance of the reflected rarefaction wave head in frames 2, 3 and 4 gives it a speed very close to the sound velocity of 4800 ft/sec.

In row No. 2, the blast wave appears to have travelled 2.5 inches in 11 μ sec or an apparent speed of 19,200 ft/sec. It is worth noting that the bursting pressure was also higher here. The reflected rarefaction wave head again has a velocity of nearly 4800 ft/sec, but somewhat slower. (A measurement of distance does not have the same accuracy as that of time. However, the velocities quoted are not meant to be definitive as the experiments are only of a preliminary nature.) In row No. 3, an average shock velocity of 7800 ft/sec is obtained for the first 20⅛ μ sec and is consistent with the previous results, as the shock decay is rather rapid. From frame 2, the average speed over the first 50 μ sec is 6100 ft/sec. The difference between frames 1 and 2 again gives an average velocity of 5000 ft/sec, which is approaching the acoustic value and is in agreement with the previous result.

The above preliminary data have shown that this method of generating underwater blasts offers some very worthwhile possibilities, and a systematic research program is presently underway. The apparent values quoted for the shock speeds were given for illustration purposes only and should not be miscon-

strued as being actual speeds. Further details will be found in future UTIA publications as they become available.

It is perhaps worthwhile to include the (r, t)-plane schlieren record of an underwater explosion, shown in Figure 36. A combustible mixture (0.2 H_2 + 0.1 O_2 + 0.7 He) at 200 psi was used as the driver gas. The instant of ignition is shown by the luminous horizontal line and the first shock wave appears about 1400 μ sec later. Poor quality schlieren (due to the flexing of the thin glass plates perhaps) make the passage of the shock wave almost invisible except at the very edges of the film strip. In this case, the hot air bubble in contact with the water gives rise to some peculiar spreading and motions of the contact region. The record was included for its qualitative value only but it does illustrate that good quantitative records should be possible. Schlieren photographs of the (r, t)-plane would be much more definitive in accurately computing the shock and air bubble velocities from these continuous-time records.

Head-on collision of spherical shock waves

An investigation of this type of interaction, using blasts from 2 inch diameter glass spheres, has proven quite successful. Since numerical solutions existed for Air/Air and He/Air explosions for spheres at 22 and 18 atm, respectively, these were chosen for the initial studies. Consequently, by the time the spherical shock waves collided they were relatively weak. Much stronger collisions can be generated by using low ambient pressures (Figure 25b) coupled with combustible driver gases. The boundary condition at the point of

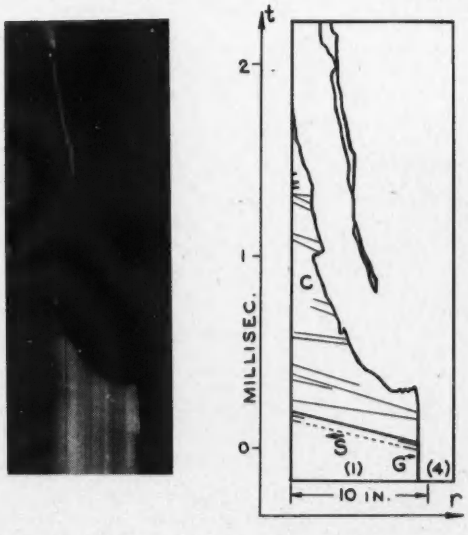

Figure 36

Underwater explosion generated from a pressurized glass sphere (a) schlieren record of the (r, t)-plane, (b) explanatory sketch: G = glass sphere, 2 inch diameter, filled with 200 psi (p_1) of a combustible mixture (0.2 H_2 + 0.1 O_2 + 0.7 He); ambient conditions, aquarium 8 inches × 16 inches × 10 inches, water depth 8 inches, surrounding atmosphere 14.7 psi at 300°K, S = main shock wave, C = constant region

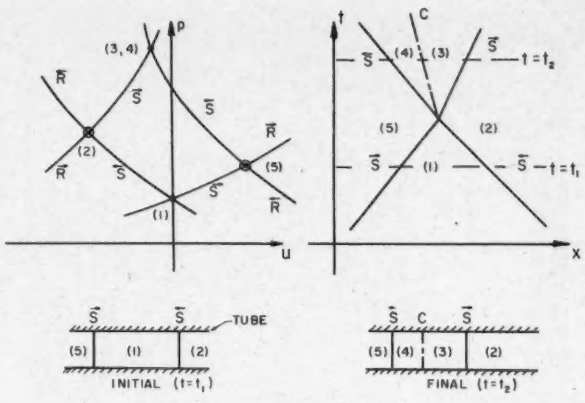

Figure 37

Head-on collision of planar shock waves in the (u, p)- and (x, t)-planes. Conditions in a shock tube before collision ($t = t_1$) and after collision ($t = t_2$) are indicated

intersection of the spherical shock waves can be determined from planar wave theory[16]. This type of interaction is illustrated in Figure 37 in the (x, t)- and (u, p)-planes. State (1) is a rest state. States (2) and (5) are the states behind the backward and forward facing approaching shock waves. It is seen that after the collision two shock waves that are separated by a contact surface recede from the point of interaction. The new states (3) and (4) have a higher pressure than the previous states and their particle velocity will follow the stronger shock wave. Once the initial shock strengths P_{21} and P_{51} and state (1) are known, the final wave strengths and states (3) and (4) can be found[14].

After the instant of interaction, new boundary conditions must be satisfied that involve both regular and Mach-type reflections. Consequently, the flow becomes asymmetrical and very complex. A solution would now contain three independent variables (two spatial and one temporal) and the reflection boundary conditions noted above. Such a solution based on the method developed by Brode has not been obtained to date.

However, the collision problem has been investigated using optical techniques, and a comparison between the planar theory and the experimental results at the point of intersection was possible. A view of the two 2 inch diameter glass spheres, with their centres 9 inches apart, and of the solenoid-operated, spring-loaded breaker mechanism, is shown in Figure 38. The same technique was employed in generating a double blast as for a single explosion, with the exception that the plunger now had two mallet heads to break the two spheres at approximately the same instant. Although there was some variation in sphere geometry and strength of the glass this was usually achieved.

Figure 39a shows a shadowgram of approaching shock waves from He/Air and Air/Air explosions. Some diffracted waves about the breaker can be seen, otherwise the blasts are as in Figure 16. In Figure 39b the shock waves have collided and penetrated. Only

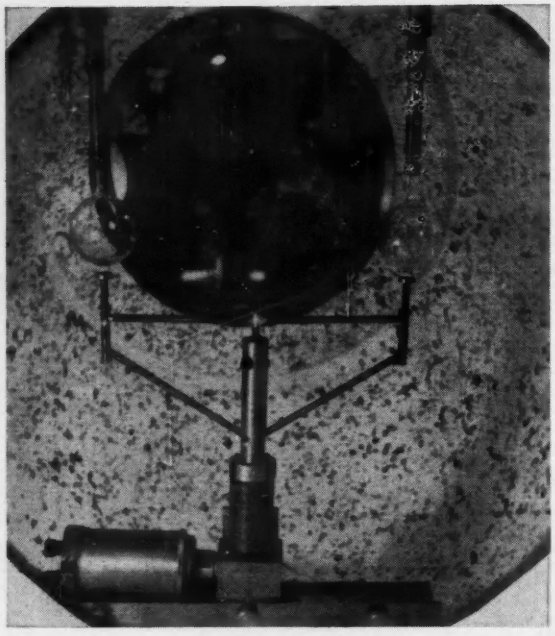

Figure 38
Breaker mechanism used for head-on collision of spherical shock waves

a small change in shock wave curvature is noted owing to the low strength of the colliding shock waves, and for the same reason no contact front can be observed in the penetration region between states (3) and (4).

A schlieren record of the (r, t)-plane of the same type of interaction is shown in Figure 40. The left-hand sphere contains helium at 500 psi and the right-hand sphere air at 250 psi. The approximate location of the contact surface is shown in the explanatory sketch. The absolute velocities of the shock waves, measured in laboratory coordinates, divided by the sound speed in state (1), are given in the caption as measured absolute shock Mach numbers. These are in fair agreement with theory. There are some difficulties involved in accurately measuring shock speeds from curved paths, and further details are given in Reference 14.

The second shock waves, in both blasts, are clearly visible. The one from the helium explosion appears sooner owing to the higher sound speed. The stationary character of the contact surfaces, after about 300 μ sec from the start of the blast, is clearly illustrated and is in keeping with the model noted previously for the generation of the second shock wave. In this record the glass fragments attain speeds of 210 and 240 ft/sec for the air and helium blasts, respectively. The fragments collide about 1500 μ sec after the initiation of the explosions. At approximately this time the shocks reflected from the steel walls of the 3 ft diameter sphere are also seen, and they implode and reflect at the origin. This process is repeated manifold.

Figure 41 shows the details of the interaction region in the (r, t)-plane for the case of two 2 inch diameter glass spheres under identical conditions, He/Air, 326 psi/14.7 psi, $T = 295°K$, except that the left sphere breaks 160 μ sec earlier. As a result a collision of unequal shock waves takes place as shown. Figure 42 shows a typical schlieren record of the head-on collision process, taken at nominal time intervals of 50 μ sec, or at a framing rate of 20,000 pictures per second. In this case, both spheres contained helium at an initial pressure of 326 psi. The series of photographs start at frame 1, where it is seen that the left sphere breaks first and as a result the shocks when they collide are of unequal strength. The development of the wave systems appears in frames 1 to 8, inclusive, and covers an interval from 100 to 500 μ sec. The shocks approach the collision point in frame 5 and have collided in frame 6. In frames 7 and 8 the forward facing shock is interacting with

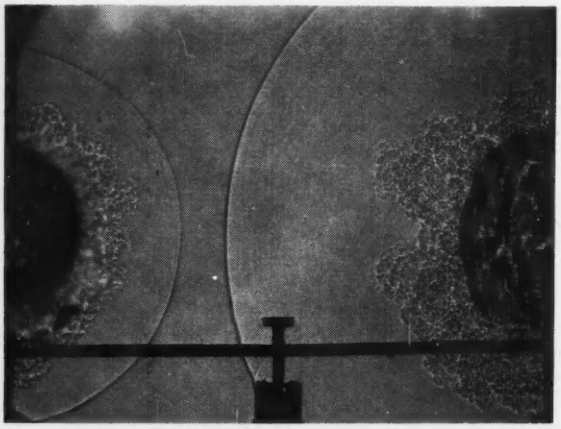

(a) left sphere, Air/Air, 400 psi/14.7 psi. Right sphere, He/Air, 326 psi/14.7 psi, $T = 298°K$, 2 inch diameter spheres, time delay 297 μ sec

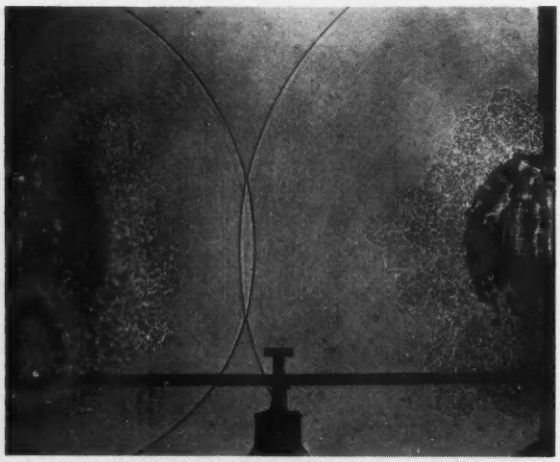

(b) left sphere, Air/Air, 400 psi/14.7 psi. Right sphere, He/Air, 326 psi/14.7 psi, $T = 295°K$, time delay = 373 μ sec

Figure 39
Shadowgrams of the head-on collision of spherical shock waves

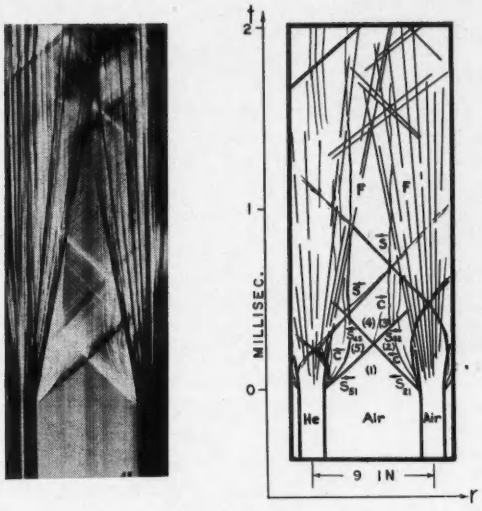

Figure 40

Schlieren record of the (r, t)-plane showing the head-on collision of spherical shock waves. Left sphere, He/Air, 500 psi/14.7 psi, right sphere, Air/Air, 250 psi/14.7 psi, $T = 296°K$, $S_{21} = 1.04$, $S_{51} = 1.24$, $S_{31} = 1.07$, $S_{41} = 0.91$

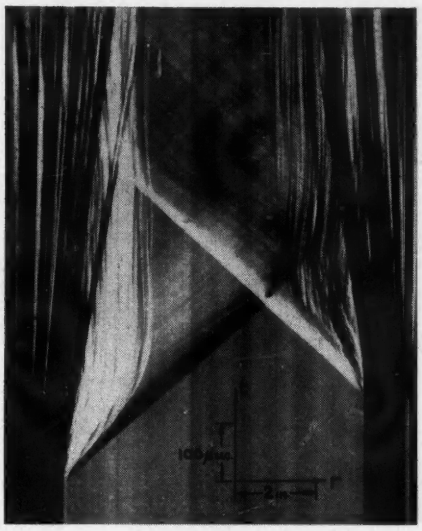

Figure 41

Detailed view of the collision of two unequal spherical shock waves. Both spheres 2 inch diameter, He/Air, 326 psi/14.7 psi, $T = 295°K$, time interval between breaks 160 μ sec

the contact region from the right sphere. The stationary character of the contact regions beyond frame 4 is quite noticeable.

Figure 43 shows a similar result at a slightly later time of 252 to 605 μ sec. Of particular interest in this series is the second shock, which has reflected at the origin and is seen to pass through the contact region in frame 4, and appears prominently in frame 6. The second shock wave from the right-hand sphere is more difficult to detect, since the schlieren knife edge is on the right and the shock tends to blend into the dark background on the photograph. Further examples and interesting details may be found in Reference 14. The above work has indicated that it is possible to generate head-on collision interactions. The actual experiments were conducted at low shock strength because of the availability of numerical solutions only for the primary blast cases. However, the same methods can be used to generate stronger shock collisions by simply using low pressure ambient atmospheres. A complete theoretical-experimental comparison was not possible owing to the lack of numerical solution for an asymmetric problem of this type. Where it was possible to apply planar wave theory, such as to the point of interaction, fair to good agreement was obtained.

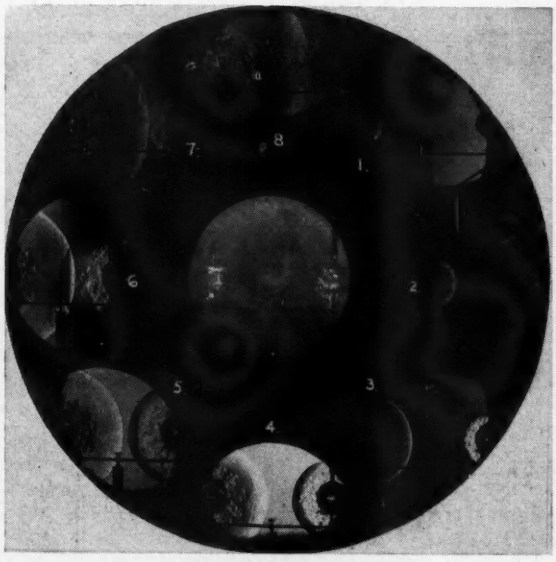

Figure 42

High speed schlieren photographs of the collision of two spherical shock waves. Both spheres 1.9 inch diameter, He/Air, 326 psi/14.5 psi, $T = 296°K$, time delays in μ sec for frames 1 to 8, 100, 150, 250, 300, 350, 400, 450, 500

CONCLUSION

Analytical solutions exist both for explosions and implosions when they are very intense and for explosions when they are very weak. For example, Taylor's self-similar solution for an intense point-source blast has been substantiated from shock speed measurements of an atomic explosion at small times, when the assumptions of constant energy and a perfect gas do not appear to seriously affect the solution. At later times when the strong shock conditions cease to apply and considerable energy has been lost through radiation, the experimental results are in good agreement with the numerical solution for the blast generated from a high pressure sphere of very hot gas. The analytical extensions to intense cylindrical and planar blast waves do not appear to be well represented by exploding wires or magnetogasdynamically driven shock waves in a T tube. In these cases it may be necessary to treat the explosion as a finite source with a more complex type of relation for the addition

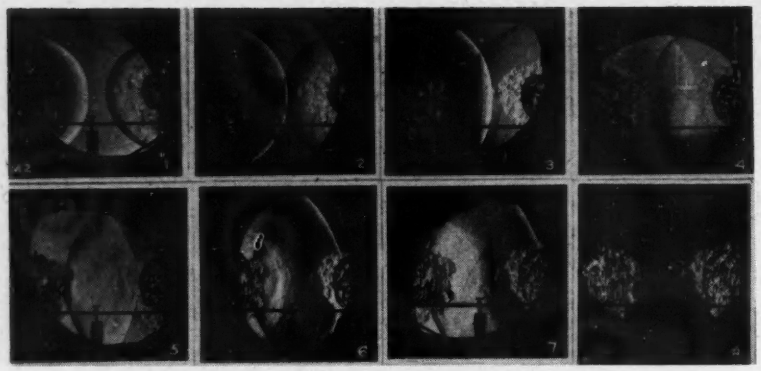

Figure 43

High speed schlieren photographs of the collision of spherical shock waves. Both spheres, 1.9 inch diameter, He/Air, 326 psi/14.5 psi, $T = 295°K$, time delays in μ sec for frames 1 to 8, in 50 μ sec intervals, 250 to 600

of the blast energy. However, the use of blast wave theory for the analysis of the related problems in steady, hypersonic, two-dimensional and axisymmetric flows have been very successful.

The theoretically predicted wave systems from finite source explosions generated by pressurized glass spheres, including the motion of the second shock wave, have been satisfactorily verified from schlieren records of the (r, t)-plane, considering that limitations are imposed by an actual diaphragm of finite strength and mass during the early development of the blast. Ample scope for the measurement of pressure, temperature, density and velocity profiles still remains in order to fully substantiate the numerical predictions. Various driver gases and combustible gas mixtures have been successfully used to produce explosions of varying initial energy and intensity. As for intensity, a low pressure atmosphere provides a simple means of producing initially strong blast waves.

The technique of using pressurized glass spheres has been successfully extended to the production of cylindrical explosions by using pressurized open or sealed end glass cylinders. Compressed gases and combustible gas mixtures ignited by exploding wires have been used as drivers. However, the cylindrical explosions are not as consistently symmetrical or as easily generated as spherical blasts. The same methods when applied to spherical and cylindrical implosions have to date not yielded the desired results, owing to the severe asymmetrical bursting properties of glass spheres and cylinders under compressive loading. More sophisticated materials or rupturing methods may be required.

The attenuation of spherical shock waves from various finite source explosions appear to have a decay rate similar to that of a point-source explosion, after the blast wave has engulfed a mass of air equal to approximately ten times the initial mass of the explosive. Consequently, it might appear that explosions from different sources would be completely scaleable. However, as Brode points out, the initial history of an explosion persists and identical scaling may not be possible even if the decay rate is similar. However, for the purposes of some aerodynamic simulation this may not be a serious obstacle, and for structural simulation even cruder types of explosion generators may be used as long as they supply a blast pressure profile of sufficient duration compared with the response time of the structure.

Use can be made of pressurized glass spheres to generate more complex types of blast phenomena and wave interactions. Some preliminary results of underwater explosions have already substantiated the worth of this method and a detailed study of such blasts is now underway. The head-on collision of spherical shock waves has been successfully produced using this method for weak shock interactions, since for this case only were numerical solutions of the initial explosions available. The experimental work could readily be extended to stronger shock waves, but a comparison with theory would not be possible because numerical solutions of the interacting flows are too difficult to handle on present day, high speed computers. Such a comparison was only possible near the point of the shock intersection, where only the application of planar shock wave interaction theory gave fair to good agreement with the shock wave paths in the (r, t)-plane.

Similar remarks regarding numerical analyses would also apply to studies of spherical and cylindrical shock diffraction and refraction in gases or in water, or to explosions from pressurized glass spheres and cylinders in supersonic flows. Pressurized glass cylinders and spheres also appear to have useful applications in combustion investigations and for spherical shock wave transition studies in a rarefied atmosphere. The latter would have the advantage of a complete absence of interference from the viscous boundary layer, which is always present in shock tube flows.

ACKNOWLEDGEMENT

I wish to thank Dr. G. N. Patterson for his encouragement to prepare this paper and for his support of the reported investigations. The valuable contributions made by Dr. D. W. Boyer, Dr. H. L. Brode, Dr. J. G. Hall, Mr. R. Collins and Mr. L. E. Heuckroth are sincerely appreciated and are listed in the references. I am grateful to Dr. J. H. deLeeuw for reading the manuscript and for his helpful suggestions.

The Rand Corporation, Santa Monica, California deserves special thanks for their cooperation in the computation of the explosions generated from pressurized glass spheres.

The financial support received from the Defence Research Board of Canada and the US Office of Naval Research is gratefully acknowledged.

REFERENCES

(1) Cook, M. A. – *The Science of High Explosives*, Reinhold Publishing Corp., New York, 1958.

(2) Bernstein, B., et al. – *On the Dynamics of a Bull Whip*, Jl. Acoust. Soc. America 30, 12, p 1112, 1958.

(3) Glasstone, S., editor – *The Effects of Nuclear Weapons*, US Government Printing Office, Washington, 1957.

(4) Taylor, G. I. – *The Formation of a Blast Wave by a Very Intense Explosion*, Proc. Roy. Soc. A201, p 159 and p 175, 1950.

(5) Sedov, L. I. – *Similarity and Dimensional Methods in Mechanics*, Academic Press Inc., New York, 1959.

(6) Bethe, H. A., Fuchs, K., von Neumann, J., Peierls, R., and Penney, W. G. – *Shock Hydrodynamics and Blast Waves*, Los Alamos Scientific Laboratory Report AECD – 2860, 1944.

(7) Brode, H. L. – *Numerical Solutions of Spherical Blast Waves*, Rand Corp. Report RM-1363-AEC, 1954. Jl. Appl. Phys. 26, 6, p 766, 1955.

(8) Brode, H. L. – *The Blast Wave in Air Resulting from a High Temperature, High Pressure Sphere of Air*, Rand Corp. Report RM-1825-AEC, 1956.

(9) Hayes, W. D., and Probstein, R. F. – *Hypersonic Flow Theory*, Academic Press, New York, 1959.

(10) Lin, S. C. – *Cylindrical Shock Waves Produced by Instantaneous Energy Release*, Jl. Appl. Phys., 25, 1, p 54, 1954.

(11) Lees, L., and Kubota, T. – *Inviscid Hypersonic Flow Over Blunt-Nosed Slender Bodies*, Jl. Aeronaut. Scl. 24, 3, p 195, 1957.

(12) Sakurai, A. – *On the Propagation and Structure of the Blast Wave*, Jl. Phys. Soc. Japan 8, 5, p 662, 1953, and 9, 2, p 256, 1954.

(13) Glass, I. I. – *Spherical Flows and Shock Waves*, UTIA Decennial Symposium, 14-16 October, Vol. 3, p 233, 1959.

(14) Glass, I. I., and Heuckroth, L. E. – *Head-On Collision of Spherical Shock Waves*, UTIA Report No. 59, 1960. See also, Phys. Fluids, 2, 5, p 542, 1959.

(15) Chace, W. G., and Moore, H. K., editors – *Exploding Wires*, Plenum Press, Inc., New York, 1959.

(16) Glass, I. I., and Hall, J. G. – *Shock Tubes*, Navord 1488, Section 18, US Government Printing Office, Washington, 1960.

(17) Dukowicz, J. – *Determination of the Performance of a Magnetically Driven Shock Tube*, M.A.Sc. Thesis, UTIA, 1960.

(18) Brode, H. L. – *Blast Wave from a Spherical Charge*, Phys. Fluids, 2, 2, p 217, 1959.

(19) McFadden, J. A. – *Initial Behaviour of a Spherical Blast*, Navord Report No. 2378, 1952.

(20) Holt, M. – *The Initial Behaviour of a Spherical Explosion*, Proc. Roy. Soc., London, A234, p 89, 1956.

(21) Brode, H. L. – *The Blast from a Sphere of High Pressure Gas*, Rand Corp. Report P-582, 1955.

(22) von Neumann, J., and Richtmyer, R. D. – *A Method for the Numerical Calculation of Hydrodynamic Shock*, Jl. Appl. Phys., 21, p 332, 1950.

(23) Brode, H. L. – *Numerical Calculations of Blast Waves*, Rand Corp. Report P-1933, 1960.

(24) Boyer, D. W., Brode, H. L., Glass, I. I., and Hall, J. G. – *Blast from a Pressurized Sphere*, UTIA Report No. 48, 1958.

(25) Boyer, D. W. – *Spherical Implosions and Explosions*, UTIA Report No. 58, 1959.

(26) Guderley, G. – *Starke Kugelige und Zylindrische Verdichtungstosse in der Nahe des Kugelmittelpunktes bzw. der Zylinderachse*, Luftfahrtforschung 19, p 302, 1942.

(27) Glass, I. I., and Hall, J. G. – *Shock Sphere – An Apparatus for Generating Spherical Flows*, Jl. Appl. Phys., 28, p 424, 1957.

(28) deLeeuw, J. H., Glass, I. I., and Heuckroth, L. E. – *A High-Speed Multi-Source Spark Camera*, UTIA Technical Note No. 26, 1960.

(29) Glass, I. I. – *Design of a Wave Interaction Tube*, UTIA Report No. 6, 1950.

(30) Glass, I. I., Martin, W. A., and Patterson, G. N. – *A Theoretical and Experimental Study of the Shock Tube*, UTIA Report No. 2, 1953.

(31) Schardin, H. – *Measurement of Spherical Shock Waves*, Communs. Pure and Appl. Math. 7, 1, p 223, 1954.

(32) Collins, R. – *Some Methods of Generating Cylindrical Explosions*, UTIA Technical Note No. 43, 1960.

(33) Lewis, B., and von Elbe, G. – *Combustion, Flames and Explosions of Gases*, Academic Press Inc., New York, 1951.

(34) Heuckroth, L. E. – *Some Experiments on Cylindrical and Spherical Implosions*, UTIA Technical Note (to be published).

(35) Payne, R. B. – *A Numerical Method for a Converging Cylindrical Shock*, Jl. Fluid Mech. 2, 2, p 185, 1957.

(36) Groves, T. K. – *A Photo-Optical System of Recording Shock Profiles from Chemical Explosions*, Suffield Technical Paper No. 192, DRB, Canada, 1960.

(37) Jones, G. H. S., Slater, W. J., and Muirhead, J. C. – *Model Studies of Blast Effects*, Parts 1, 2 and 4, Suffield Technical Paper Nos. 154, 163, 174, DRB, Canada, 1959-1960.

(38) Filler, W. S. – *Measurements on the Blast Wave in a Conical Tube*, Phys. Fluids, 3, 3, p 444, 1960.

(39) Shaw, W. A., and Allgood, J. R. – *An Atomic Blast Simulator*, Proc. Soc. Exptl. Stress Anal., 12, 1, p 127, 1959.

(40) Bleakney, W., White, D. R., and Griffith, W. C. – *Measurements of Diffraction of Shock Waves and Resulting Loading of Structures*, Jl. Appl. Mech. p 439, December, 1950.

(41) Waldron, H. F. – *An Experimental Study of a Spiral Vortex Formed by a Shock Wave*, UTIA Technical Note No. 2, 1955.

(42) Cole, R. H. – *Underwater Explosions*, Princeton University Press, 1948.


CANADIAN AERONAUTICAL
INSTITUTE

DESIGN OF AN INLET DUCT FOR THE PROPELLER-TURBINE INSTALLATION ON A STOL AIRCRAFT†

by Dr. D. H. Henshaw,* A.F.C.A.I.

The De Havilland Aircraft of Canada Limited

Figure 1
STOL Caribou

THE De Havilland Aircraft of Canada Limited is currently designing a propeller-turbine installation for its STOL Caribou. The Caribou is a twin-engined utility aircraft capable of performing exceptionally short takeoffs and landings from rough, unprepared fields. It is currently in production and powered by the reliable Pratt and Whitney R2000 reciprocating engine (Figure 1).

With STOL aircraft, the engine installation must be such as to provide the maximum possible power for the takeoff manoeuvre. Special design problems are encountered with the Caribou because of the low takeoff speeds permitted by the exceptionally effective flaps, which operate in the strong flow of air from the propeller. The installation must also be suited to the high speed cruise condition.

The turbine engine that is being fitted to the Caribou is manufactured by the General Electric Company under the designation T-64. This unit has a remote propeller gear box driven by a shaft protruding forward along the axis of the compressor. The general arrangement of the engine may be seen in Figure 2.

With the T-64 type of engine, the airframe manufacturer assumes responsibility for the air supply to the compressor. On the Caribou, the air is conveniently supplied by means of an S shaped duct with entry above the propeller spinner. The flow is then over the gear box, downwards past the power shaft and thence into the engine intake. Figure 3 illustrates the T-64 engine and intake installation as adopted for the DHC-4 turbine application.

The design of the intake is of interest because of its influence on engine performance. Engine power can be increased, fuel consumption decreased and engine operation improved by the use of a duct that supplies the engine with a uniform flow of air at the highest possible pressure. Performance calculations have shown that appreciable increases of payload can be achieved through the careful refinement of the nacelle and duct details.

The inlet arrangement chosen for the T-64 is in the form of a scoop above the propeller spinner. The inlet is canted and raked to provide the optimum arrangement for pressure recovery and drag at both low and high speeds. A high critical Mach number has been assured by an appropriate choice of NACA Series 1 Cowl lines[1]. A boundary layer by-pass has been fitted to prevent ingestion of the disturbed airflow from the propeller root sections.

The difficult factors in the inlet design were the wide ranges of angle of attack and inlet velocity ratio.

High angles of attack tend to give external flow separation over the upper intake lip, particularly for the "dead" engine in single-engine climbs. Highly

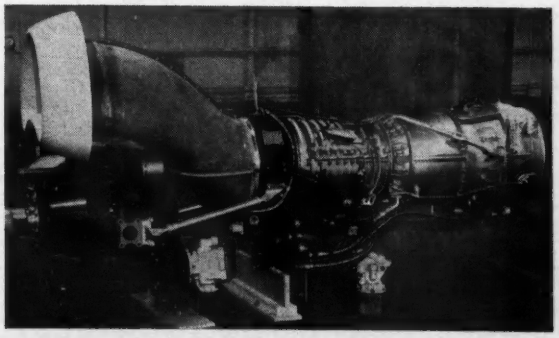

Figure 2
Intake duct on General Electric T-64

†Paper read at the Joint I.A.S./C.A.I. Meeting in Montreal on the 18th October, 1960.
*Project Engineer

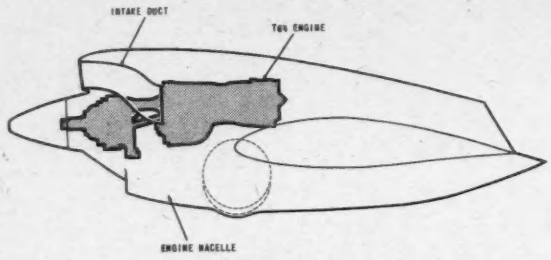

Figure 3
Caribou installation of T-64 turbine

cambered cowl lines were adopted to minimize drag under these conditions. In addition, a slight downward inclination of the intake axis reduced the effective angle of attack. The rake of the inlet reduces the tendency to external flow separation on the upper lip at high angles of attack.

For the high inlet velocity ratios occurring in takeoff, some internal flow separation will occur on the inner lips of the intake duct. According to Seddon[3], the duct immediately downstream of the inlet should be so proportioned that flow reattachment can take place. This generally requires a constant area duct for a length of about one inlet radius immediately downstream of the inlet. Inlet losses have also been reduced by the use of as large an inlet area and internal lip radii as are compatible with the external flow requirements in the high speed cruise condition.

In the formulation of the internal design of the duct, calculations were carried out to determine the nature of the potential flow solutions. The vectorial equations describing the flow in the duct are

$$\rho\vec{u_1} = -\rho \operatorname{grad} \phi$$

$$\operatorname{div}(\rho\vec{u_1}) = 0$$

To simplify the equations, the flow was assumed to be incompressible and so the above equations reduce to the familiar La Place equation $\nabla^2\phi = 0$.

To avoid the formidable difficulties encountered in analytical or digital calculations, it was decided to use analogue methods.

The analogue considered in the present connection was one relying on the properties of an isotropic conducting medium. The current flow is described as

$$\vec{i} = \sigma \operatorname{grad} e$$

$$\operatorname{div} \vec{i} = 0$$

where $\vec{i}$ is the current vector, e is the voltage and σ is the conductivity. When σ is independent of position, the equations reduce to the La Place equation $\nabla^2 e = 0$.

The velocity potential for the fluid flow and the electric potential both satisfy the La Place equation. Experimental solutions for the electric potential may, therefore, be interpreted as solutions for the velocity potential ϕ.

One of the more prominent names in the literature of electrical analogues is Malavard. He and his coworkers have carried out an extensive development of analogue techniques for the solution of many varied problems. His early studies were based to some extent on the pioneering efforts of E. F. Relf, 1924, and G. I. Taylor, 1928.

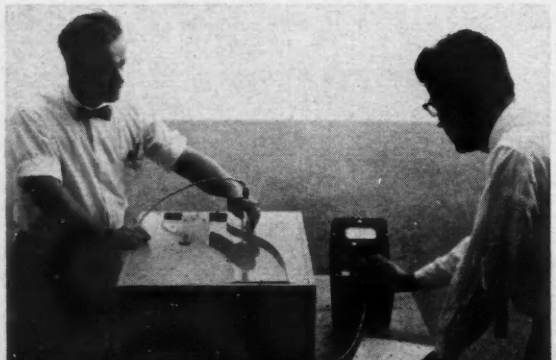

Figure 4
Electrical analogue for duct flow

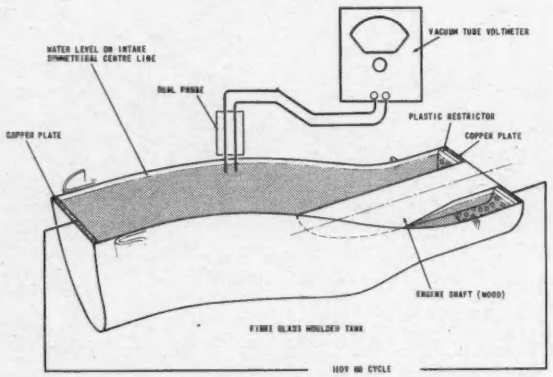

Figure 5
Electric analogy tank for duct

Studies of three-dimensional flow problems have been rather limited, because of difficulties encountered in the representation of lifting surfaces. The general literature refers almost exclusively to the two-dimensional flow problems associated with plane or axially symmetric flow. In fact, Dr. J. H. T. Wade[5] has recently discussed the application of analogue techniques to the design of an axially symmetric air intake for a small gas turbine. Popularity of the two-dimensional analogues is perhaps limited by the availability of alternative numerical methods. For the case of two-dimensional plane flow, a rapid approximate analysis has been developed by Valentine[4]. In addition, the relaxation methods of Southwell may be applied to both plane and axially symmetric flows.

For three-dimensional flows, the alternatives to the analogue techniques are generally unattractive because of the effort required for even approximate solutions. An invesigation was therefore made to ascertain the suitability of analogue techniques for the study of flow in a three-dimensional duct. As a result of discussions with R. J. Templin of the National Research Council, Ottawa, it was decided to proceed with an

electrical analogy using a conducting fluid such as tap water.

Following some exploratory measurements with a two-dimensional analogy, a three-dimensional model of the duct was molded to exact contour using a fiberglass material. The electric potential of 110 volts, 60 cycles, was applied through copper plates at each end of the duct. The electric potential distribution was measured with a voltmeter as shown in Figure 4. Note that the symmetry of the duct has permitted the adoption of the half model technique (Figure 5).

Many of the measurements were concerned with the determination of the flow velocities (Figure 6). For this purpose, a dual probe was used; this had two electrodes at a fixed distance apart. The voltage difference was proportional to the component of velocity in the direction of the line joining the electrodes.

Velocity measurements were made at the engine inlet. These were useful for the development of a design capable of meeting the engine manufacturer's specification for flow uniformity. In this investigation, an effort was made to assess the sensitivity of the inlet flow velocities to the method of simulation of the compressor inlet. It was anticipated that the compressor would tend to smooth out the distribution of flow into the engine. This smoothing effect was simulated by the introduction of a perforated sheet of plexiglass at the compressor face position. The relatively high voltage drop across the plexiglass resulted in a more uniform flow of electric current at the compressor face. The measurements showed that compressor restraint effects were small compared with the turning effects.

Another calculation was performed to determine the flow velocities in the neighbourhood of the power shaft. This shaft was circular in cross section but was to be fitted with a streamline fairing. The beneficial effects of a favourable pressure gradient on the fairing induced flow losses have already been noted by Seddon and Spence[5].

Calculations showed that the original fairing proposal was situated in an adverse pressure gradient and so could be expected to generate relatively large flow losses. It was determined that a somewhat longer fairing would position the trailing edge in a favourable gradient. The resultant beneficial effects on the flow in the wake were expected to reduce the flow losses to a low level.

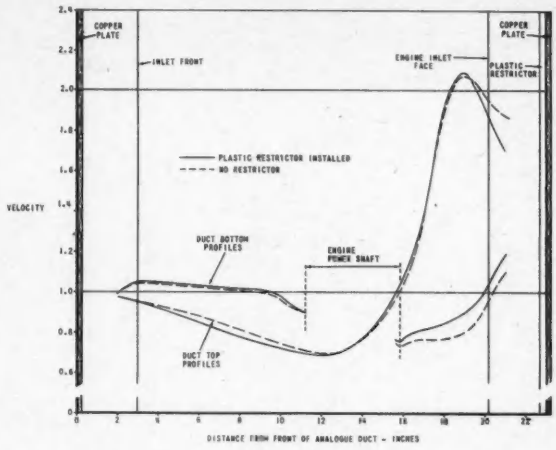

Figure 6
Electrical analogue flow velocity on plane of symmetry

In the design of the Caribou propeller-turbine installation, flow calculations carried out by the electrical analogue method have contributed to the rapid and economic development of a high efficiency airflow system. It is hoped that this brief presentation will contribute to a more widespread application of the analogue method to the design of high efficiency flow systems.

REFERENCES

(1) Baals, D. D., Smith, N. F., and Wright, J. B. – *The Development and Application of High-Critical-Speed Nose Inlets*, NACA Technical Report 920, 1948.

(2) Seddon, J. – *Air Intake for Gas Turbine Engines*, Jour. R.Ae.S., October, 1952.

(3) Wade, Dr. J. H. T. – *The Design and Testing of an Air Intake for a Small Shaft Power Gas Turbine*, Canadian Aeronautical Journal, Vol. 6, No. 6, June, 1960.

(4) Valentine, E. F. – *An Approximate Method for Design or Analysis of Two-Dimensional Sub-sonic Flow Passages*, NACA Technical Note 4241, April, 1958.

(5) Seddon, J., and Spence, A. – *A Wind Tunnel Investigation of Entry Loss on Propeller Turbine Installation*, Parts I and II, ARC Report and Memo. No. 2894, 1954.


CANADIAN AERONAUTICAL
INSTITUTE

C.A.I. LOG

SECRETARY'S LETTER

My annual tour of the western Branches has always been a most enjoyable interlude and since I have been making these tours with the President they have become even more fun. This year the tour took place from the 16th to the 20th January; the weather was kind to us – it fact it was bright and clear all the time – and all our journeyings worked out as planned.

VANCOUVER

The President and I joined forces in Vancouver on the Monday. He had come up from a business trip to the States and I had come by DC-8 (what an aeroplane!) across Canada. On my arrival and before I met the President, Mr. Hartley, the Branch Chairman, took me around the Canadian Pacific Air Lines shops. Spending, as I do, so much time in Headquarters, these rare glimpses of reality are most refreshing.

In the afternoon we had a meeting with the Branch Executive Committee and in the evening we attended the January meeting of the Branch, which had been rearranged from the 18th to enable us to be present. In Vancouver, as in most of our Branches, I recognize so many faces nowadays – and forget so many names, alas – that much as I enjoy these meetings I always leave them feeling a little guilty at not having greeted personally some of my old friends. I hope that they will understand how bewildering this sudden reunion with fifty or sixty people can be.

CALGARY

Next morning bright and early we set out for Calgary, where we were met by Mr. Fenby and and F/O Flaherty, the Chairman and Secretary of the Branch, respectively. The President went on into town but the rest of us waited at the airport to meet Dr. Whyte of the NRC, who was coming from Ottawa to speak to the Branch. Dr. Whyte and I were taken to lunch at Canadian Pacific Air Lines (Repairs) at Lincoln Park. I had not been there before and was interested to see this modern version of the "Mod Centre", which I knew so well in the States during the war.

Later in the afternoon we had an informal meeting with the Branch Executive Committee in the President's room in the hotel, a room I might add with a magnificent view of the foothills country, rimmed by the white peaks of the Rockies across the entire horizon. The Branch held a dinner meeting in the evening. I think that the highlights were an unexpected burst of French from the President in opening his excellent (I nearly said "otherwise excellent") address – this was brought on by a few pointed remarks about la Belle Province by Mr. Fenby in introducing him – Dr. Whyte's paper, and the customary western hospitality and renewal of acquaintances. It was a most enjoyable visit.

COLD LAKE

On the Wednesday we were due at Cold Lake and the President, Dr. Whyte and I flew up to Edmonton in the morning. I had spoken to F/L Smith, the Chairman of the Cold Lake Branch, on the telephone from Calgary and as a result it was decided that the President and Dr. Whyte should remain in Edmonton; the membership of the Cold Lake Branch has fallen considerably during the last year, due to transfers and for other reasons, and it is becoming an increasingly difficult job to get there; we felt that it would be rather an imposition on the President and the Speaker to ask them to tackle the journey for perhaps a rather small meeting. So I went alone; and had a wonderful time.

A seven hour bus ride took me there. This in itself was a worthwhile experience, running through that remote country with brief stops at half a dozen isolated communities, with their Ukranian churches and grain elevators along the railway. I was met by F/O Bailey, the Branch Secretary, who kindly entertained me to dinner at his home before we went on to the meeting. It was a small meeting, but very pleasant and chatty; S/L Fryers stepped into the breach as speaker, and discussed his recent paper on Pressure Altitude Altimetry, which was published in the December issue of the Journal. We also discussed some of the current difficulties of the Branch.

Cold Lake: Mr. C. B. Jeffery, F/L N. H. Smith and the Taylorcraft — running

I had intended to return to Edmonton by train but Mr. Jeffery offered to fly me back in his rather elderly Taylorcraft and I readily accepted. Accordingly Mr. Jeffery, F/L Smith and I duly assembled next morning on the frozen surface of Cold Lake itself (this is a little way from the RCAF Station) where some half dozen small aircraft, some on skis and some on wheels, were soaking in the near-zero temperature. Mr. Jeffery's Taylorcraft is an admirable aeroplane but easy starting when cold is not one of its virtues. When we had got it started, it suffered rather severely from mag drop and we had to take all the plugs out. All this was a lot of fun, if a little chilling; another return to reality. I hadn't swung a prop for about 25 years, and then on wet English grass rather than Northern Alberta ice. However we duly arrived at Edmonton, where I found the President wondering whether he should begin looking for a new Secretary or whether it was worth alerting Search and Rescue to look for the old one.

EDMONTON

Late that afternoon Mr. van Horne, Chairman of the Edmonton Branch, and Mr. Quick, the Chairman of his Programmes Committee, met us in the President's hotel room and we discussed Branch and Institute affairs. After dinner together, with Dr. Whyte, we proceeded to the Branch meeting, where again we met many old friends; both the President and I had, of course, attended the Mid-season Meeting in Edmonton last year and had very pleasant memories of Edmonton hospitality.

This was another good meeting and fortunately the President was able to stay to the end, though he had to leave that night on his return journey to the east.

WINNIPEG

Because the President could not be with me on the Friday and because Friday is a bad night for meetings and because we would all be back in Winnipeg again for the Mid-season Meeting, no Branch meeting had been arranged in Winnipeg when I arrived on the last visit of my tour. However I reached Winnipeg by mid-day and was taken by Mr. Baker, the Branch Secretary, to see the site of the forthcoming Mid-season Meeting and to talk over our plans with the hotel. This done, we went to the Flying Club where I conferred with the Committee which had been working on the Mid-season Meeting plans. At the time of writing, I think that all that can be done to make this Meeting a success has been done and the Branch is to be congratulated on the preparation it has made.

I spent the evening with the Branch Executive Committee at the home of W/C Evans, their Chairman, and we talked about all manner of administrative and policy matters, with a few digressions into such topics as man-powered flight and snowboats (which, for the uninitiated as I was, are in effect aero-engine-powered sleds).

And so home by the late night plane. It was a good tour. Somewhere along the way someone mentioned that my correspondence lately had been so full of the Institute's woes that they had felt it was high time for me to come and see them and be cheered up. Cheered up I certainly was; it is most encouraging to witness the work that the Institute is doing across the country and the momentum that the western Branches have built up. I am sure that the President was similarly impressed.

DUES DUE

March is the end of our fiscal year and April the beginning of the next. During March we send out next year's dues bills and I would suggest that they should be paid promptly. Certainly the Bylaws provide for a period of grace – technically a member does not become "in arrears" until October – but if payment is put off till then, we have all sorts of complications about loss of privileges and reminder letters, which we should avoid if we can. And we can, if members would pay when they get their bills and before they forget all about them.

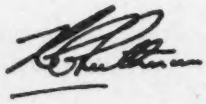

BRANCHES

Vancouver

Reported by M. G. Brechin

January Meeting

The monthly meeting of the Branch was held on January 16th, 1961, at the RCAF Officers' Mess Sea Island, and was attended by 46 members and 4 guests.

Mr. F. L. Hartley, Branch Chairman, called the meeting to order and introduced Mr. David Boyd, President of the CAI, and Mr. H. C. Luttman, Secretary, to the members and guests present.

Mr. Boyd addressed the meeting with a few informal words, saying how pleased he was to be able to meet the members of the Vancouver Branch. He went on to say that the CAI was going through a few difficult years due to the "cut-back" in aircraft manufacturing in Canada, and "where we were approaching future plans on horseback we are now walking". However, membership in the Institute is growing steadily in spite of the difficulties. He urged more membership from the hangar people such as Mechanics, Inspectors and Air Engineers – people who know their way around aircraft. These people are as interested as the "brass hats and slide rule boys". Our future lies in development – not in size but in how effective we are. Aeronautics is the people, knowledge and education in aviation.

Vancouver Branch Executive Committee and guests (l to r) Mr. M. G. Brechin, S/L A. E. Falls, Mr. David Boyd, Mr. F. L. Hartley, Mr. H. C. Luttman, Mr. R. J. McWilliams, Mr. A. G. Reddy and Mr. G. W. T. Roper.

Mr. Luttman, in his address to the membership, said how pleased he was to be back visiting the Vancouver Branch. He laid emphasis on participation for membership from the hangar and the shortage of papers for the Journal, especially those papers which lend themselves to the interest of people on the hangar floor.

Presentation of membership certificate was made to Mr. C. F. Tinley by the President.

The Programme Chairman, Mr. A. G. Reddy, presented a short report advising that the hopes of the Vancouver Branch in obtaining Sir Frank Whittle to address the joint CAI/SAE meeting in February were still high.

The programme for the evening consisted of a panel discussion on the subject, "Constant Frequency vs Frequency Wild Generating Systems for Aircraft". The panel members were Mr. F. P. Schregardus from Boeing Aircraft and Mr. L. C. Bryan, being the proponents of constant frequency, and Mr. J. A. Love and Mr. R. L. Jubinville for frequency wild systems. The moderator, Mr. G. A. Worden, was hard pressed at times to keep the discussion at a constant frequency, as the lively discussion which followed could be described as frequency wild.

The panel members were thanked by Mr. W. E. Regan for their participation and for the lively interest aroused.

Presentation of membership certificate to Mr. C. F. Tinley by the President

Calgary

Reported by F/O L. A. Flaherty

January Meeting

The January meeting of the Calgary Branch was a dinner meeting held at the Al San Club on 17th January, 1961, at 7.30 pm. The meeting was presided over by the Chairman, Mr. G. H. Fenby. There were 16 members and 10 guests present. Among the guests, we were honoured in having our President, Mr. David Boyd, and the National Secretary, Mr. H. C. Luttman, present.

Before the introduction of the guest speaker, Mr. Luttman spoke briefly to the members on the general policies affecting the CAI. He gave a short résumé of the SAE International Congress and Exposition which he attended in Detroit. He also extended an invitation for the submission of individual papers for the Journal, and explained how the new layout of the Journal would permit individual binding of papers.

Mr. Boyd then addressed the members, beginning his address in French, but switching quickly to English, when he saw the consternation on the faces of some of the members. He suggested later, that we should all endeavour to learn French. Mr. Boyd expressed the hope that the CAI collectively and individually, by Branches and members, would endeavour to take the lead in putting the spirit of romance back into aviation. He stressed the need for encouraging students to be interested in the aircraft business. He urged the members to make an effort to increase the membership, and he touched briefly on the financial situation of the CAI. Upon the conclusion of his address, he was thanked by Mr. Fenby.

Mr. W. E. Jamison introduced the guest speaker, Dr. R. B. Whyte, whose subject was "Qualification Testing of Fuels and Lubricants at the NRC".

Dr. Whyte explained the methods and purposes for qualification testing, and supported his talk with slides showing the actual equipment in use at the National Research Laboratories in Ottawa. It was interesting to note that these facilities are now available to any oil company wishing to become a supplier to the armed forces. Through this facility, the company can obtain qualification testing and, if acceptable, be certified by that branch of the armed forces concerned. Prior to this facility being made available, oil companies in Canada were at a considerable disadvantage.

Dr. Whyte's talk was followed by a question and answer period, at the conclusion of which S/L R. S. Crosby thanked Dr. Whyte on behalf of the Calgary Branch.

The Chairman, Mr. Fenby, then extended the thanks of the Calgary Branch to the President and the National Secretary for visiting us and expressed the hope of continued liaison and good will.

Halifax-Dartmouth

Reported by Lt A. M. Percy

January Meeting

The regular meeting was held in the cinema of the CPOs' Mess, HMCS Shearwater, on Wednesday, 18th January, 1961. A total of 45 members and guests were present. The meeting was presided over by LCDR G. M. Cummings, the Branch Chairman.

The Chairman stated that CPO G. E. Blackwell had offered his services as Secretary since the former Secretary, CPO A. C. Green, was now serving at sea, and that Lt A. M. Percy had been elected as Vice Chairman of Publicity.

The Chairman then invited Mr. W. G. Stewart to introduce the guest speaker, Mr. L. A. Dickinson. Mr. Dickinson, who is Head of the Rocket Engine Development Section, Propulsion Wing, CARDE, gave a very interesting and informative lecture entitled "Rocket Engine Development in Canada".

The speaker presented his lecture in two sections. The first, which was illustrated by a number of slides, was devoted to describing the factors influencing the design of a rocket motor and the choice of a suitable propellant to satisfy the many and varied requirements. The second section was a film showing stages in the production and testing of a rocket propulsion vehicle of the Black Brant type culminating in the successful launching of such a vehicle.

The lecture was followed by a lively discussion period during which Mr. Dickinson mentioned that Canadian research was now taking place to investigate the chemistry of the upper atmosphere, with a view to improving long range weather forecasting and long range radio communications.

Mr. R. Wallworth thanked the speaker for the interesting presentation of his lecture and for the ready and informative answers to the varied questions raised during the discussion period.

Cold Lake

Reported by F/O D. N. Bailey

January Meeting

The January meeting of the Branch was held in the GIS Theatre on the 18th January, 1961. 7 members and 2 guests attended.

After welcoming those present, the Branch Chairman, F/L N. H. Smith, introduced the Secretary of the CAI, Mr. H. C. Luttman, who gave a short talk on the purpose and aims of the CAI. This was followed by a short discussion of Branch problems, with special reference to the future of the Cold Lake Branch.

The speaker for the evening, S/L W. R. Fryers, was introduced by Mr. C. B. Jeffery. The speaker's subject "Pressure Method of Measuring Altitude", covered the research and planning he had done on the measuring of aircraft altitude with reference to pressure levels rather than to feet or kilometers. He had obviously gone into the problem thoroughly and had solutions to the problems of aircraft flight level separation, a standard flight level indication and had a tentative design for method of presentation to the pilot.

After an informal discussion period, the speaker was thanked on behalf of those present by F/O D. N. Bailey.

COMING EVENTS

CAI

25th-26th May, 1961—*Annual General Meeting*, TORONTO, ONT.

BRANCHES

Vancouver

22nd April — CANYON GARDENS, *Annual General Meeting and Dance.*

Tour Speakers

Advanced Systems Planning Looks at VTOL in Peace and War,

W. S. GEDDES.

20th March — Vancouver
21st March — Edmonton
22nd March — Calgary
23rd March — Winnipeg

A Review of Technical Requirements for the Operation of Aircraft at Sea,

CDR J. F. FRANK.

22nd March — Montreal
23rd March — Quebec

Solutions to Aircraft Store Separation Problems, T. B. FESSENDEN.

19th April — Halifax-Dartmouth
20th April — Quebec

BOOKS

Transport Phenomena. By R. B. Bird, W. E. Stewart and E. N. Lightfoot. John Wiley and Sons, New York, 1960. 780 pages. Illus. $13.75.

This book, written by three members of the Chemical Engineering Department at the University of Wisconsin, is an important addition to the literature of fundamental engineering science. It deals with those physical phenomena in which the transport in fluid or solid media of momentum, energy or mass are the central features. Thus the topics dealt with include, among others, viscous flows (momentum transport), heat transfer (energy transport) and diffusion (mass transport). The close correspondence and mathematical analogies among these transport processes are emphasized. The material is cleverly organized on a "two-coordinate" basis; that is, each of the 22 chapters is defined by (a) the type of transport and (b) the entity being transported. The entities are those already mentioned (momentum, energy and mass) and the types of transport include transport by molecular motion, by laminar and turbulent flow, transport across fluid and solid interfaces, and transport by radiation. These and other associated phenomena are basic to many engineering processes and design problems. They have widespread and important applications in aeronautics and astronautics, of which one noteworthy example is the re-entry heating problem. In the case of ablation, all three processes take place simultaneously and are strongly coupled.

Since the book is intended for use as a text book, many excellent problems are included at the end of each chapter to be worked by the student. These should prove to be of great help to teachers.

The level of scholarship is gratifyingly high. The authors exhibit a comprehensive and fundamental grasp of an extremely wide variety of subject matter, and have effectively put this across in the text. However, it must be said that students will not find this book 'easy going'. The details of the mathematical arguments are rather condensed, and the level of mathematics employed is quite advanced (but not unnecessarily so).

This book may be said in a sense to be three in one – Viscous Flow, Heat Transfer and Mass Transfer. The case for a unified treatment in a single volume has been well put by the authors, and this reviewer has no doubt of the value of this approach in a work of reference. He has some reservations as to its desirability from the pedagogical standpoint, however. The volume of material included in this way may be too much for one course. Experience with classroom use will show how correctly the authors have anticipated future developments in engineering curricula. Indeed this important book may exert a substantial influence on them.

B. Etkin

An Introduction to the Theory of Aircraft Structures. By Dr. D. Williams. MacMillan Co. Canada, 1960. 448 pages. Illus. $10.25.

The first sentence of the preface sums up this book admirably: "The aim of this book is to provide a background for the solution of aircraft structural problems as distinct from providing a collection of solutions to individual problems".

Dr. Williams is Deputy Chief Scientific Officer in the Structures Department of the Royal Aircraft Establishment, Farnborough. He has had many papers published in various technical journals, plus many RAE reports, to establish him as an authority on the subject of aircraft structures.

Chapter 1 presents a sufficient amount of the theory of elasticity that is required later in the book. It is well presented and easy to follow. The two chapters on strain energy methods and strain energy examples are a welcome addition in books of this type. Too often strain energy theories are derived and it is up to the student to apply them. Chapters 4 and 5 deal with "individual displacements" and application and removal of constraints. This latter chapter only touches on the basic elements of the subject, with the author himself suggesting reference to Southwell's work on relaxation methods for a more comprehensive background. Chapter 6 deals with torsion of shells and box beams and considers axial warping of box beams. Chapter 7 deals with bending shear stresses in thin walled beams, both open and closed sections. Both these chapters contain much that can be found in appropriate textbooks. Chapter 8 deals with shear lag and is presented in an excellent manner. Rectangular box beams and beams representative of fuselages are considered. An excellent collection of references on shear lag are added at the end of the chapter. Chapter 9 deals with pressure cabin problems and includes such items as neutral holes, reinforcing around holes and effect of cabin frames and bulkheads. An interesting example of a typical fuselage shows that conventional frames at 20 inch pitch can at best be only 38% effective in helping to reduce the maximum hoop stress in the skin. It was disappointing to see only about four pages on the subject of fatigue and fail-safe aspects of pressure cabins. Dr. Williams could have reduced the contents of the last four chapters in order to discuss this subject in more detail. The last four chapters deal with the dynamics of the aeroplane. They will be especially useful to the aircraft stressmen in providing a good background on the problems his neighbour engineer in the dynamics department is confronted with. More could have been included on power spectrum analysis of gusts since this "new" technique is now an accepted procedure of analysis. Throughout the book, Dr. Williams has emphasized the importance of stiffness as well as strength. In present day design, for instance, wing flexibility is one of the most important problems, and therefore the addition of these four chapters is not out of place in a structures book of this kind.

The mathematics involved are of such a level that the graduate engineer should not have too much trouble in reading this book.

The book is one which can be recommended to the post-graduate engineer and the aircraft stressman – the former for studying, the latter as a reference book.

E. Aubrey

Avionics Research: Satellites and Problems of Long Range Detection and Tracking. Edited by E. V. D. GLAZIER, E. RICHTER AND J. VOGE. Pergamon Press, 1960. 257 pages. Illus. $10.00.

The 19 papers published in this book were presented at the AGARD Symposium held in Copenhagen in October, 1958, under NATO auspices.

Immediately after the unannounced launching of Sputnik I, radio astronomy equipments were converted to radar sets and the Minitrack stations modified to operate on 20 mc/sec and 40 mc/sec. Eight of the papers discuss the results obtained. Radar detection was not reliable; its failures being attributed to polarisation rotations in the ionosphere and to satellite motions causing the effective echoing area to fluctuate over wide limits. Such motions could also be inferred from the amplitude variations of the signals from the satellite radio transmitters.

Detection of large ground targets by ionospheric radar is discussed and mention is made of the probable detection of a satellite using this technique. Some observers, however, feel that the echo was returned from the ionization trail behind the satellite, a view which could be supported by the data on auroral echoes and the responses from meteor trails.

Other papers deal with the electrohydrodynamic effects of an ionized medium on the motion of the satellite. The connection between this and the detection problem seems somewhat tenuous; and a similar criticism could be levelled at the description of the re-entry of an IRBM where initial detection was by a chance visual observation.

A paper on echoing area characteristics deals with simple shapes, meteor trails and the size of the moon. Unfortunately the continuation of the discussion to artificial satellites was not attempted.

The theory and philosophy of radar detection receive cursory treatment in two other papers. One interesting paper describes the use of noise radiated by the sun as a remote signal source in the measurement of antenna patterns, particularly when ground reflection effects are encountered.

The "principal purpose of the Avionics Panel of AGARD is to highlight profitable areas of avionics research and development". This aim is not realized in these papers, other than to point out the incomplete knowledge, at the time, of what might be loosely called "propagation phenomena". The book is not likely to provide much background data for aeronautical engineers unless many of the references are consulted; for the electronics specialist recent literature supplants much of the information presented.

J. CHISHOLM

APPOINTMENT NOTICES

The facilities of the Journal are offered free of charge to individual members of the Institute seeking new positions and to Sustaining Member companies wishing to give notice of positions vacant. Notices will be published for two consecutive months and will thereafter be discontinued, unless their reinstatement is specifically requested. A Box No., to which enquiries may be addressed (c/o The Secretary), will be assigned to each notice submitted by an individual.

The Institute reserves the right to decline any notice considered unsuitable for this service or temporarily to withhold pulication if circumstances so demand.

POSITION WANTED

Box 111 **Technician:** Aircraft Maintenance Technology graduate from the Southern Alberta Institute of Technology and Art desires position in industry. Will appreciate all offers. Excellent references available.

SUMMER EMPLOYMENT

Box 112 **Student:** Second year engineering student at Ecole Polytechnique de Montréal seeks position for the period 15th May to 15th September. Bilingual with technical drawing and surveying experience.

Box 113 **Student:** First year student in Aircraft Maintenance Technology at the Southern Alberta Institute of Technology and Art seeks position, in western Canada, for the period May 15th to September 1st.

Box 114 **Student:** First year student in Aircraft Maintenance Technology at the Southern Alberta Institute of Technology and Art seeks position, preferably in Ontario, for the period May 15th to September 15th.

Box 115 **Student:** Student having completed his first year in the Aircraft Maintenance Technology course at the Southern Alberta Institute of Technology and Art seeks position in the Edmonton or Calgary areas.

Box 116 **Student:** Second year postgraduate student in Mechanical Engineering at Nova Scotia Technical College seeks position from the 1st May in the propulsion field, with an outlook for permanent employment after graduation. No geographical preference. Experienced in supervision.

Box 117 **Student:** First year student in Aircraft Maintenance Technology at the Southern Alberta Institute of Technology and Art seeks position, preferably in western Canada, for the period March 20th to September 1st. Hard worker and willing to learn.

Box 118 **Student:** Second year student in Aeronautical Engineering at the Southern Alberta Institute of Technology and Art seeks position, preferably in western Canada, for the period May 15th to September 15th. Experience includes two years Mechanical, structural and topographical drafting.

Box 119 **Student:** First year student at the Southern Institute of Technology and Art seeks position anywhere in western Canada. Experience includes a Private Pilot's Licence and two months service in the RCAF Reserve Tradesmen Training Plan towards an Airframe Technician Group I rating.

Box 102 **Student:** Fourth year Mechanical Sciences student at McGill University seeks position in plant engineering. Experience includes four years workshop and drafting prior to entering university.

SUSTAINING MEMBERS

of the

CANADIAN AERONAUTICAL INSTITUTE

1960-61

Aeroquip (Canada) Limited

Aircraft Industries of Canada Limited

Alloy Metal Sales Limited

Aviation Electric Limited

A. V. Roe Canada Limited, Aeronautical Group

BP Canada Limited

Bourne & Weir Limited

Bristol Aero-Industries Limited

Canadair Limited

Canadian Flight Equipment Cobourg Ltd.

Canadian Pacific Air Lines Limited

Canadian Pratt & Whitney Aircraft Company Limited

Cannon Electric Canada Limited

Carriere and MacFeeters Limited

Collins Radio Company of Canada Limited

Computing Devices of Canada Limited

DeHavilland Aircraft of Canada Limited

D. Napier & Son (Canada) Limited

Dowty Equipment of Canada Limited

Enamel & Heating Products Limited

Fairey Aviation Company of Canada Limited

Field Aviation Company Limited

Fort Garry Tire & Auto Supplies

Garrett Manufacturing Limited

General Controls Co. (Canadian) Limited

Godfrey Engineering Company Limited

Honeywell Controls Limited

Imperial Oil Limited

Irvin Air Chute Limited

Jarry Hydraulics Limited

Lucas-Rotax Limited

Moffats Limited (Avco of Canada)

Normalair (Canada) Limited

Northwest Industries Limited

Okanagan Helicopters Limited

Prenco Progress & Engineering Corporation Limited

Railway & Power Engineering Corporation Limited

Rolls-Royce of Canada Limited

Rousseau Controls Limited

Shell Oil Company of Canada Limited

Simmonds Aerocessories of Canada Limited

Smith (A.M.I.) Canada Limited

Standard Aero Engine Limited

Timmins Aviation Limited

Trans-Canada Air Lines

Walter Kidde & Company Limited

York Gears Limited

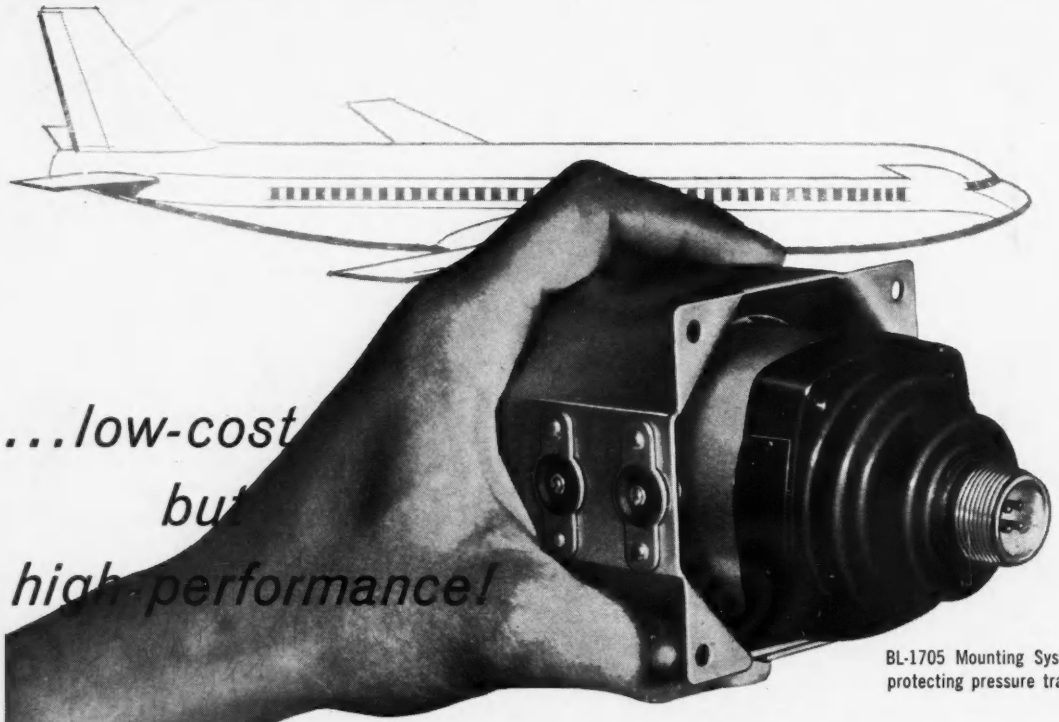

...low-cost
but
high-performance!

BL-1705 Mounting System — shown protecting pressure transducer.

vibration control for aircraft instruments

Here's a new Lord mounting system for small equipment or instruments on jet aircraft that offers big advantages!

It's versatile. Basic design is adaptable to a variety of units: transducers, indicators, electronic tubes, gages, warning and timing devices, baroswitches. Mounting arrangements permit use in instrument panel, nacelle or other airframe locations.

It's high-performance. Lightweight system provides excellent all-attitude control of high-frequency excitations plus attenuation of shock and structure-borne noise. BTR® Elastomeric Mountings possess extreme environmental resistance, excellent damping, superior endurance, consistent performance over −65° to +300°F. range.

It's economical. Simplified design gives you Lord quality at a lower price than competitive bases. Long service life means your maintenance costs will be lower, too.

It's proved. The advanced design and performance of this Lord system have been thoroughly proved in actual service on today's jet airliners.

This mounting system is an example of Lord ingenuity. It indicates why you can continue to expect Lord to produce the best in vibration/shock/noise control for the aerospace environment. To put this ingenuity to work on your project, or to get further data on the BL-1705 base, contact *the nearest office of Railway & Power Engineering Corporation, Limited.*

typical specifications

Application: pressure transducer. **Weight: equipment** — 1.2 lbs., **base** — .38 lbs. **Shock/vibration protection:** all-attitude. **Isolators:** four Special BTR Multiplane Mountings. **System natural frequency:** 45 cps. **Operating temperature range:** −65° to +300°F. **Environmental resistance:** unaffected by fungi, dust, sand, salt atmosphere, oil, ozone. **Construction:** center-of-gravity suspension, fail-safe. **Mounting arrangements:** clearance holes or clinch nuts for base, bulkhead or overhead attachment.

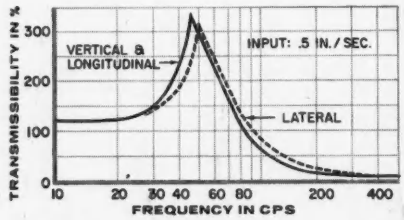

LORD®

RAILWAY & POWER
Engineering Corporation, Limited

NEW GLASGOW - QUEBEC - MONTREAL - NORANDA - NORTH BAY - OTTAWA - TORONTO - HAMILTON - WINDSOR - SAULT STE. MARIE - WINNIPEG - CALGARY - EDMONTON - VANCOUVER